

Mathematical Modelling of the Intrarenal Renin Angiotensin System in Hypertension

by

Delaney Smith

A thesis
presented to the University of Waterloo
in fulfillment of the
thesis requirement for the degree of
Master of Mathematics
in
Applied Mathematics

Waterloo, Ontario, Canada, 2023

© Delaney Smith 2023

Author's Declaration

This thesis consists of material all of which I authored or co-authored: see Statement of Contributions included in the thesis. This is a true copy of the thesis, including any required final revisions, as accepted by my examiners.

I understand that my thesis may be made electronically available to the public.

Statement of Contributions

This thesis contains one research work that has been published in a scientific journal. The author lists for the paper and contributions made by myself and my coauthor are as follows:

The intrarenal renin-angiotensin system in hypertension: Insights from mathematical modelling

Delaney Smith¹ and Anita Layton^{1, 2, 3, 4}

1 Department of Applied Mathematics, University of Waterloo, Waterloo, Ontario, Canada

2 Cheriton School of Computer Science, University of Waterloo, Waterloo, Ontario, Canada

3 Department of Biology, University of Waterloo, Waterloo, Ontario, Canada

4 School of Pharmacy, University of Waterloo, Waterloo, Ontario, Canada

D. Smith contributed to the design of the mathematical model, design of the computer code, running of simulations, analysis of the data, interpretation of the results, preparation of the figures as well as the drafting and revision of the manuscript. A. Layton contributed to the design of the mathematical model, analysis of the data, interpretation of the results as well as the drafting and revision of the manuscript.

Abstract

Hypertension is the leading cause of cardiovascular disease and premature death worldwide. It is a highly multi-factorial disease associated with multiple risk factors and patho-physiological changes, including impaired kidney function and an over-active renin-angiotensin system (RAS). Many hypertensive actions of [angiotensin II \(Ang II\)](#), the primary bio-active product of the RAS, are mediated within the kidney; an organ that also expresses and independently regulates all RAS constituents. The interconnected nature of the systems involved makes it difficult, and in many cases impossible, to identify their individual contributions to the observed pathology *in vivo*. Thus, the goal of this thesis is to investigate the role of the local intrarenal RAS in the pathogenesis and progression of hypertension *in silico*. In particular, we first developed a computational model of the intrarenal and systemic RASs in isolation to unravel the mechanisms that mediate the former's over-activity in Ang II infused hypertensive rats (an experimental model of hypertension). Then, by extending the model to include a [pharmacokinetic \(PK\)](#) representation of an [angiotensin receptor blocker \(ARB\)](#), a common RAS-modulating anti-hypertensive therapy, we examined the impact of this class of medication on the kidney. Lastly, by coupling our model to one of whole-body blood pressure regulation in the rat and creating the first model of long-term blood pressure regulation that considers an intrarenal RAS, we zoomed back out to determine how the aforementioned effects actually contribute to blood pressure dis-regulation.

Our results suggest that Ang II accumulates in the kidney during the development of Ang II-induced hypertension because of enhanced [angiotensin type 1 receptor \(AT1R\)](#)-mediated uptake of circulating Ang II, which is facilitated by positive feedback on intrarenal AT1R expression. By inhibiting this feedback loop, and others inherent to the intrarenal RAS, ARBs effectively prevent intrarenal Ang II levels from increasing. However, it is rather by restricting Ang II to extracellular regions of the kidney that ARBs effectively restore normotension. In the absence of treatment, rising concentrations of cell-associated Ang II act to increase blood pressure by stimulating sodium reabsorption along the [nephron](#). The timing of this response also affects blood pressure dynamics. Indeed, slow-pressor hypertension is a consequence of systemic and intrarenal RAS decoupling: The progressive accumulation of Ang II in the kidney permits the sequential activation of sodium reabsorption by aldosterone, then Ang II. Our results shed light on the functional importance of the intrarenal RAS in hypertension induced by Ang II infusion, and thus clinical hypertension associated with an over-active RAS.

Acknowledgements

I would like to thank my supervisor Dr. Anita Layton for her unwavering support and guidance throughout this degree. She has provided me with ample opportunities to grow both as a researcher and a person, and has always encouraged me to find my own path. For that, I will always be grateful.

I would also like to thank my committee members, Dr. Sue Ann Campbell, Dr. Brian Ingalls, and Dr. Anita Layton who graciously took the time to review my thesis.

Thank you to my lab members: Melissa Stadt, Chris West, Stéphanie Abo, Shervin Hakimi, Pritha Dutta, Mehrshad Sadria, William Bell, Anderson White, Matt Wiens, Kaixin Zheng, Chi-Chung Cheung, and Amandeep Kaur. I have learned something from each of you. I would also like to thank Dr. Robert Arntfield, Blake VanBerlo, and my many other colleagues at Deep Breathe for their support. It is an honour to be a part of your team.

Finally, I would like to thank my family, my friends, and my partner for always encouraging me to do what I love, whatever that may be. I wouldn't be who I am today without each of you.

Dedication

This thesis is dedicated to my parents, without whom none of this would have been possible.

Table of Contents

List of Figures	xii
List of Tables	xiii
List of Abbreviations	xiv
1 Introduction	1
1.1 Regulators of blood pressure	3
1.1.1 The kidney	3
1.1.2 The renin-angiotensin system	4
1.2 History of computational models	9
1.2.1 Renin-angiotensin system models	9
1.2.2 Blood pressure regulation models	11
1.3 Outline of thesis	12
2 Modelling the rat intrarenal renin angiotensin system	14
2.1 Intrarenal RAS model	15
2.1.1 General model equations	17
2.1.2 Glomerular compartment	19
2.1.3 Tubular compartment	20
2.1.4 Peritubular compartment	20

2.1.5	Vasculature compartment	21
2.1.6	Whole kidney concentrations	21
2.2	Systemic RAS model	22
2.3	Parameter identification	25
2.3.1	Parameter derivations	27
2.3.2	Parameter fitting	28
2.4	Steady state results	32
2.4.1	Local sensitivity analysis	32
3	The intrarenal renin angiotensin system and angiotensin II infusions	35
3.1	Introduction	36
3.2	Methods	38
3.2.1	Modelling positive feedback	38
3.2.2	Simulating Ang II infusion experiments	40
3.2.3	Separating exogenous Ang II from endogenous Ang II	41
3.2.4	Parameter fitting	42
3.3	Results	43
3.3.1	Model validation	43
3.3.2	Model predictions	48
3.3.3	Local sensitivity analysis	50
3.4	Discussion	52
3.4.1	Model limitations and future extensions	55
4	The intrarenal renin angiotensin system and angiotensin-receptor blockers	57
4.1	Introduction	58
4.2	Methods	59
4.2.1	Pharmacokinetic model	59

4.2.2	Coupling the RAS and pharmacokinetic models	63
4.2.3	Model parameter identification	66
4.3	Results	67
4.3.1	Model parameter identification	67
4.3.2	Model validation	67
4.3.3	Model predictions	70
4.3.4	Local sensitivity analysis	72
4.4	Discussion	76
4.4.1	Model limitations and future extensions	78
5	The intrarenal renin-angiotensin system and slow-pressor hypertension	80
5.1	Introduction	81
5.2	Methods	82
5.2.1	Blood pressure regulation model	82
5.2.2	Simulating Ang II infusion experiments	90
5.2.3	Parameter identification	90
5.2.4	Systemic RAS-only blood pressure regulation model	92
5.3	Results	93
5.3.1	Model parameter identification and validation	93
5.3.2	Model predictions	97
5.4	Discussion	101
5.4.1	Model limitations and future extensions	103
6	Conclusions	106
6.1	Model limitations and future extensions	109
	References	112
	APPENDICES	131

A	Intrarenal RAS model equations	132
A.1	Glomerular compartment	132
A.2	Tubular compartment	133
A.3	Peritubular compartment	135
A.4	Post-glomerular blood vasculature compartment	136
B	Intrarenal Losartan and EXP3174 model equations	138
C	Blood pressure model equations	140
C.1	Cardiovascular function	140
C.2	Renal hemodynamics	141
C.3	Renal fluid handling	141
C.4	Renin-angiotensin systems	142
C.5	Miscellaneous	143
	Glossary	148

List of Figures

1.1	Diagram of a superficial nephron and the associated vasculature.	5
1.2	Schematic representation of the RAS cascade and its hypertensive effects.	6
2.1	Schematic representation of the RAS model compartments.	16
2.2	Schematic representation of the connections between model variables.	26
2.3	Percent change in the predicted steady state concentrations caused by a 10% increase in each model parameter value.	34
3.1	Schematic representation of the model's positive and negative feedback loops	40
3.2	Simulated vs. experimental plasma AGT, PRA, and plasma and whole kidney Ang I time series following 13 days of 40 ng/min SC Ang II infusion	45
3.3	Simulated vs. experimental subcutaneous and intravenous Ang II dose-plasma Ang II response curves	46
3.4	Comparing the model fit to renal compartmental Ang II data following 13 days of 80 ng/min subcutaneous Ang II infusion when mechanism (i) vs. mechanism (ii) is simulated.	47
3.5	Model validation against whole kidney Ang II time series data following subcutaneous, 40ng/min Ang II infusion	49
3.6	Temporal change in the renal distribution of Ang II throughout 13 days of SC Ang II infusion at 40 ng/min.	51
3.7	Percent change in the predicted systemic and intrarenal RAS concentrations after 13 days of 40 ng/min subcutaneous (SC) Ang II infusion to a 10% increase in each parameter value.	53

4.1	Schematic representation of the Losartan-EXP3174 pharmacokinetic model	61
4.2	Model fit (curves) to plasma Losartan and EXP3174 concentration time series data (markers) following a single oral dose (10 mg/kg) of Losartan. .	68
4.3	Model validation against RAS peptide data following experiments (i), (ii), and (iii) of Ref. [184]	69
4.4	Plasma and intrarenal exogenous and endogenous Ang II concentration following experiments (i), (ii), and (iii) of Ref. [184]	71
4.5	Temporal change in the intrarenal distribution of Ang II throughout 13 days of SC Ang II infusion at 40 ng/min alone and in conjunction with 30 mg/kg/day Losartan administration	73
4.6	The effect of Losartan on the intrarenal concentration and distribution of Ang II in a hypertensive rat	74
4.7	Percent change in the predicted average compartmental Losartan and EXP3174 concentrations following 13 days of 40 ng/min SC Ang II infusion alongside 30 mg/kg/day Losartan administration in drinking water when each parameter value is increased by 10%.	75
4.8	Percent change in the predicted average systemic and intrarenal RAS peptide concentrations following 13 days of 40 ng/min SC Ang II infusion alongside 30 mg/kg/day Losartan administration in drinking water when each parameter value is increased by 10%.	76
5.1	Schematic model of blood pressure regulation	84
5.2	RAS-related parameter fitting results	94
5.3	Impact of Ang II bioavailability on intrarenal and systemic RAS peptide time series'	95
5.4	Impact of Ang II infusion experiments on sodium and fluid balance	96
5.5	Impact of the intrarenal RAS on the blood pressure response induced by prolonged Ang II infusion	97
5.6	Mechanisms that mediate slow-pressor hypertension induced by Ang II infusion	98
5.7	Role of intrarenal Ang II in the development of slow-pressor hypertension .	101
5.8	Schematic representation of the mechanisms governing Ang II-induced hypertension	102

List of Tables

2.1	Sub-compartment-specific parameters corresponding to Eqs. 2.1–2.5.	23
2.2	Parameters derived from the literature	27
2.3	Fitted parameters	29
2.4	Experimental bounds for steady state concentrations	30
2.5	Steady state concentrations of model variables	31
3.1	Ang II infusion data used for feedback parameter estimation	42
3.2	Feedback parameters	44
4.1	Intrarenal sub-compartment-specific parameters corresponding to Eq. 4.5. .	64
4.2	Losartan-EXP3174 pharmacokinetic model parameters	67
C.1	Long-term blood pressure regulation model parameters	145
C.2	Long-term blood pressure regulation model steady state variable values. . .	147

List of Abbreviations

- [**Ang II**] **Ang II** concentration 2, 8, 30, 36, 37, 39, 86, 90, 91, 93
- ACE** angiotensin-converting enzyme 5, 8, 17, 19, 24, 29, 39, 148
- ACE2** angiotensin-converting enzyme 2 24
- ACEi** angiotensin-converting enzyme inhibitor 8, 9, 11, 55, 79, 104, 110
- AGT** angiotensinogen 4, 9, 18, 22, 27, 31, 36, 39, 150
- Ang (1-7)** angiotensin (1-7) 24, 31
- Ang I** angiotensin I 4, 9, 15, 17–22, 24, 27, 29–32, 39, 148, 150
- Ang II** angiotensin II iv, xiv, 1, 2, 4, 7, 9, 15, 17–24, 27, 29–32, 35, 38, 39, 81, 148
- ARB** angiotensin receptor blocker iv, 8–10, 12, 14, 52, 55, 58, 72, 77–79, 104, 109, 149
- AT1R** angiotensin type 1 receptor iv, 5, 7, 9, 15, 18–23, 25, 27, 29–31, 35, 38, 39, 63
- AT2R** angiotensin type 2 receptor 5, 9
- GI** gastrointestinal 59–61, 73
- IV** intravenous 41, 46
- NEP** neprilysin 24, 29
- PD** pharmacodynamic 10
- PK** pharmacokinetic iv, 10, 12, 55, 59, 63, 66, 68, 76, 79, 104, 108, 109

PK/PD pharmacokinetic/pharmacodynamic 10, 12, 57, 77, 104, 109

PRA plasma renin activity 4, 22, 29, 67, 68

PRC plasma renin concentration 22, 23, 29

RAS renin-angiotensin system 1, 4, 29, 35, 81, 150

RSNA renal sympathetic nervous activity 1, 11, 12

SC subcutaneous xi, 41, 45–47, 49–51, 53

Chapter 1

Introduction

Cardiovascular disease affects nearly half of the American population and has been a leading cause of death in Canada and the United States for over two decades [16, 8]. Globally, the number of deaths attributed to cardiovascular disease is rising. Hypertension, or chronic high blood pressure, is the world's number one risk factor for cardiovascular mortality [8]. It is estimated to have impacted nearly 25% of all Canadian adults over 20 years of age from 2016 to 2019 [15]. In 2015, 1.52 billion adults were affected around the world [8].

Hypertension is a highly complex, multi-factorial disease associated with many pathological changes, including arterial stiffening, impaired renal sodium handling, increased renal sympathetic tone, and an over-active [renin-angiotensin system \(RAS\)](#). Since many of these systems interact with one another, it is difficult, and in many cases impossible, to narrow the conditions inception to a single cause. Nevertheless, treatments that target one of two main components – the kidney and the RAS – have proven highly effective in reducing elevated blood pressure [60, 130]. Many experimental models of hypertension have therefore been devised to study clinical hypertension stemming from the impairment of each of these systems [88, 134]. In the studies presented in this thesis, clinical hypertension associated with an overactive RAS in particular will be examined through the lens one such experimental model – hypertension induced by [Ang II](#) infusion.

[Ang II](#) is the primary bio-active product of the RAS. It increases blood pressure by inducing vasoconstriction, increasing [renal sympathetic nervous activity \(RSNA\)](#), and stimulating sodium reabsorption [36, 144]. Given that many of these actions take place within the kidney, an organ which has recently been found to not only express, but independently regulate, all components of the RAS [122, 109, 38, 37, 107, 70, 40, 180, 182, 21, 114], the

significance of the local intrarenal RAS to the pathology and development of hypertension has recently come into focus.

In Ang II-induced hypertensive rats, there is a progressive rise in intrarenal Ang II that cannot be explained on the basis of equilibration with the plasma [Ang II concentration](#) ([\[Ang II\]](#)) [\[184, 31, 40, 93\]](#). A similar decoupling of the systemic and intrarenal RAS has also been observed in other experimental models of hypertension, such as: two-kidney, one-clip Goldblatt hypertension [\[18\]](#), salt-sensitive rats [\[168\]](#), and spontaneously hypertensive rats [\[150\]](#). Given the commonality of this signature across pre-clinical models, our understanding of clinical hypertension would necessarily be improved by studying the mechanisms both upstream (causes) and downstream (effects) of intrarenal RAS over-activation.

For many decades, computational modelling has provided a useful tool to study a broad range of physiological and patho-physiological systems and applications in medicine [\[68\]](#). These models prove particularly useful when studying systems that are multi-factorial in nature, such as blood pressure regulation, because once a model is developed that includes all components of interest, they can be individually turned on/off to examine their impact on the network as a whole. These *in silico* experiments are difficult to perform *in vivo*, because the contributing mechanisms are often fundamentally connected. Furthermore, when one mechanism is removed experimentally, the others often adjust to compensate.

In the studies presented in this thesis, we take advantage of these computational benefits to gain insight into role of the intrarenal RAS in hypertension. In particular, novel computational models of the intrarenal RAS and of a common RAS-modulating anti-hypertensive therapy are developed and used to simulate hypertension induced by Ang II infusion under control and treated conditions. In these studies, we seek to answer the questions: *What mechanisms mediate the progressive rise in intrarenal Ang II that accompanies hypertension induced by Ang II infusion? How does this over-activation contribute to blood pressure dis-regulation? How are these responses altered by treatment with RAS-modulating anti-hypertensive therapies? How does this explain the effectiveness of these treatment strategies in preventing clinical hypertension?* To motivate these questions and the techniques used to answer them, we first discuss the relevant background of blood pressure physiology (Section [1.1](#)) and provide a history of existing computational models in the field (Section [1.2](#)). Then, in the Chapters that follow, hypotheses for each of these questions will be developed, tested, and discussed.

1.1 Regulators of blood pressure

Blood pressure is a highly regulated variable in the body, with stabilizing mechanisms acting on both short and long time scales. Central to the pathogenesis of hypertension is the disruption of the body’s long-term regulators – the kidney and the RAS.

1.1.1 The kidney

The kidney is a collection of **nephrons**; small “filters” specially designed to reabsorb useful substances while allowing waste to pass and be excreted in urine [121]. Each nephron comprises of the **renal corpuscle** and the **renal tubule**. Solutes and water from the blood are filtered at the level of the renal corpuscle by the **glomerulus**, a tightly interconnected cluster of capillaries, into Bowman’s capsule. The glomerulus is structurally supported by the mesangium, which comprises of **mesangial cells** and the **mesangial matrix** [100, 137]. From Bowman’s capsule, the filtered fluid (the **filtrate**) enters the renal tubule to be fine-tuned via **reabsorption** (removing solutes or volume) and **secretion** (adding solutes) prior to its excretion in urine. The renal tubule is lined by a single layer of epithelial cells that separate the **luminal fluid** from the surrounding **interstitial space**. The apical membrane of these **tubular epithelial cells** faces the lumen, while their basolateral membrane faces the interstitial space. These membranes express a variety of transporters to facilitate the transcellular (through-cell) reabsorption and secretion of solutes and volume, though paracellular (between-cell) transport also occurs. The expression of these transporters and the inter-cell permeability are highly regulated using a combination of hormonal, neural, and intrarenal signals to maintain proper solute and volume balance in the body [121]. Importantly, different segments of the nephron are regulated by different factors and contain different epithelial cell types and transporters to specialize their function. The main (ordered) segments of the nephron include: the proximal tubule, the loop of Henle, the distal tubule, and the collecting duct. A diagram of the nephron and its vasculature (summarized below) is provided in Figure 1.1.

Blood flows into the kidney via the renal artery at the level of the renal hilum at a rate referred to as the **renal blood flow** [161]. In the kidney, the renal artery branches into smaller and smaller vessels before eventually becoming the **afferent arterioles** – the vessels that supply blood to the **glomerulus**. What remains of the blood after glomerular filtration is taken away by the **efferent arterioles**. The efferent arterioles subsequently become the **peritubular capillaries**; the vessels which descend into the kidney and wrap around the renal tubules. This capillary network not only supplies renal cells with the oxygen and

nutrients they need to survive, but it also facilitates the reabsorption and secretion of substances between the blood and the renal tubules. The tree-like nature of the renal arterial vasculature is mirrored by the renal venous vasculature. Ultimately, the newly filtered blood leaves the kidney via the renal vein.

Because the afferent/efferent arterioles surround the [glomerulus](#), their resistance is a key determinant of the [glomerular filtration rate](#) and of glomerular pressure [161]. If glomerular pressure is too high, as indicated by a high glomerular filtration rate, the delicate capillaries of the glomerulus could be damaged, rendering the filter unusable. If the filtration rate is too low, then the tubular epithelium may not receive the blood flow that it needs to effectively fine-tune the filtrate. Hence, glomerular filtration is tightly regulated through the control of afferent/efferent arteriole diameter via a variety of auto-regulatory mechanisms (e.g., tubuloglomerular feedback [78, 74] and myogenic response [19], hormones and neural factors, including [Ang II](#) (see Section 1.1.2).

The kidney and blood pressure regulation Kidney function is the body’s primary determinant of blood pressure over long time scales [44]. Indeed, transplantation studies have shown that hypertension “goes with” the kidney; transplanting a kidney from a hypertensive rat into a normotensive rat causes hypertension in the recipient [41]. The kidney primarily regulates blood pressure via the [pressure natriuresis](#) effect, whereby increases in renal perfusion pressure cause greater amounts of sodium to be excreted in urine [63]. Since water reabsorption largely “follows” sodium, this also results in a greater fluid excretion, which lowers blood volume and therefore, blood pressure. An abnormal pressure natriuresis mechanism is observed in all cases of chronic hypertension: Sodium excretion is maintained despite the increased blood pressure [48]. As detailed below, the RAS is one of the most powerful regulators of this pressure natriuresis mechanism and consequently, of blood pressure [1, 63].

1.1.2 The renin-angiotensin system

Since the discovery of [renin](#) in 1898, the concept of a systemic [RAS](#) as an important endocrine regulator of blood pressure has long been established [7]. The cascade begins with the release of the substrate [angiotensinogen \(AGT\)](#) from the liver [175, 114] and its conversion into [angiotensin I \(Ang I\)](#) by [plasma renin activity \(PRA\)](#). Renin is secreted from the [juxtaglomerular apparatus](#) of the kidney; a structure which lies adjacent to the glomerulus [175, 114]. As Ang I circulates in the bloodstream, it is cleaved into many other forms of angiotensin, including [Ang II](#) and Ang (1-7), which each have their own

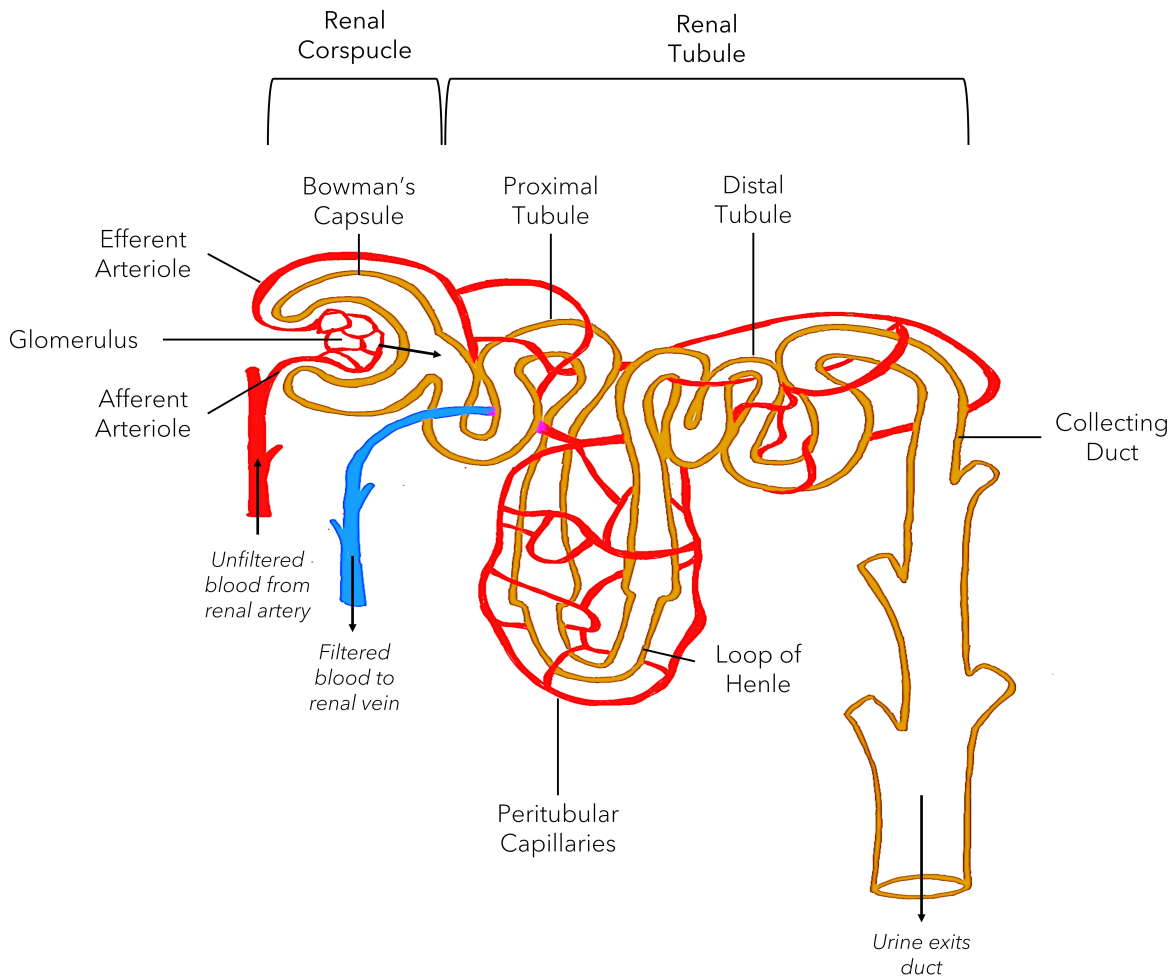
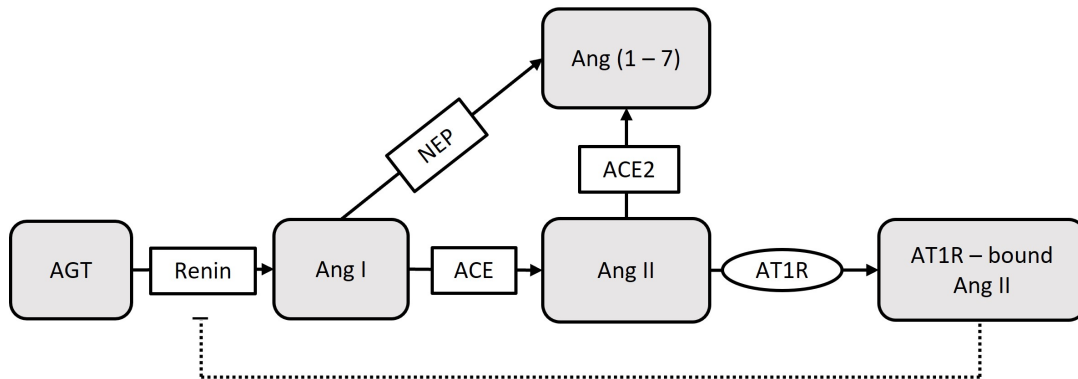
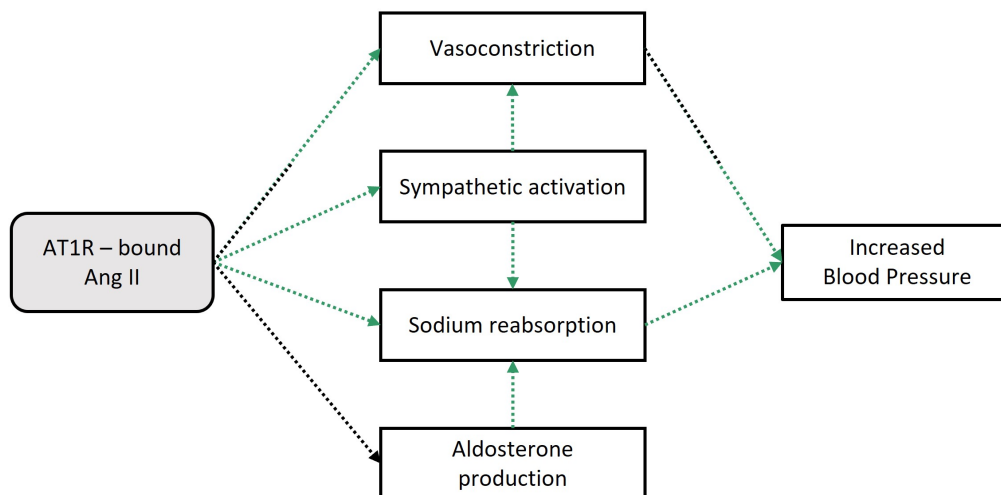


Figure 1.1: Diagram of a superficial nephron and the associated vasculature.

effects in the body. The most well-studied pathway is Ang I's conversion into Ang II by [chymase](#) and [angiotensin-converting enzyme \(ACE\)](#) activity. To prevent the system's under- or over-activation, Ang II moderates renin's secretion into the circulation via a feedback response [84]. This process, along with all hypertensive actions of Ang II (see below), are mediated by its binding to [AT1Rs](#). Ang II may also bind to [angiotensin type 2 receptors \(AT2Rs\)](#) to induce opposing effects on blood pressure, however this process is less well-studied. Therefore, in this thesis we focus primarily on the ACE/Ang II/AT1R axis. A schematic representation of this axis of the cascade is provided in Figure 1.2a.



(a) Hormones (grey), enzymes (white squares), and receptors (white ovals) of the classical RAS cascade. Dotted blunted arrow represents negative feedback.



(b) AT1R-mediated intrarenal (green) and systemic (black) effects of Ang II.

Figure 1.2: Schematic representation of the RAS cascade and its hypertensive effects.

In the past two decades, the traditional view of the RAS has been expanded with the discovery of functional local RASs in diverse tissues and organs, including the pancreas, liver, intestine, heart, kidney, vasculature, carotid body, and adipose, as well as the nervous, reproductive, and digestive systems [89]. Over the years, the clinical importance of these local systems has continued to gain traction, especially with regards to cardiovascular

disease [89]. Specifically in the context of hypertension, the importance of the intrarenal RAS has been particularly emphasized given the centrality of the kidney in blood pressure regulation and the many connections that exist between this organ and the RAS (see below).

All key components of the RAS are expressed within the kidney, including, but not limited to AGT, renin, Ang I, ACE, Ang I, Ang II, and AT1Rs [122, 109, 38, 37, 107, 70, 40, 180, 182, 21, 114, 71, 175, 93]. These components are also independently regulated, resulting in local Ang II production from multiple mechanisms that are independent of the systemic RAS [71]. In particular, AGT [107, 109, 70, 40, 72, 138] and renin [122, 109, 38, 37] are synthesized and secreted in the proximal tubule and collecting duct, respectively. The local production of both of these molecules is up-regulated by Ang II itself via an AT1R-dependent mechanism, creating a positive feedback loop with regards to endogenous Ang II production in the kidney. Another source of intrarenal positive feedback is the Ang II- and AT1R-dependent up-regulation of apical and basolateral proximal tubule epithelial cell AT1R expression [180, 182, 21]. Greater AT1R expression enhances AT1R-Ang II binding and intracellular uptake, which leads to more AT1R expression, and so on and so forth. Each of these positive feedback loops, up-regulated Ang II production and AT1R expression, have been hypothesized to play a role in how the intrarenal RAS becomes over-activated and de-coupled from the systemic RAS in hypertensive conditions [71, 180].

The renin-angiotensin system and blood pressure regulation The RAS primarily regulates blood pressure by modifying kidney function and therefore, fluid homeostasis. It does so by controlling the [glomerular filtration rate](#) and sodium reabsorption via a combination of direct and indirect, but interconnected factors (summarized in Figure 1.2b). Indeed, by binding to [AT1Rs](#), [Ang II](#) stimulates vasoconstriction, renal sympathetic activity, [aldosterone](#) production, and the activity of various sodium transporters along the nephron [36, 144]. Both renal vasoconstriction and increased renal sympathetic activity effect glomerular filtration rate by adjusting afferent and efferent arteriole diameter. Increased aldosterone production, a hormone secreted from the adrenal glands, stimulates sodium reabsorption in the distal tubule and collecting duct [9]. This, in combination with Ang II's direct effects on sodium transporters in the proximal tubule, leads to greater sodium and fluid reabsorption along the entire length of the nephron. Given the significant interactions between Ang II and kidney function, improving our understanding of intrarenal RAS activity in control and pathophysiological conditions is critical, should we wish to fully comprehend blood pressure regulation and its related pathologies.

To study the behaviour of the intrarenal RAS in hypertension in particular, many studies have relied on Ang II infusion experiments, a common protocol used to induce

hypertension in pre-clinical models. One aspect of this protocol that remains to be understood is: there is a progressive rise in intrarenal Ang II that cannot be explained on the basis of equilibration with the plasma [Ang II] [184, 31, 40, 93]. Several mechanisms have been proposed to explain the renal accumulation of Ang II in [Ang II-induced hypertension](#), including: enhanced AT1R-mediated uptake of circulating Ang II and increased intrarenal endogenous Ang II production [71, 109, 141, 142, 159, 180, 70, 72, 35, 40, 94, 141, 183]. Each pathway relies on a different source of intrarenal positive feedback (summarized above). However, their individual contribution to the over-activation of the intrarenal RAS in hypertension has yet to be delineated. Answering this question is the primary focus of Chapter 3. The functional importance of these effects in the context of blood pressure dis-regulation is studied in Chapter 5.

In general, the importance of the RAS in blood pressure regulation is evidenced by the effectiveness of RAS inhibitors as anti-hypertensive treatment strategies [60]. Indeed, between 2005 and 2016 over 60% of American adult hypertensive patients were prescribed an [angiotensin-converting enzyme inhibitor \(ACEi\)](#) or an [ARB](#) as part of their mono- or poly-therapeutic hypertension treatment regiment [26]. Both of these drugs function to inhibit the hypertensive actions of Ang II, but they do this via different mechanisms: ARBs selectively bind to and block AT1Rs to prevent Ang II binding and signalling, while ACEi reduce the pool of Ang II available to bind to AT1Rs by targeting [ACE](#) activity.

Despite their popularity, the manner in which these anti-hypertensive therapies target the intrarenal RAS remains incompletely understood. To yield better insights, many of the Ang II infusion studies outlined above have been accompanied by treatment with a RAS inhibitor, most commonly the [ARB Losartan](#) [184, 183]. During these experiments, Losartan restores normotension and consistently prevents intrarenal Ang II levels from rising. Whether the latter effect functionally contributes to the former response has yet to be elucidated. Nevertheless, the blockage of all intrarenal positive feedback loops, also known as the “key point breakdown effect” has been proposed to explain this behaviour [170]. In Chapter 4, we explore this hypothesis using a novel computational model of Losartan and RAS peptide dynamics. In doing so, we elucidate the ways in which ARBs target intrarenal RAS activity to prevent hypertension. This computational approach has frequently been used to investigate the effects of anti-hypertensive therapies on the systemic RAS and blood pressure. Below, we provide a summary of these models, among others that describe the RAS and blood pressure regulation.

1.2 History of computational models

As aforementioned, to investigate the role of the intrarenal RAS in blood pressure regulation and to study how ARBs target this local RAS to treat hypertension, we use computational models to describe each of these components – the RAS, ARBs, and blood pressure regulation. Many published models have been built to describe each of these systems both separately and in combination. Below, we describe some of the major contributions to the field to contextualize and motivate the models and studies presented in this thesis.

1.2.1 Renin-angiotensin system models

Systemic RAS models A number of computational models of the RAS have been published, though the vast majority focus on the systemic RAS. Most of these models have been designed to study the effects of RAS-modulating anti-hypertensive therapies and thus focus primarily on the ACE/Ang II/AT1R axis [149, 54, 123]. To explain why ACEis lower blood pressure, even though genetic variations in ACE expression have little impact on blood pressure, Takahashi et al. [149] developed a model of the ACE/Ang II/AT1R axis that also incorporates bradykinin’s effects on ACE and blood pressure. Model simulations suggest that small variations in ACE activity, such as those resulting from genetic variation, may be offset by bradykinin to regulate Ang II levels. This is no longer the case for large variations in ACE activity, such as those resulting from ACEis, causing Ang II levels and thus, blood pressure to decrease.

In 2018, a more comprehensive model that considers key RAS peptides, including AGT, Ang I, Ang II, Ang (1-7), Ang IV, AT1Rs, and AT2Rs, was developed by Leete et al. [84]. Four distinct parameter sets were identified to describe the behaviour of male/female normotensive/hypertensive rats. The models were used to explain sex differences in anti-hypertensive treatment efficacy [147]. The male model’s dynamic equations form the basis for the systemic RAS model outlined in Chapter 2.

Intrarenal RAS models Only two models of the intrarenal RAS have been developed previously [135, 95]. The first model [135] was designed to estimate the intrarenal distribution of Ang II and AT1/2Rs at steady state. Schalekamp and Danser [135] found that arterially-delivered (endocrine) Ang II mainly acts in the renal corpuscle, whereas intrarenally-produced (paracrine) Ang II mainly acts in the renal tubule. These regional distinctions were proposed to explain why the kidney responds to low levels of endocrine Ang II despite expressing high levels of paracrine Ang II. A key limitation of this model

however is that it does not consider temporal dynamics and therefore it cannot be used to study how the intrarenal RAS changes as blood pressure rises during the development of hypertension or as blood pressure falls following treatment with RAS-modulating anti-hypertensive therapies.

The second model [95] was developed as a case study to showcase the potential benefits of computational modelling in the drug development process. In particular, Lo et al. proposed several model extensions and *in silico* experiments that could be used to study the effects of anti-hypertensive therapies on the intrarenal RAS. While their baseline model does consider the rate of change of key RAS peptides (unlike that of Ref. [135]), it is limited in that it does not differentiate between intracellular and extracellular compartments of the kidney. This distinction must be made to effectively study intrarenal RAS over-activation in hypertension, given the hypothesized importance of AT1R-mediated uptake of circulating Ang II to this response. Indeed, this Ang II accumulation mechanism relies on the uptake of Ang II into distinct intracellular compartments where the peptide is protected from degradation. If these compartments are not represented in the model, then this mechanism cannot be simulated.

Importantly, neither Lo et al.'s [95] nor Schalekamp and Danser's [135] intrarenal RAS models include positive feedback on AGT, renin, or AT1R expression in the kidney. Since these pathways are the hypothesized mediators of intrarenal RAS dis-regulation in hypertension and the proposed targets of ARB treatment, they must be considered by any model aimed at studying the role of the intrarenal RAS in the development of hypertension.

Angiotensin receptor blocker models In published computational models, the effect of ARBs on the RAS is often represented implicitly via a parameter that reduces Ang II-AT1R binding by an arbitrary target amount [84, 95]. This approach is beneficial when aiming to study or compare the qualitative effects of ARB administration on one or more populations. For example, Leete et al. [84] used this approach to compare how male and female rats may respond to an ARB that reduces Ang II-AT1R binding by 50% and 90% of control. However, a similar approach is not possible when we know how much of a specific ARB has been administered and we want to predict its effect. This is because the relationship between drug dosage and Ang II-AT1R binding is rarely, if ever, explicitly experimentally quantified.

In these cases, a pharmacokinetic/pharmacodynamic (PK/PD) model can be of value. PKs describe the concentration-time series of a drug following its administration at a certain dosage and pharmacodynamics (PDs) describe the resulting effect on the system of interest [99]. Therefore, a PK/PD model of an ARB may describe the drugs plasma

concentration-time series and its resulting effect on blood pressure. Ten PK/PD models of this nature were developed by Csajka et al. [24] to inform drug dosage recommendations for different ARBs. However, the models were limited in that their PD component consisted of a hypothetical effect compartment whose drug concentration was assumed to directly decrease blood pressure; the physiological processes connecting the drug with its effect were not considered. More detailed PK models of commonly prescribed ARBs have also been created, such as that of [Losartan](#) by Karatza and Karalis [65], which was used to study gastric emptying in humans. To our knowledge, such a PK model has yet to be coupled to a detailed physiology-based model of the intrarenal RAS or of blood pressure regulation (see below). As discussed in Chapter 4, the resulting PK/PD model would provide an excellent opportunity to study the mechanisms underlying ARB pharmacodynamics [23]. A similar approach – coupling a PK model of a common RAS inhibitor to a pharmacodynamic model of the ACE/Ang II/AT1R axis – has been used to study the effects of other classes of RAS inhibitors, such as direct renin inhibitors [54] and [ACEis](#) [123] previously.

1.2.2 Blood pressure regulation models

In 1972, Guyton and Coleman [45] pioneered the field of computational physiology with their seminal circulation model. Their model comprises of components that describe cardiovascular function, circulatory dynamics, renal hemodynamics, kidney function, respiratory function, neurohormonal feedback, autonomic nervous system activity, and electrolyte balance. Model simulations highlight the paramount importance of kidney function and in particular, the regulation of sodium and water balance, in the control of blood volume, and thus blood pressure. Since its development, the Guyton model has been rigorously studied, validated, and extended to answer a variety of questions related to blood pressure regulation.

To design a human physiological model capable of targeting both the short- and the long-term regulation of blood pressure, Thomas et al. [152] incorporated Ikeda et al. [61]’s detailed representation of body fluid regulation and kidney function into the Guyton model. In 2010, Guillaud and Hannaert [42] added AGT, Ang I, Ang II, aldosterone, and their effects on vascular resistance to the resultant model, creating the first blood pressure regulation model that incorporated the RAS. This extension allowed the modelling of patients with hypertension and cardiovascular renal disease.

In 2005, Karaaslaan et al. [64] took the Guyton model in another direction when they added the effect of [RSNA](#) on sodium reabsorption and renin secretion. A detailed RAS sub-model was then added to this version of the Guyton model by Hallow et al. [49]

to simulate RAS-modulating anti-hypertensive therapies with more accuracy. In 2019, this RAS sub-model was replaced with one that is sex-specific [84, 85]. By additionally representing sex differences in baseline aldosterone levels and the reactivity of [RSNA](#), Leete and Layton [85] aimed to identify which factors contribute to sexually dimorphic responses to anti-hypertensive therapies.

The first sex-specific computational model of long-term blood pressure regulation *in the rat* came in 2020, following the re-parameterization of Leete and Layton [85]’s human model by Ahmed and Layton [1]. The resultant model, which accounted for differences in size, renal hemodynamics, and RAS hormone concentrations, was used to interpret the results of various animal experiments relating to pressure natriuresis, sodium sensitivity, and Ang II infusion.

While the aforementioned models provide valuable insights into the many different aspects of blood pressure regulation, none of these models incorporate the intrarenal RAS. As a result, all actions of the RAS, even those mediated within the kidney, are assumed to be regulated by systemic Ang II levels. This simplification becomes particularly problematic during an investigation of hypertension where the systemic and intrarenal RASs become de-coupled. Therefore, in this thesis (Chapter 5) the first long-term blood pressure regulation model in the rat that accounts for the intrarenal RAS is developed by building on the model of Ahmed and Layton [1].

1.3 Outline of thesis

We begin our analysis of the intrarenal RAS in hypertension by developing a compartmental ODE model of the RAS in Chapter 2. Following our analysis of the system at steady state, the baseline model is extended and built upon in subsequent Chapters to answer a variety of questions. Indeed, in Chapter 3 various sources of intrarenal positive feedback are added to the model to elucidate the mechanisms by which Ang II accumulates in the kidney during the development of Ang II-induced hypertension. A mathematical formalism to simulate Ang II infusion experiments is also introduced. Chapter 2 and Chapter 3 are largely based on our published work in the *Journal of Mathematical Biology* [143]. In Chapter 4, a PK model of the [ARB Losartan](#) and its bio-active metabolite [EXP3174](#) is developed and coupled to our RAS model to investigate the local effects of ARBs within the kidney. Coupling is achieved via Losartan- and EXP3174-AT1R-binding in the systemic and intrarenal compartments. Simulation results obtained using the resultant [PK/PD](#) model shed light on how ARBs influence the general activity of the intrarenal RAS, and therefore blood pressure regulation. In Chapter 5, we couple our RAS model

to one of whole-body blood pressure regulation in the rat [1] to create the first long-term blood pressure regulation model that considers the intrarenal RAS. Results highlight the functional importance of the intrarenal RAS in the development of hypertension induced by Ang II infusion, and consequently, clinical hypertension associated with an over-active RAS. Finally, in Chapter 6 we summarize the results presented in this thesis and discuss directions for future work.

Chapter 2

Computational modelling of the rat intrarenal and systemic renin angiotensin system: Steady state results and analysis

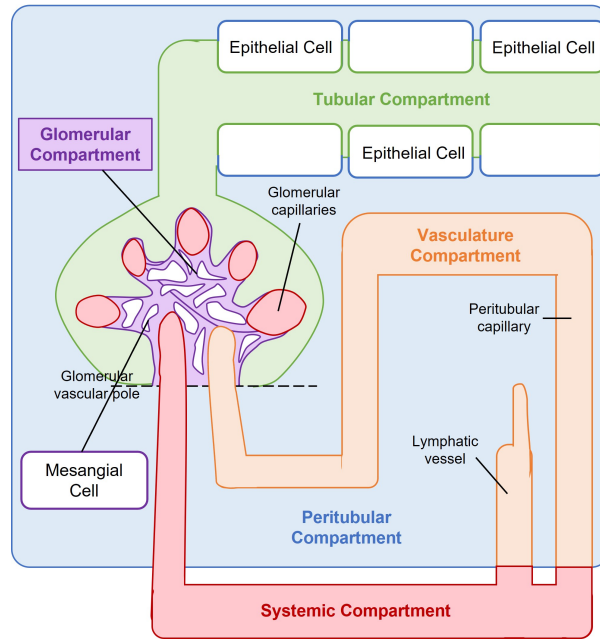
In this Chapter, a novel computational model of the intrarenal and systemic RAS is introduced. This model forms the basis for all subsequent studies presented in this thesis, focused on the role of the intrarenal RAS in hypertension. How the model is extended to simulate [Ang II infusion](#) experiments and the administration of the [ARB Losartan](#) is outlined in Chapters [3](#) and [4](#), respectively. The model's coupling to a whole-body blood pressure regulation model is discussed in Chapter [5](#).

2.1 Intrarenal RAS model

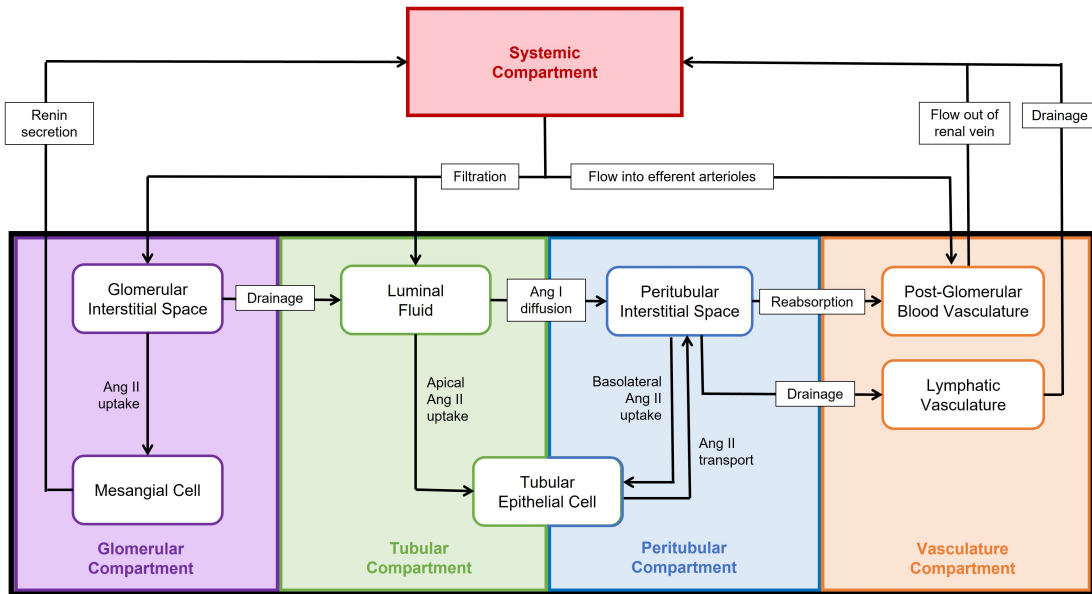
The intrarenal model considers [Ang I](#) and [Ang II](#) dynamics across four tissue compartments: the [glomerular compartment](#), the [peritubular compartment](#), the [tubular compartment](#), and the [vasculature compartment](#). The vasculature compartment comprises both the lymphatic vasculature and the post-glomerular blood vasculature. The pre-glomerular blood vasculature is considered part of the systemic circulation compartment (Section 2.2). The other compartments are subdivided into extracellular and intracellular regions, connected to one another via [AT1R](#)- and [megalin](#)-dependent [39, 120] [Ang II](#) internalization. Since [Ang I](#) does not bind to [AT1Rs](#) and its binding to [megalin](#) is unknown, [Ang I](#) is assumed to be restricted to the extracellular regions. This assumption is consistent with data from [62], which indicates that intracellular [Ang I](#) comprises a negligible portion of total renal [Ang I](#) (4%).

The [luminal fluid](#) constitutes the extracellular region of the [tubular compartment](#) and the extracellular matrix and interstitial fluid of the renal interstitial space [178], hereafter referred to as the [interstitial space](#), comprises the extracellular region of both the [glomerular compartment](#) and the [peritubular compartment](#). The glomerular and peritubular interstitial space is separated at the level of the glomerular vascular pole, such that the glomerular interstitial space represents the [mesangial matrix](#) and extraglomerular fluid, while the peritubular interstitial space represents the intertubular and extravascular space of the kidney. The intracellular region of the glomerular compartment comprises [mesangial cells](#), whereas that of the tubular and peritubular compartments comprises [tubular epithelial cells](#). The intracellular tubular and peritubular regions differ in that the former is specific to apically-derived molecular structures, while the latter is specific to basolaterally-derived molecular structures. The model compartments are consistent with those of Schalekamp and Danser [135]’s steady state model. A visual representation of each compartment as they appear in the kidney is presented in Figure 2.1a, with the physiological processes connecting the compartments outlined in Fig 2.1b.

The mathematical formalisms used to model the aforementioned processes are described in detail below. The structure of the equations describing [Ang I](#), [Ang II](#), [AT1R](#)-bound [Ang II](#), and [AT1R](#) dynamics are similar, albeit not exactly the same, across all renal compartments. Therefore, we introduce general equations describing each variable in the intracellular ($L = Cell$), membrane-bound ($L = Memb$), and extracellular ($L = Ext$) regions of each compartment C ($C = Gl, Tb, Pt, Pv$) in Section 2.1.1, before detailing the specifics of each compartment in Sections 2.1.2 – 2.1.5.



(a) Visualization of each model compartment.



(b) Physiological processes that connect each model compartment.

Figure 2.1: Schematic representation of the RAS model compartments.

2.1.1 General model equations

The **Ang I** and **Ang II** dynamics in renal sub-compartment C_L ($L = Ext, Cell$) can be described by the following equations:

$$\begin{aligned}
\frac{d[AngI]_C^{Ext}}{dt}(t) &= \frac{1}{V_C^{Ext}} \left(\sum_j Q_{inj}^{C_{Ext}} [AngI]_{C_{inj}}^{Ext}(t) - Q_{out}^{C_{Ext}} [AngI]_C^{Ext}(t) \right) \\
&\quad - c_{ACE}^C [AngI]_C^L(t) \\
&\quad - k_{lys}^{C_L} [AngI]_C^L(t) \\
&\quad + k_{AngI}^C(t)
\end{aligned} \tag{2.1}$$

$$\begin{aligned}
\frac{d[AngII]_C^L}{dt}(t) &= \frac{1}{V_C^L} \left(\sum_j Q_{inj}^{C_L} [AngII]_{C_{inj}}^{L_{inj}}(t) - Q_{out}^{C_L} [AngII]_C^L(t) \right) \\
&\quad + c_{ACE}^C [AngI]_C^L(t) \\
&\quad - k_{lys}^{C_L} [AngII]_C^L(t) \\
&\quad + k_{diss} [AT1R - bound AngII]_C^L(t) \\
&\quad - k_{ass} [AngII]_C^L(t) [AT1R]_C^L(t)
\end{aligned} \tag{2.2}$$

The first line of each equation represents the balance between the j fluxes into sub-compartment C_L from sub-compartment C_{inj} with rate $Q_{inj}^{C_L}$ and the flux out of sub-compartment C_L with rate $Q_{out}^{C_L}$. The number of incoming fluxes j differs for each compartment, as summarized in Table 2.1. V_C^L is a parameter describing the volume of each sub-compartment (Table 2.2). The second line represents the conversion of **Ang I** to **Ang II** by local **ACE** activity with rate c_{ACE}^C . The third line represents peptide degradation with rate $k_{lys}^{C_L}$. Intracellular Ang II is assumed to be degraded by lysosomes and peptide X ($X = \text{Ang I, Ang II}$) in the renal post-glomerular blood vasculature is assumed to decay according to its half life h_X :

$$k_{lys}^{CL} = \begin{cases} 0 & \text{if } C \neq Pv, L = Ext \\ k_{lys} & \text{if } C \neq Pv, L = Cell \\ \ln 2/h_X & \text{if } C = Pv \end{cases}$$

The rest of the expressions used to describe the dynamics of [Ang I](#) and [Ang II](#) differ. Indeed, the fourth and fifth lines of Eq. 2.2 represent the unbinding and binding of Ang II to [AT1R](#)s with rates k_{diss} and k_{ass} , respectively. Finally, as described by the last line of Eq. 2.1, Ang I is endogenously produced from local [AGT](#) and renin activity. k_{AngI}^C (Eq. 3.4) is assumed to be constant, given that renal renin activity has been shown to be conserved during Ang II infusion experiments [141].

The equation describing membrane-bound ($L = Memb$) and intracellular ($L = Cell$) [AT1R](#)-bound [Ang II](#) dynamics in each compartment C is given by:

$$\begin{aligned} \frac{d[AT1R - \text{bound } AngII]_C^L}{dt}(t) &= k_{ass}[AngII]_C^L(t)[AT1R]_C^L(t) \\ &\quad - k_{diss}[AT1R - \text{bound } AngII]_C^L(t) \\ &\quad + k_{int}^{CL}[AT1R - \text{bound } AngII]_C^{Memb}(t) \end{aligned} \quad (2.3)$$

The first line represents the binding of [Ang II](#) to [AT1R](#)s with rate k_{ass} , the second line represents the unbinding of Ang II from [AT1R](#)s with rate k_{diss} , and the third line represents membrane-bound [AT1R](#)-bound Ang II internalization. We allow for intracellular Ang II and [AT1R](#) re-binding given the recent evidence that internalized Ang II can interact with cytoplasmic [AT1R](#)s to induce intracellular signalling cascades [31]. A simplified model of [AT1R](#) binding that does not consider membrane-bound [AT1R](#)-bound Ang II internalization was implemented in the renal post-glomerular blood [vasculature compartment](#) (and systemic model, see Section 2.2), due to the substantial uncertainties in key variables such as the volume of such an intracellular compartment and the concentration of intracellular endothelial Ang II. Hence:

$$k_{int}^{CL} = \begin{cases} -k_{int} & \text{if } C \neq Pv \text{ and } L = Memb \\ k_{int} \frac{V_C^{Ext}}{V_C^{Cell}} & \text{if } C \neq Pv \text{ and } L = Cell \\ 0 & \text{if } C = Pv \end{cases}$$

The equation describing intracellular [AT1R](#) dynamics in the glomerular, tubular, and peritubular compartments ($C = Gl, Tb, Pt$) is given by:

$$\begin{aligned}
\frac{d[AT1R]_C^{Cell}}{dt}(t) &= k_{diss}[AT1R - \text{bound } AngII]_C^{Cell}(t) \\
&\quad - k_{ass}[AngII]_C^{Cell}(t)[AT1R]_C^{Cell}(t) \\
&\quad - k_{rec}[AT1R]_C^{Cell}(t)
\end{aligned} \tag{2.4}$$

The first line represents the unbinding of [Ang II](#) from [AT1Rs](#) with rate k_{diss} , the second line represents the binding of [Ang II](#) to [AT1Rs](#) with rate k_{ass} , and the third line represents the recycling of internalized [AT1Rs](#) back to the cell membrane. It is assumed that the [AT1Rs](#) are recycled back to the same membrane (basolateral or apical) and thus compartment (peritubular or tubular) from which they originate in [tubular epithelial cells](#).

Finally, the equation describing the concentration of membrane-bound [AT1Rs](#), $[AT1R]_C^{Mem}(t)$ in the tubular and peritubular compartments ($C = Tb, Pt$) is given by:

$$\begin{aligned}
\frac{d[AT1R]_C^{Mem}}{dt}(t) &= k_{diss}[AT1R - \text{bound } AngII]_C^{Mem}(t) \\
&\quad - k_{ass}[AT1R]_C^{Mem}(t)[AngII]_C^{Ext}(t) \\
&\quad + k_{rec} \frac{V_C^{Ext}}{V_{Tb,Pt}^{Cell}} [AT1R]_C^{Cell}(t)
\end{aligned} \tag{2.5}$$

Consistent with intracellular [AT1R](#) dynamics in these two compartments (Eq. 2.4), the first line represents the unbinding of [Ang II](#) from [AT1Rs](#) with rate k_{diss} , the second line represents the binding of [Ang II](#) to [AT1Rs](#) with rate k_{ass} , and the third line represents the recycling of internalized [AT1Rs](#) back to the cell membrane from which they originate. This equation differs in the glomerular and vasculature compartments, hence a compartment-specific derivation of these equations as well as a description of those outlined above is given in Sections 2.1.2–2.1.5 below.

2.1.2 Glomerular compartment

A small fraction of the [renal plasma flow](#) ϕ_{RPF} enters the glomerular [interstitial space](#) (denoted ϕ_{Gl}) [87], contributing to an influx of circulating [Ang I](#) and [Ang II](#) to this sub-compartment. This influx is balanced by drainage into the [luminal fluid](#) with flow rate ϕ_{Gl} . Given the lack of data surrounding [ACE](#) activity and the concentration of [Ang I](#) and

Ang II in the [glomerulus](#), we set $k_{AngI}^{Gl} = c_{ACE}^{Gl} = 0$. Furthermore, to derive the equation for membrane-bound AT1R dynamics, we assume that the total amount of AT1Rs in the glomerular compartment is conserved, such that:

$$\begin{aligned}
V_{Gl}^{Exp}[AT1R]_{Gl}^{Memb}(t) &= AT1R_{Gl}^{tot} - \left(V_{Gl}^{Exp}[AT1R - bound AngII]_{Gl}^{Memb}(t) \right. \\
&\quad + V_{Gl}^{Cell}[AT1R - bound AngII]_{Gl}^{Cell}(t) \quad (2.6) \\
&\quad \left. + V_{Gl}^{Cell}[AT1R]_{Gl}^{Cell}(t) \right)
\end{aligned}$$

2.1.3 Tubular compartment

[Ang I](#) and [Ang II](#) are filtered from the systemic circulation with rate ϕ_{GFR} , reabsorbed transcellularly across the [tubular epithelium](#), and cleared in the urine with rate ϕ_U . Since the mechanism underlying Ang I reabsorption across the tubular epithelium is largely unknown, we model this as a simple diffusion between extracellular compartments with rate k_{diff} , as done in Ref. [135]. In contrast, Ang II [transcytosis](#) has been shown to depend on both [megalin](#)- and [AT1R](#)-binding in cultured opossum kidney cells, a model of proximal epithelia [120]. Therefore, both megalin- and AT1R-Ang II binding are modelled along the apical membrane. However, given that far less is known about megalin as a receptor for Ang II, megalin is assumed to bind and internalize Ang II at a constant rate k_{meg} for simplicity. In terms of AT1R-bound Ang II [endocytosis](#), as in the glomerular compartment, we assume that the total amount of tubular AT1Rs is conserved in healthy steady state conditions. Nevertheless, a dynamic equation for $[AT1R]_{Tb}^{Memb}$ is given in Eq. 2.5 to facilitate extending the model in Section 3.2.1 to consider positive feedback on apical AT1Rs in conditions where local Ang II concentrations are elevated.

2.1.4 Peritubular compartment

[Ang I](#) and [Ang II](#) are reabsorbed transcellularly from the luminal fluid into the peritubular [interstitial space](#) as described in Section 2.1.3. In particular, Ang I diffuses along its concentration gradient with rate k_{diff} and apically-derived intracellular Ang II is transported into the peritubular interstitial space with rate k_{trans} . Peritubular interstitial peptides are then drained via the lymphatic vasculature and reabsorbed into the renal post-glomerular blood vasculature at rates proportional to fluid flow ϕ_L and ϕ_{Pv} , respectively. Conservation of flow is assumed, such that $\phi_{Pv} = \phi_{Gl} + \phi_{GFR} - \phi_L - \phi_U$. Moreover, peritubular

AT1Rs behave identically to tubular AT1Rs in that their total concentration is conserved in healthy steady state conditions (Eq. 2.5). Once again however, a dynamic equation for $[AT1R]_{Pt}^{Memb}$ is given in Eq. 2.5 to facilitate the addition of positive feedback on basolateral AT1Rs in conditions where local Ang II concentrations are elevated (Section 3.2.1).

2.1.5 Post-glomerular blood vasculature compartment

The amount of renal plasma flow that does not enter the nephron or glomerular interstitial space, i.e. $\phi_{RPF} - \phi_{Gl} - \phi_{GFR}$, enters the efferent arterioles, bringing a proportional amount of circulating Ang I and Ang II with it. Also impacting the rate of change of the Ang I and II concentrations at this level is re-absorption from the peritubular interstitial space at a rate proportional to fluid flow ϕ_{Pv} and loss via the renal vein. Once again, flow is assumed to be conserved with concentrations of Ang I and II proportional to

$$\begin{aligned}\phi_{RPF} - \phi_{Gl} - \phi_{GFR} + \phi_{Pv} &= \phi_{RPF} - \phi_{Gl} - \phi_{GFR} + \phi_{Gl} + \phi_{GFR} - \phi_L - \phi_U \\ &= \phi_{RPF} - \phi_L - \phi_U\end{aligned}$$

being returned to the systemic circulation.

As aforementioned, a simplified model of AT1R binding that does not consider membrane-bound AT1R-bound Ang II internalization was implemented in the post-glomerular blood vasculature. Instead, the total concentration of AT1Rs in this compartment $[AT1R]_{Pv}^{tot}$ is assumed to remain constant:

$$[AT1R]_{Pv}^{Memb}(t) = [AT1R]_{Pv}^{tot} - [AT1R - \text{bound } AngII]_{Pv}^{Memb}(t) \quad (2.7)$$

2.1.6 Whole kidney concentrations

The amount of Ang I and Ang II in each renal compartment described above are summed to equal total renal concentrations in units of $fmol/g$ kidney.

$$\begin{aligned}[AngI]_T(t) &= V_{Gl}^{Ext}[AngI]_{Gl}^{Ext}(t) + V_{Pt}^{Ext}[AngI]_{Pt}^{Ext}(t) \\ &\quad + V_{Tb}^{Ext}[AngI]_{Tb}^{Ext}(t) + V_{Pv}[AngI]_{Pv}(t)\end{aligned} \quad (2.8)$$

$$\begin{aligned}
[AngII]_T(t) = & V_{Pt,Tb}^{Cell} ([AngII]_{Pt}^{Cell}(t) + [AT1R - \text{bound } AngII]_{Pt}^{Cell}(t)) \\
& + V_{Pt,Tb}^{Cell} ([AngII]_{Tb}^{Cell}(t) + [AT1R - \text{bound } AngII]_{Tb}^{Cell}(t)) \\
& + V_{Gl}^{Cell} ([AngII]_{Gl}^{Cell}(t) + [AT1R - \text{bound } AngII]_{Gl}^{Cell}(t)) \\
& + V_{Pt}^{Ext} ([AngII]_{Pt}^{Ext}(t) + [AT1R - \text{bound } AngII]_{Pt}^{Memb}(t)) \\
& + V_{Tb}^{Ext} ([AngII]_{Tb}^{Ext}(t) + [AT1R - \text{bound } AngII]_{Tb}^{Memb}(t)) \\
& + V_{Gl}^{Ext} ([AngII]_{Gl}^{Ext}(t) + [AT1R - \text{bound } AngII]_{Gl}^{Memb}(t)) \\
& + V_{Pv} ([AngII]_{Pv}(t) + [AT1R - \text{bound } AngII]_{Pv}^{Memb}(t))
\end{aligned} \tag{2.9}$$

A summary of the parameters outlined in Eqs. 2.1 – 2.5 specific to each sub-compartment is given in Table 2.1. The complete set of intrarenal model equations is provided in Appendix A.

2.2 Systemic RAS model

The systemic RAS model is based on those in Refs. [84] and [1]. Modifications were made to couple the systemic model to the intrarenal model, as well as to the AT1R–Ang II binding and plasma renin activity formalisms.

The rate of change of the plasma AGT concentration ($[AGT]_{circ}$) is governed by its endogenous production at a constant rate k_{AGT} , conversion to Ang I by renin, and degradation with a half-life h_{AGT} .

$$\frac{d[AGT]_{circ}}{dt}(t) = k_{AGT} - PRA(t) - \frac{\ln 2}{h_{AGT}}[AGT]_{circ}(t) \tag{2.10}$$

As in Ref. [84], PRA is assumed to follow Michaelis-menten kinetics, with the Michaelis constant K_M reflecting the concentration of AGT where PRA is half-maximal. However, similarly to the formulation by Ahmed and Layton [1], the maximal activity is assumed to depend linearly on the plasma renin concentration (PRC), with rate constant v_{max} . In this way, sufficient concentrations of both renin and AGT are required to generate sufficient PRA:

$$PRA(t) = v_{max} PRC(t) \frac{[AGT]_{circ}(t)}{K_M + [AGT]_{circ}(t)} \tag{2.11}$$

L	C	Parameters							
		Ang	Q_{inj}^{CL}	$[AngX]_{C_{inj}}^{L_{inj}}(t)$	Q_{out}^{CL}	c_{ACE}^C	k_{lys}^{CL}	$k_{AngI}^C(t)$	k_{int}^{CL}
	<i>Gl</i>	<i>I, II</i>	ϕ_L	$[AngX]_{circ}(t)$	ϕ_L	0	0	0	–
<i>Ext</i>	<i>Tb</i>	<i>I</i>	ϕ_{GFR}	$[AngI]_{circ}(t)$	$k_{diff} + \phi_U$			k_{AngI}^{Tb}	
			ϕ_{GI}	$[AngI]_{GI}^{Ext}(t)$		c_{ACE}^{Tb}	0		–
	<i>II</i>		ϕ_{GFR}	$[AngII]_{circ}(t)$	$k_{meg} + \phi_U$			–	
			ϕ_{GI}	$[AngII]_{GI}^{Ext}(t)$					
<i>Pt</i>	<i>I</i>		k_{diff}	$[AngI]_{Tb}^{Ext}(t)$	$\phi_{Pv} + \phi_L$	c_{ACE}^{Pt}	0	k_{AngI}^{Pt}	–
	<i>II</i>		$k_{trans}^{V_{Tb, Pt}^{Cell}/V_{Pt}^{Ext}}$	$[AngII]_{Tb}^{Cell}(t)$				–	–
<i>Pv</i>	<i>I, II</i>		$\phi_{RPF} - \phi_{GFR} - \phi_{GI}$	$[AngX]_{circ}(t)$	$\phi_{RPF} - \phi_L - \phi_U$	0	$\frac{\ln 2}{h_X}$	0	–
			ϕ_{Pv}	$[AngX]_{Pt}^{Ext}(t)$					
<i>Cell</i>	<i>Gl</i>	<i>II</i>	0	–	0	0	k_{lys}	–	$k_{int}^{V_{Gl}^{Ext}/V_{Gl}^{Cell}}$
	<i>Tb</i>	<i>II</i>	$k_{meg}^{V_{Tb}^{Ext}/V_{Tb, Pt}^{Cell}}$	$[AngII]_{Tb}^{Ext}(t)$	k_{trans}	0	k_{lys}	–	$k_{int}^{V_{Tb}^{Ext}/V_{Tb, Pt}^{Cell}}$
	<i>Pt</i>	<i>II</i>	0	–	0	0	k_{lys}	–	$k_{int}^{V_{Pt}^{Ext}/V_{Tb, Pt}^{Cell}}$
<i>Memb</i>	<i>Gl</i>	<i>II</i>	–	–	–	–	–	–	$-k_{int}$
	<i>Tb</i>	<i>II</i>	–	–	–	–	–	–	$-k_{int}$
	<i>Pt</i>	<i>II</i>	–	–	–	–	–	–	$-k_{int}$
	<i>Pv</i>	<i>II</i>	–	–	–	–	–	–	0

Table 2.1: Sub-compartment-specific parameters corresponding to Eqs. 2.1–2.5.

Renin is secreted from the [juxtaglomerular apparatus](#) of the kidney at a basal rate R_{sec} . This secretion rate is modified by the concentration of glomerular membrane-bound [AT1R](#)–bound [Ang II](#), $[AT1R - \text{bound } AngII]_{Gl}^{Memb}$, via the feedback function ν_{AT1R} (Eq. 2.13). Since the exponent B_{AT1R} is positive, ν_{AT1R} drops below 1 to inhibit renin secretion when $[AT1R - \text{bound } AngII]_{Gl}^{Memb}$ rises above its healthy steady state $[AT1R - \text{bound } AngII]_{Gl}^{Memb, eq}$, i.e. when their ratio R_{Gl} rises above 1. The opposite effect is observed if $[AT1R - \text{bound } AngII]_{Gl}^{Memb}$ drops below its steady state, i.e. when R_{Gl} drops below 1. Also contributing to the rate of change of [PRC](#) is the peptide’s decay according to its half-life h_{renin} , resulting in the equation:

$$\frac{dPRC}{dt}(t) = R_{sec} \cdot \nu_{AT1R}(R_{Gl}^{Memb}(t)) - \frac{\ln 2}{h_{renin}} PRC(t) \quad (2.12)$$

where

$$\nu_{AT1R}(R_{Gl}^{Memb}(t)) = R_{Gl}^{Memb}(t)^{-B_{AT1R}}, \quad (2.13)$$

Plasma **Ang I**, $AngI_{circ}$ decays with a half-life h_{AngI} and is converted into other forms by **ACE**, **neprilysin (NEP)**, and **chymase** activity with rates $c_{ACE_{circ}}$, c_{NEP} , and c_{chym} , respectively. In addition, plasma Ang I enters the kidney via the renal artery. In doing so, an amount of Ang I proportional to ϕ_{RPF} gets distributed to the various renal compartments as described above. Following local renal modifications, Ang I from the renal post-glomerular blood vasculature and the peritubular **interstitial space** gets returned to the systemic circulation via the renal vein and lymphatic vasculature, respectively, with corresponding flow rates $\phi_{RPF} - \phi_L - \phi_U$ and ϕ_L . In this way, fluid flow into and out of the kidney is conserved, differing only by a factor of ϕ_U which is assumed to be balanced by the bodies water sources and other sinks, such as; water intake, metabolic reactions, and insensitive loss:

$$\begin{aligned}
\frac{d[AngI]_{circ}(t)}{dt} &= PRA(t) - (c_{chym} + c_{ACE}^{circ}) [AngI]_{circ}(t) \\
&\quad - \left(c_{NEP} + \frac{\ln 2}{h_{AngI}} \right) [AngI]_{circ}(t) \\
&\quad + \frac{W_K}{V_{circ}} \phi_L [AngI]_{Pt}^{Ext}(t) \\
&\quad + \frac{W_K}{V_{circ}} (\phi_{RPF} - \phi_L - \phi_U) [AngI]_{Pv}(t) \\
&\quad - \frac{W_K}{V_{circ}} \phi_{RPF} [AngI]_{circ}(t)
\end{aligned} \tag{2.14}$$

The rate of change of the plasma Ang (1-7) concentration, $[Ang(1-7)]_{circ}$, is governed by its production from **Ang I** by **NEP** and **Ang II** by **angiotensin-converting enzyme 2 (ACE2)** with respective rate constants c_{NEP} and c_{ACE2} , and its decay according to its half-life h_{Ang17} :

$$\begin{aligned}
\frac{d[Ang(1-7)]_{circ}(t)}{dt} &= c_{NEP} [AngI]_{circ}(t) + c_{ACE2} [AngII]_{circ}(t) \\
&\quad - \frac{\ln 2}{h_{Ang17}} [Ang(1-7)]_{circ}(t)
\end{aligned} \tag{2.15}$$

Systemic **Ang II**, $AngII_{circ}$, is produced from **Ang I** by **chymase** and **ACE** activity, converted to **angiotensin (1-7) (Ang (1-7))** by **ACE2** activity, and decays with half-life h_{AngII} . Identically to Ang I, systemic Ang II enters the kidney via the renal artery, undergoes local modifications, and is returned to the circulation via the renal vein and lymphatic

vasculature. Unlike Ang I however, Ang II may bind to [AT1Rs](#) in the systemic vasculature endothelium, $AT1R_{circ}^{Memb}$ with rate k_{ass} to form membrane-bound AT1R-Ang II complexes, $AT1R$ – bound $AngII_{circ}^{Memb}$. This binding is reversible, with dissociation rate k_{diss} . As in the renal post-glomerular blood vasculature, the total concentration of systemic AT1Rs ($[AT1R]_{circ}^{tot}$) is assumed constant:

$$\begin{aligned}
\frac{d[AngII]_{circ}(t)}{dt} &= (c_{chym} + c_{ACE}^{circ}) [AngI]_{circ}(t) \\
&\quad - \left(c_{ACE2} + \frac{\ln 2}{h_{AngII}} \right) [AngII]_{circ}(t) \\
&\quad + \frac{W_K}{V_{circ}} \phi_L [AngII]_{Pt}^{Ext}(t) \\
&\quad + \frac{W_K}{V_{circ}} (\phi_{RPF} - \phi_L - \phi_U) [AngII]_{Pv}(t) \\
&\quad - \frac{W_K}{V_{circ}} \phi_{RPF} [AngII]_{circ}(t) \\
&\quad + k_{diss} [AT1R - bound AngII]_{circ}^{Memb}(t) \\
&\quad - k_{ass} [AT1R]_{circ}^{Memb}(t) [AngII]_{circ}(t)
\end{aligned} \tag{2.16}$$

$$\begin{aligned}
\frac{d[AT1R - bound AngII]_{circ}^{Memb}}{dt}(t) &= k_{ass} [AT1R]_{circ}^{Memb}(t) [AngII]_{circ}(t) \\
&\quad - k_{diss} [AT1R - bound AngII]_{circ}^{Memb}(t)
\end{aligned} \tag{2.17}$$

$$[AT1R]_{circ}^{Memb}(t) = [AT1R]_{circ}^{tot} - [AT1R - bound AngII]_{circ}^{Memb}(t) \tag{2.18}$$

A schematic diagram of the connections between model variables is shown in [Figure 2.2](#).

2.3 Parameter identification

The majority of the model's parameters were derived from the literature ([Table 2.2](#); [Section 2.3.1](#)). The remaining minority ([Table 2.3](#); [Section 3.2.4](#)) were fit to available steady state ([Table 2.4](#)) and kinetic data.

Parameter	Description	Value	Unit	Reference
General				
W_b	Body weight	284	g	[105]
$W_{K/b}$	Kidney-to-body weight ratio	5.23	mg/g	[184]
W_K	Kidney weight	1.49	g	[105, 184]
V_B	Circulating blood volume	17.8	mL	[83]
V_{circ}	Circulating plasma volume	10.3	mL	[83, 105]
Hct	Hematocrit	0.42	-	[105]
Renal Volumes				
V_{Gl}^{Ext}	Volume density of the glomerular interstitial space	0.0019		[6, 159]
V_{Gl}^{Cell}	Volume density of mesangial cells	0.0019		[6, 159]
V_{Pt}^{Ext}	Volume density of the peritubular interstitial space	0.0236		[6, 51]
$V_{Tb,Pt}^{Cell}$	Volume density of tubular epithelial cells	0.294	mL/g kidney	[6, 51]
V_{Tb}^{Ext}	Volume density of the luminal fluid	0.102		[6, 51]
V_{Pv}	Volume density of the renal vasculature plasma	0.085		[6, 51]
Renal Hemodynamics				
ϕ_{RPF}	Renal plasma flow	7.79		[105, 184]
ϕ_{GFR}	Glomerular filtration rate	2.02		[105, 184]
ϕ_U	Urine flow rate	0.041		[131, 105, 184]
ϕ_{Pv}	Flow from peritubular interstitial space to renal post-glomerular blood vasculature	1.98	mL/min per g kidney	[105, 146, 184, 131]
ϕ_L	Renal lymph flow rate	0.041		[105, 146, 184, 131]
ϕ_{Gl}	Flow from glomerular interstitial space to luminal fluid	0.041		[105, 146, 184, 131]
Ang II-AT1R-binding kinetics				
K_D	Dissociation constant for Ang II-AT1R binding	1000	fmol/mL	[135]
k_{ass}	Ang II-AT1R association rate	$2.4e - 5$	/(fmol/mL) per min	[135]
k_{diss}	Ang II-AT1R dissociation rate	0.024	/min	[135]
Systemic Compartment				
h_{AGT}	AGT half-life	240		[53]
h_{renin}	Renin half-life	3		[3]
h_{AngI}	Ang I half-life	0.5	min	[1]
h_{AngII}	Ang II half-life	0.267		[3]
h_{Ang17}	Ang (1-7) half-life	0.167		[171]
R_{sec}	Basal renin secretion rate	1	-	[1]
K_M	AGT affinity for renin	2.8×10^6	fmol/mL	[43]

Table 2.2: Parameters derived from the literature

2.3.1 Parameter derivations

General parameters Many whole-body parameters are based on the 284 g male Sprague Dawley rat described by Munger and Baylis [105]. Indeed, given a kidney-to-body weight ratio of 5.23 mg per g [184], we assume a kidney weight W_K of 1.49 g. Based on the body weight-to-blood volume relationship from Lee et al. [83], we assume a circulating blood volume of 17.8 mL. This corresponds to a circulating plasma volume V_{circ} of 10.3 mL, given a hematocrit of 0.42 [105].

Renal volume parameters The cortical volume shares of the [luminal fluid](#) (0.16), [tubular epithelial cells](#) (0.46), and the interstitial tissue including peritubular capillaries (0.30) were extracted from Hegedus et al. [51]. Moreover, we know the cortical volume share of the extracellular peritubular [interstitial space](#) (0.037) and the entire peritubular interstitial space including interstitial cells (0.07) from Lemley et al. [86], allowing us to compute that of the peritubular capillaries (renal post-glomerular blood [vasculature compartment](#)) alone ($0.30 - 0.07 = 0.23$). Since the kidney is 70% cortex by volume [6], and the ratio of kidney volume-to-kidney weight is 0.912 mL per g (extracted from Fig 3F of Baldelomar et al. [6]), we obtain:

$$\begin{aligned} V_{Tb}^{Ext} &= 0.16 * 0.70 * 0.912 = 0.102 \text{ mL per g kidney} \\ V_{Tb,Pt}^{Cell} &= 0.46 * 0.70 * 0.912 = 0.294 \text{ mL per g kidney} \\ V_{Pt}^{Ext} &= 0.037 * 0.70 * 0.912 = 0.0236 \text{ mL per g kidney} \\ V_{Pv} &= 0.23 * 0.70 * 0.912 * (1 - \text{Hct}) = 0.085 \text{ mL per g kidney} \end{aligned}$$

The volume of the [glomerular compartment](#) is computed based on the known volume fractions in mice [66]. Indeed, with a [mesangial matrix](#) and [mesangial cells](#)-to-glomerulus fractional volume of 0.09, a glomerulus-to-whole kidney fraction volume of 0.023, and a kidney volume-to-kidney weight ratio of 0.912 [6], we obtain:

$$V_{Gl}^{Cell} = V_{Gl}^{Ext} = 0.09 * 0.023 * 0.912 = 0.0019 \text{ mL/g kidney}$$

Renal hemodynamic parameters [Renal plasma flow](#) ϕ_{RPF} and [glomerular filtration rate](#) ϕ_{GFR} are taken directly from Munger and Baylis [105] and scaled by W_K to obtain the appropriate units of mL per g kidney. Moreover, we assume that renal lymphatic flow accounts for 2% of total fluid reabsorption from the kidney ($\phi_L = 0.02 * \phi_{GFR} + \phi_{Gl} - \phi_U$) [146] and that it is the same as drainage from the glomerular [interstitial space](#) as well as urine flow ($\phi_{Gl} = \phi_U = \phi_L$) [131]. In this way, all remaining hemodynamic parameters can be computed from the known ϕ_{GFR} [105], since $\phi_{Gl} = \phi_L = \phi_U = 0.02\phi_{GFR}$ and $\phi_{Pv} = \phi_{Gl} + \phi_{GFR} - \phi_L - \phi_U$.

2.3.2 Parameter fitting

The remaining parameters in the baseline set p_0 (Table 2.3) were identified by solving the system at steady state x_0 (Table 2.5) and imposing the following constraints using MATLAB's nonlinear programming solver `fmincon`:

Parameter	Description	Value	Unit
k_{int}	Rate constant for AT1R-bound Ang II internalization	0.193	/min
k_{rec}	Rate constant for AT1R recycling to the membrane	0.277	/min
k_{lys}	Rate constant for lysosomal degradation of intracellular Ang II	0.208	/min
k_{trans}	Rate constant for Ang II transport into the interstitial space	32.9	/min
k_{meg}	Rate of megalin -dependent uptake of Ang II	4.68	/min
k_{diff}	Rate of Ang I diffusion across the tubular epithelium	0.478	mL/min per g kidney
$AT1R_{Gl}^{tot}$	Total amount of glomerular AT1Rs	115	fmol/g kidney
c_{ACE}^{circ}	Reaction rate of circulating ACE	1.035	/min
c_{chym}	Reaction rate of circulating chymase	0.115	/min
c_{NEP}	Reaction rate of circulating NEP	0.293	/min
c_{ACE2}	Reaction rate of circulating ACE2	0.062	/min
v_{max}	Maximal rate of PRC to PRA conversion	99.7	/min
k_{AngI}^{Pt}	Production rate of Ang I in the peritubular interstitial space	6746	fmol/mL per min
c_{ACE}^{Pt}	Reaction rate of ACE in the peritubular interstitial space	2.0	/min
k_{AngI}^{Tb}	Production rate of Ang I in the luminal fluid	9992	fmol/mL per min
c_{ACE}^{Tb}	Reaction rate of ACE in the proximal luminal fluid	1.83	/min

Table 2.3: Fitted parameters

1. Since [Ang II–AT1R–mediated endocytosis](#) occurs with a half-life of 2 to 10 minutes [153], the rate constant describing [AT1R–bound Ang II](#) internalization, k_{int} (Eq. 2.3), was restricted to the interval [0.07, 0.35] /min [135]. The same upper bound (0.35/min) was assumed for the rate constants describing receptor recycling k_{rec} (Eqs. 2.4, 2.5) and lysosomal degradation k_{lys} (Eq. 2.2).
2. The total amount of glomerular [AT1Rs](#), $AT1R_{Gl}^{tot}$ (Eq. 2.6), was fit to ensure that the total concentration of glomerular receptors was greater than the total concentration of tubular and peritubular receptors at baseline [181], but less than the upper bound of $1000K_D$ [135]. $K_D = k_{diss}/k_{ass}$ is the dissociation constant of [Ang II](#) from [AT1Rs](#). The same value ($1000K_D$) was used to bound the total concentration of [AT1Rs](#) in all other compartments.
3. Ensuring that the steady state concentrations of all model variables (Table 2.5) were within the range of the renal and systemic [RAS](#) concentrations that have been observed experimentally (Table 2.4).

The resulting parameter set p_0 was subsequently validated against data collected from various [Ang II](#) infusion experiments (see Chapter 3). In future work, the size of the

parameter regime that satisfies the above constraints should be quantified via a global parametric sensitivity analysis.

Variable	Bounds	Units	Reference
$[AGT]_{circ}$	[554, 598]	pmol/mL	[14]
$[AngI]_{circ}$	$[[AngII]_{circ}, 228]$	fmol/mL	[115, 14, 184, 183]
$[AngII]_{circ}$	[30, 114]	fmol/mL	[115, 14, 184, 183, 141]
$[Ang(1 - 7)]_{circ}$	[3, 7]	fmol/mL	[14]
PRA	[61, 100]	fmol/mL per min	[184]
$[AngI]_T$	[121, 267]	fmol/g kidney	[115, 184, 183, 14]
$[AngII]_T$	[105, 371]	fmol/g kidney	[115, 184, 183, 14, 141]
$[AngII]_{Tb}^{Cell} + [AT1R - bound AngII]_{Tb}^{Cell}$	$[0.12, 0.33] * \frac{[AngII]_T}{V_{Tb, Pt}^{Cell}}$	fmol/g kidney	[62] ^a
$[AngII]_{Pt}^{Cell} + [AT1R - bound AngII]_{Pt}^{Cell}$	$[0.05, 0.10] * \frac{[AngII]_T}{V_{Tb, Pt}^{Cell}}$	fmol/g kidney	[62] ^a
$[AngI]_{Tb}^{Ext}$	[494, 7340]	fmol/mL	[108] ^b
$[AngII]_{Tb}^{Ext}$	[250, 9700]	fmol/mL	[108, 103, 162] ^b
$[AngI]_{Pt}^{Ext}$	$[[AngI]_{circ}, 880]$	fmol/mL	[115] ^c
$[AngII]_{Pt}^{Ext}$	$[[AngII]_{circ}, 3500]$	fmol/mL	[115] ^c

Table 2.4: Experimental bounds for steady state concentrations

^aApical and basolateral endosomes of **tubular epithelial cells** account for 12 – 33% and 5 – 10% of total renal **[Ang II]**, respectively [62].

^bUsing micropuncture techniques, the **Ang I** [108] and **Ang II** [108, 103, 162] concentrations in the proximal luminal fluid have been measured to within [4940, 7340] fmol/mL and [2500, 9700] fmol/mL, respectively. However, it has been proposed by [108] that concentrations under undisturbed conditions may be as low as 10-20% of those aforementioned, due to the experimental set-up required to collect the fluid. Hence, we allow $[AngI]_{Tb}^{Ext}$ (Eq. A.8) and $[AngII]_{Tb}^{Ext}$ (Eq. A.9) to be as low as 10% of the values reported at steady state.

^cUsing microdialysis techniques, Nishiyama et al. [115] measured the **Ang I** and **Ang II** concentration in the renal interstitial fluid to within [800, 880] fmol/mL and [2640, 3500] fmol/mL, respectively. However, it has been suggested by [159] that such high concentrations are an artifact. Indeed, the microdialysis probe increases the extracellular space separating the cells by 150-fold, decreasing the concentration of **AT1Rs** available for **Ang II** binding, resulting in artificially high free **Ang II** concentrations. Smaller interstitial concentrations would also be more consistent with the concentrations reported in the renal lymph and venous plasma of dogs [165]. Hence, we allow $[AngI]_{Pt}^{Ext}$ (Eq. A.15) and $[AngII]_{Pt}^{Ext}$ (Eq. A.16) to be as low as their respective plasma concentrations at steady state.

Variable	Description	Steady State	Unit
Systemic compartment			
$[AGT]_{circ}$	Plasma [AGT]	575941	
$[AngI]_{circ}$	Plasma [Ang I]	65.2	
$[AngII]_{circ}$	Plasma [Ang II]	43.3	
$[AT1R - bound AngII]_{circ}^{Memb}$	Membrane-bound [AT1R-Ang II complex]	21662	fmol/mL
$[AT1R]_{circ}^{Memb}$	Membrane-bound free [AT1R]	499837	
$[Ang(1-7)]_{circ}$	Plasma [Ang (1-7)]	5.25	
PRC	Plasma [renin]	4.33	
PRA	Plasma renin activity	73.6	fmol/mL per min
Glomerular compartment			
$[AngI]_{Gl}^{Ext}$	Interstitial [Ang I]	65.2	
$[AngII]_{Gl}^{Ext}$	Interstitial [Ang II]	40.9	
$[AT1R - bound AngII]_{Gl}^{Memb}$	Glomerular membrane-bound [AT1R-Ang II complex]	262.2	
$[AT1R - bound AngII]_{Gl}^{Cell}$	Intracellular [AT1R-Ang II complex]	2153	fmol/mL
$[AngII]_{Gl}^{Cell}$	Free intracellular [Ang II]	243.2	
$[AT1R]_{Gl}^{Memb}$	Free membrane-bound [AT1R]	57927	
$[AT1R]_{Gl}^{Cell}$	Free intracellular [AT1R]	182.4	
Peritubular compartment			
$[AngI]_{Pt}^{Ext}$	Interstitial [Ang I]	455	
$[AngII]_{Pt}^{Ext}$	Interstitial [Ang II]	190	
$[AT1R - bound AngII]_{Pt}^{Memb}$	Basolateral membrane-bound [AT1R-Ang II complex]	66.7	
$[AT1R - bound AngII]_{Pt}^{Cell}$	Basolateral intracellular [AT1R-Ang II complex]	43.0	fmol/mL
$[AngII]_{Pt}^{Cell}$	Free basolateral intracellular [Ang II]	4.96	
$[AT1R]_{Pt}^{Memb}$	Free basolateral membrane-bound [AT1R]	3172	
$[AT1R]_{Pt}^{Cell}$	Free basolateral intracellular [AT1R]	3.72	
Tubular compartment			
$[AngI]_{Tb}^{Ext}$	Luminal fluid [Ang I]	1638	
$[AngII]_{Tb}^{Ext}$	luminal fluid [Ang II]	763	
$[AT1R - bound AngII]_{Tb}^{Memb}$	Apical membrane-bound [AT1R-Ang II complex]	27.0	
$[AT1R - bound AngII]_{Tb}^{Cell}$	Apical intracellular [AT1R-Ang II complex]	75.7	fmol/mL
$[AngII]_{Tb}^{Cell}$	Free apical intracellular [Ang II]	37.57	
$[AT1R]_{Tb}^{Memb}$	Free apical membrane-bound [AT1R]	320	
$[AT1R]_{Tb}^{Cell}$	Free apical intracellular [AT1R]	6.53	
Renal post-glomerular blood vasculature compartment			
$[AngI]_{Pv}$	Renal plasma [Ang I]	163.9	
$[AngII]_{Pv}$	Renal plasma [Ang II]	79.2	
$[AT1R - bound AngII]_{Pv}^{Memb}$	Membrane-bound [AT1R-Ang II complex]	36.7	fmol/mL
$[AT1R]_{Pv}^{Memb}$	Free membrane-bound [AT1R]	463	
Whole kidney			
$[AngI]_T$	Whole kidney [Ang I]	192	
$[AngII]_T$	Whole kidney [Ang II]	149	fmol/g kidney

Table 2.5: Steady state concentrations of model variables

2.4 Steady state results

Following the procedure outlined in Section 2.3.2, a parameter set (Table 2.3) and model steady state (Table 2.5) were identified that satisfy all bounds outlined in Table 2.4. Of note, the model predicts steady state concentrations of $[AngI]_{Pt}^{Ext}$ (455 fmol/mL) and $[AngII]_{Pt}^{Ext}$ (190 fmol/mL) that are 51–57% and 5–7% of those reported by Nishiyama et al. [115], respectively. In fact, none of the parameterizations considered with peritubular interstitial angiotensin concentrations within the ranges reported by Nishiyama et al. [115] were able to satisfy the other model constraints. This discrepancy has been previously addressed by Van Kats et al. [159], who hypothesized that concentrations collected using microdialysis techniques may be artificially high due to a disturbed cell micro-environment. Moreover, the predicted concentrations of $[AngI]_{Tb}^{Ext}$ (1637 fmol/mL) and $[AngII]_{Tb}^{Ext}$ (763 fmol/mL) are 22–33% and 8–30% of those reported by Navar et al. [108], Mitchell et al. [103], and Wang et al. [162]. This supports the claim made by Navar and colleagues [108] that in unperturbed conditions luminal fluid Ang II concentrations may be only 10–20% of those collected using micro-puncture techniques, or under 1000 fmol/mL. In summary, it is likely that the high experimental renal interstitial and luminal fluid angiotensin concentrations are artifacts of the sample collection procedure.

2.4.1 Local sensitivity analysis

To determine the robustness of the steady state (Table 2.5), we perform a local parametric sensitivity analysis. In particular, we examine the percent change in each predicted concentration that is caused by a 10% increase in each model parameter.

As shown in Figure 2.3, the steady state is most (least) sensitive to changes in the parameters specific to the tubular (peritubular) compartment, in particular, the rate of megalin-mediated uptake k_{meg} as well as the rates of endogenous Ang I k_{AngI}^{Tb} (k_{AngI}^{Pt}) and Ang II c_{ACE}^{Tb} (c_{ACE}^{Pt}) production in the luminal (interstitial) fluid. The model is also sensitive to the rate of Ang I diffusion across the tubular epithelium k_{diff} . Indeed, the majority of the renal variables (apart from those in the upstream glomerular compartment) are altered by this parameter. Given its significant effect on the model’s predicted steady state, future experimental work should focus on identifying the mechanisms that mediate this process. Finally, the behaviour of the systemic, glomerular, and renal (post-glomerular blood) vasculature free Ang I and Ang II concentrations at steady state appear to be correlated. Specifically, since systemic angiotensin is the main source of glomerular and renal (post-glomerular blood) vasculature angiotensin, the variables in these compartments

are most affected by changes to parameters relating to systemic peptide production (k_{AGT} , v_{max} , and c_{chym}). Nevertheless, a 10% change in each parameter never elicits more than a 10% change any model variable and as a result, the model's steady state remains within the bounds presented in Table 2.4 in all cases considered.

Having now developed a model that is accurate and robust at the steady-state level, we can use it to study the role of the intrarenal RAS in hypertension via various model perturbation experiments and extensions. We begin with the induction of hypertension via Ang II infusion.

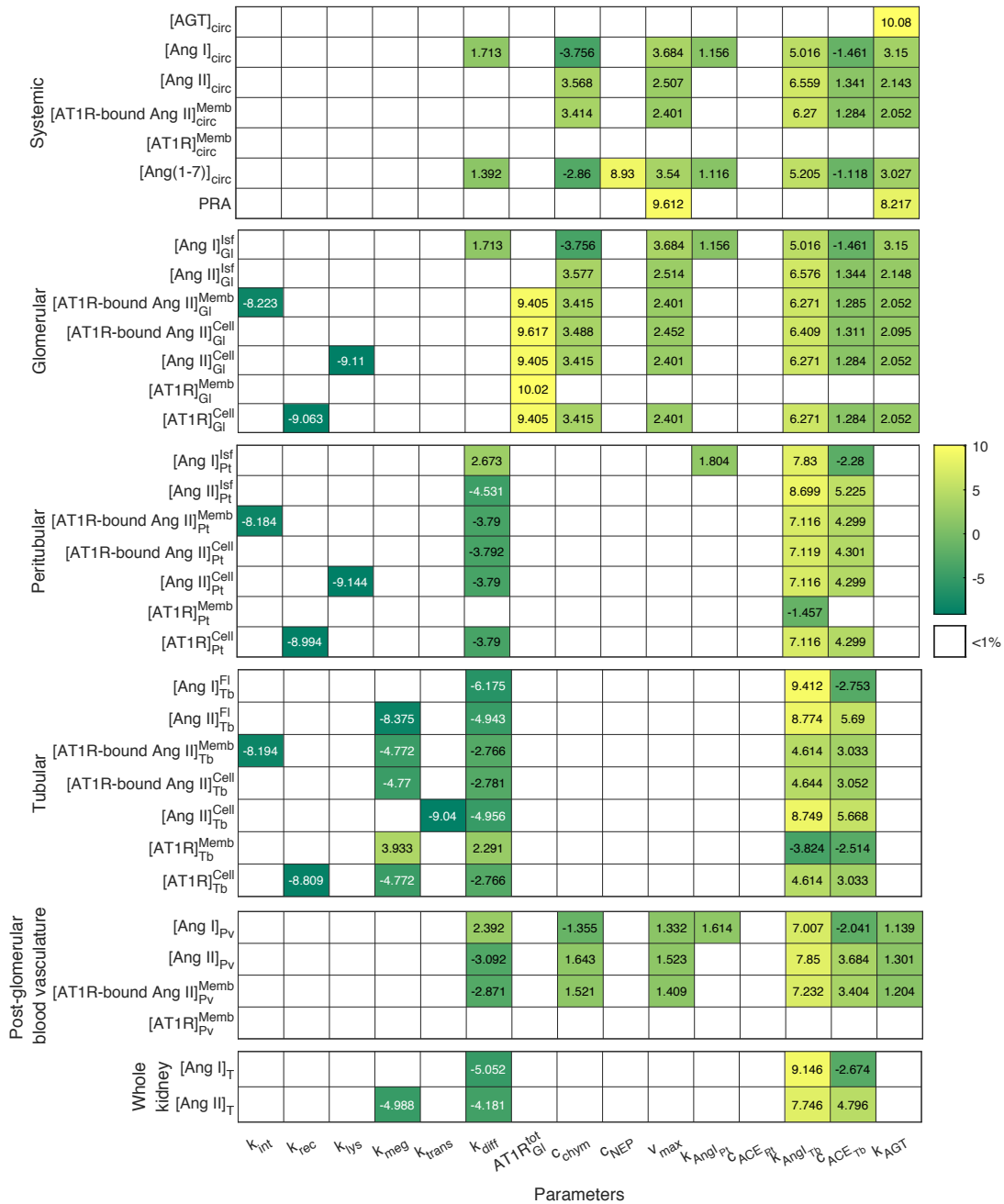


Figure 2.3: Percent change in the predicted steady state concentrations caused by a 10% increase in each model parameter value.

Chapter 3

Intrarenal renin angiotensin system activity in hypertension induced by angiotensin II infusion: Insights from mathematical modelling

Abstract

The **RAS** plays a pivotal role in the maintenance of volume homeostasis and blood pressure. In addition to the well-studied systemic RAS, local RAS have been documented in various tissues, including the kidney. Given the role of the intrarenal RAS in the pathogenesis of hypertension, a role established via various pharmacologic and genetic studies, substantial efforts have been made to unravel the processes that govern intrarenal RAS activity. In particular, several mechanisms have been proposed to explain the rise in intrarenal **Ang II** that accompanies **Ang II infusion**, including increased **AT1R**-mediated uptake of Ang II and enhanced intrarenal Ang II production. However, experimentally isolating their contribution to the intrarenal accumulation of Ang II in **Ang II-induced hypertension** is challenging, given that they are fundamentally connected. Computational modelling is advantageous because the feedback underlying each mechanism can be removed and the effect on intrarenal Ang II can be studied. In this Chapter, the mechanisms governing the intrarenal accumulation of Ang II during Ang II infusion experiments are delineated and the role of the intrarenal RAS in Ang II-induced hypertension is studied. To accomplish

this, various positive feedback systems are added to the compartmental ODE model of the systemic and intrarenal RAS outlined in Chapter 2 and Ang II infusion experiments are simulated. Simulations indicate that AT1R-mediated uptake of Ang II is the primary mechanism by which Ang II accumulates in the kidney during Ang II infusion. Enhanced local Ang II production is unnecessary. The results demonstrate the role of the intrarenal RAS in the pathogenesis of Ang II-induced hypertension and consequently, clinical hypertension associated with an overactive RAS.

3.1 Introduction

Hypertension is a common, highly complex condition that promotes risk for other diseases of the vasculature. Although the underlying causes of most cases of hypertension are unknown and likely multifactorial, antihypertensive therapies targeting the renin-angiotensin system (RAS) are highly effective in reducing elevated blood pressure [60], due to the long-established role of the RAS in blood pressure regulation [36, 144]. As detailed in Chapter 1, Ang II, the primary bio-active product of the RAS, increases blood pressure primarily via its AT1R-mediated effects on kidney function, and therefore fluid homeostasis. Given the many intrarenal actions of Ang II, and the discovery that the kidney not only expresses, but independently regulates all components of the RAS, the significance of the local intrarenal RAS to the pathogenesis and progression of hypertension has recently come into focus.

Although the systemic and intrarenal RAS are connected and typically vary in tandem, a de-coupling of the two systems has been observed in various experimental models of hypertension [184, 18, 168, 150]. In Ang II-induced hypertensive rats in particular, there is a progressive rise in intrarenal Ang II that cannot be explained on the basis of equilibration with plasma [Ang II]_s[184, 31, 40, 93]. Several mechanisms have been proposed to explain this response, including: (i) *enhanced AT1R-mediated uptake of circulating Ang II*, and (ii) *increased intrarenal endogenous Ang II production* [71, 109, 141, 142, 159, 180, 70, 72, 35, 40, 94, 141, 183]. In mechanism (i), circulating Ang II enters the kidney and binds to AT1Rs on **tubular epithelial cells**. The Ang II-AT1R complexes are then actively internalized [59] into intracellular compartments where the Ang II is protected from degradation [180, 107, 158]. It is hypothesized that the Ang II-dependent up-regulation of AT1R expression in proximal tubule epithelial cells [180, 182, 21] facilitates this effect. In mechanism (ii), the endogenous production of Ang II in the **luminal fluid** is thought to be increased as a result of Ang II-dependent positive feedback on proximal tubule **AGT** [107, 109, 70, 40, 72, 138]

and collecting duct renin production [122, 109, 38, 37].

While these hypotheses are well-founded, isolating the contribution of each mechanism to the accumulation of Ang II in the kidney in Ang II-induced hypertension poses a significant experimental challenge because they are fundamentally linked. Computational modelling is advantageous in this regard, because once a model is developed that incorporates these systems, each feedback function can be individually turned on/off and the impact on the total and local intrarenal [Ang II] can be studied. As detailed in Chapter 1, two computational models of the intrarenal RAS have been developed previously [135, 95]. However, neither considers intrarenal positive feedback. The first model [135] also does not consider any temporal dynamics and thus can only be used to study the system's behaviour at steady state. While the second model [95] does consider the rate of change of key RAS peptides, it does not differentiate between the intracellular and extracellular compartments of the kidney. Therefore, it cannot be used to study the process of AT1R-mediated uptake of circulating Ang II (mechanism (i)) in detail. For these reasons, the existing models would be ineffectual in studying the contribution of the intrarenal RAS to the pathogenesis of Ang II-induced hypertension.

In this Chapter, we aim to delineate the mechanisms that mediate intrarenal Ang II accumulation during Ang II infusion and consequently, gain insight into the role of the intrarenal RAS in the development of Ang II-induced hypertension. To do so, the computational model outlined in Chapter 2 that considers temporal dynamics and distinguishes between the intracellular and extracellular regions of various intrarenal compartments is extended to incorporate intrarenal (and systemic) positive feedback. Formalisms to simulate both subcutaneous and intravenous Ang II infusion experiments are also derived to facilitate the study of Ang II-induced hypertension. After fitting the model parameters to Ang II infusion data, the model is validated and used to make predictions on the key mechanisms contributing to the rise in intrarenal [Ang II] during Ang II infusion. The robustness of the predictions is also quantified via a local parametric sensitivity analysis. The results presented provide novel insight into the role of the intrarenal RAS in the development of Ang II-induced hypertension and accordingly, any form of hypertension associated with an overactive RAS.

3.2 Methods

3.2.1 Modelling positive feedback

To investigate the mechanisms that contribute to intrarenal RAS over-activation in Ang II-induced hypertension, the model outlined in Chapter 2 was extended to include the many positive feedback loops that have been documented experimentally. Since all feedback functions to be added take a similar form across compartments, a general function fb_C^x is first introduced here, where C represents the compartment where the feedback is taking place ($C = Tb, Pt, \text{ and } circ$) and x represents which variable is being up-regulated ($x = AngI, ACE, AT1R, \text{ and } AGT$). All feedback was assumed linear for simplicity:

$$fb_C^x (R_C^L(t)) = \begin{cases} 0 & \text{if } R_C^L(t) \leq 1 \\ K_C^x (R_C^L(t) - 1) & \text{if } R_C^L(t) > 1 \end{cases} \quad (3.1)$$

where

$$R_C^L(t) = \frac{[AT1R - \text{bound } AngII]_X^L(t)}{[AT1R - \text{bound } AngII]_X^{L,eq}} \quad (3.2)$$

L represents which fraction of AT1Rs, membrane-bound ($L = memb$) or intracellular ($L = cell$), are impacting the feedback. The variables up-regulated in each compartment are described in detail below.

Intrarenal model As aforementioned, two mechanisms have been proposed to explain the rise in intrarenal Ang II that is observed during Ang II-induced hypertension. To investigate the role of mechanism (i), enhanced AT1R-mediated uptake of circulating Ang II, in Ang II-induced hypertension, we allowed **AT1R** expression to increase via an **Ang II**- and **AT1R**-dependent mechanism [180, 182, 21] in both the tubular and peritubular compartments. Indeed, we added the function fb_C^{AT1R} to Eq. 2.5 to yield Eq. 3.3, where $C = Tb$ or Pt :

$$\begin{aligned}
\frac{d[AT1R]_C^{Memb}}{dt}(t) &= k_{diss}[AT1R - \text{bound } AngII]_C^{Memb}(t) \\
&\quad - k_{ass}[AT1R]_{Tb}^{Memb}(t)[AngII]_C^{Ext}(t) \\
&\quad + k_{rec} \frac{V_C^{Ext}}{V_{Pt,Tb}^{Cell}} [AT1R]_C^{Cell}(t) \\
&\quad + fb_C^{AT1R} (R_C^{Memb}(t))
\end{aligned} \tag{3.3}$$

To study the role of mechanism (ii), enhanced endogenous **Ang II** production [107, 109, 70, 40, 72, 138, 122, 109, 38, 37]), in Ang II–induced hypertension, explicit **Ang II**–dependent positive feedback on luminal **AGT** and **renin** activity could be turned on by redefining the tubular Ang I production rate, k_{AngI}^{Tb} , such that:

$$k_{AngI}^{Tb}(t) = k_{AngI}^{Tb} + fb_{Tb}^{AngI}(R_{Tb}^{Cell}(t)) \tag{3.4}$$

Systemic model In addition to these intrarenal feedback systems, elevated systemic [**Ang II**] has been observed to increase hepatic **AGT** production in a **AT1R**–dependent manner [91, 138, 106]. This positive feedback was incorporated by modifying the rate of **AGT** production k_{AGT} in Eq. 2.10, such that:

$$k_{AGT}(t) = k_{AGT} + fb_{circ}^{AGT}(R_{circ}^{Memb}(t)) \tag{3.5}$$

Finally, we also allowed systemic **ACE** activity to increase in an **Ang II** and **AT1R**–dependent manner via the addition of the positive feedback function fb_{circ}^{ACE} to the existing rate of plasma **ACE** activity c_{ACE} :

$$c_{ACE}^{circ}(t) = c_{ACE}^{circ} + fb_{circ}^{ACE}(R_{circ}^{Memb}(t)) \tag{3.6}$$

This feedback was found to be required to replicate the decrease (increase) in plasma **Ang I** (endogenous **Ang II**) that is observed experimentally following **Ang II** infusion (see Section 3.3.1) [184, 141, 142]. Similar feedback has been documented in the kidney [132, 73].

Figure 3.1 summarizes all feedback loops considered by the model when mechanisms (i) and (ii) are simulated. In particular, all positive feedback added to the systemic model is activated for both sets of simulations. To simulate mechanism (i), we set $fb_{Tb}^{AngI} = 0$ and activate fb_{Tb}^{AT1R} and fb_{Pt}^{AT1R} . To simulate mechanism (ii), we set $fb_{Tb}^{AT1R} = fb_{Pt}^{AT1R} = 0$ and activate fb_{Tb}^{AngI} .

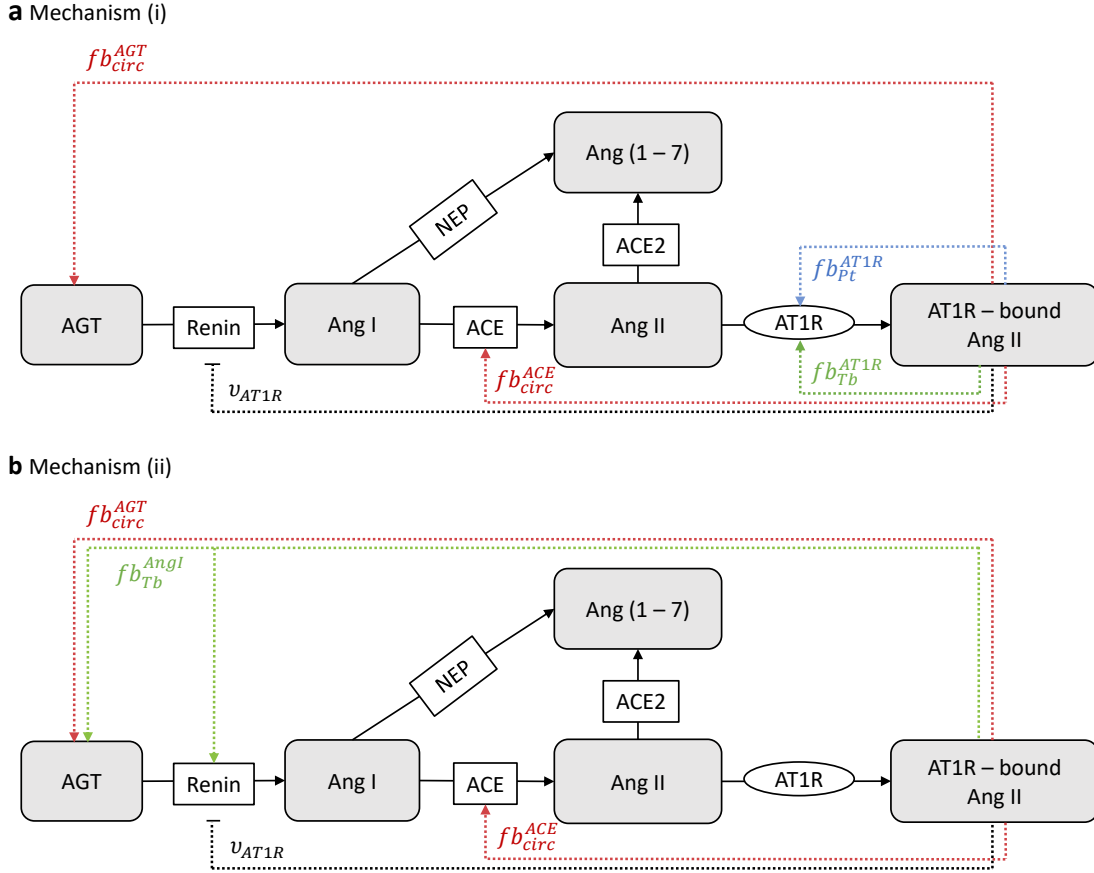


Figure 3.1: Schematic representation of the positive (arrow) and negative (blunted arrow) feedback loops included in the model when simulating **a** mechanism (i) and **b** mechanism (ii). Negative feedback on renin secretion (ν_{AT1R}) and systemic (red) positive feedback on AGT production (fb_{circ}^{AGT}) and ACE activity (fb_{circ}^{ACE}) are consistent across both mechanisms. The upregulation of AT1R expression in the peritubular (fb_{Pt}^{AT1R} ; blue) and tubular (fb_{Tb}^{AT1R} ; green) compartments is only included in mechanism (i). In contrast, the Ang II-dependent upregulation of luminal AGT and renin activity (fb_{Tb}^{AngI} ; green) is only included in mechanism (ii).

3.2.2 Simulating Ang II infusion experiments

Ang II can be infused intravenously or subcutaneously via osmotic mini-pump implantation. Each experimental technique is simulated using a different mathematical formalism.

During an **intravenous (IV)** infusion, Ang II enters the blood stream directly. Hence, it is simulated by adding the constant production term:

$$K_{inf}^{IV} = \frac{D}{V_{circ}}$$

to the original equation describing plasma Ang II dynamics (Eq. 2.16). D is the dose of Ang II in units of fmol/min, and V_{circ} is the circulating plasma volume in mL.

During a **SC** infusion, Ang II enters the blood stream indirectly following re-absorption from the SC tissue. Hence, we must consider the amount of Ang II in this compartment, $AngII_{SC}$. The rate of change of $AngII_{SC}$ is governed by the exogenous infusion of Ang II into this compartment with dose D (fmol/min) and its re-absorption into the systemic circulation with rate $k_a \text{ min}^{-1}$:

$$\frac{dAngII_{SC}(t)}{dt} = D - k_a AngII_{SC}(t) \implies AngII_{SC}(t) = \frac{D}{k_a} (1 - e^{-k_a t}) \quad (3.7)$$

Therefore, a **SC** Ang II infusion can be simulated by adding the following term to the original ODE describing $[AngII]_{circ}$ (Eq. 2.16):

$$K_{inf}^{SC}(t) = \frac{k_a}{V_{circ}} AngII_{SC}(t) = \frac{D}{V_{circ}} (1 - e^{-k_a t}) \quad (3.8)$$

3.2.3 Separating exogenous Ang II from endogenous Ang II

To better understand Ang II dynamics, we separately simulate in each compartment exogenously infused ($AngII_i$) and endogenously produced ($AngII_p$) Ang II, such that:

$$[AngII](t) = [AngII_i](t) + [AngII_p](t)$$

The equations describing exogenous and endogenous Ang II differ in their production terms: Infusion contributes to $AngII_i$ levels, while enzyme activity contributes to $AngII_p$ levels. In this way, the equations describing $AngII_p$ are analogous to those described above in Section 2.1.1 (Eqs. 2.2, 2.3) and the equations describing $AngII_i$ only differ in the compartments where the endogenous production of Ang II occurs (systemic circulation, peritubular **interstitial space**, and **luminal fluid**). Indeed, the infusion term $K_{inf}^Y(t)$ ($Y = \text{SC, IV}$) is added to the systemic circulation (Eq. 2.16) to simulate infusion and the terms describing chymase and/or ACE activity are removed in all 3 of the aforementioned compartments i.e. we set $c_{chym} = c_{ACE}^C = 0$ for $C = Tb, Pt, circ$ (Eqs. 2.2, 2.16).

In the absence of an infusion, $[AngII_i] = 0$ in all compartments and $[AngII_p]$ is the sole contributor to the total Ang II concentration, as expected.

3.2.4 Parameter fitting

Variable	Value (ratio to control)	Infusion type	Infusion dose	Time	Use	Reference
Plasma Ang I ($[AngI]_{circ}$)	0.26 ± 0.045	SC	40 ng/min	Day 3	V	[184]
	0.32 ± 0.045			Day 7	V	
	0.38 ± 0.08			Day 10	V	
	0.165 ± 0.05			Day 13	F	
Whole kidney Ang I ($[AngI]_T$)	0.93 ± 0.08	SC	40 ng/min	Day 3	V	[184]
	0.82 ± 0.094			Day 7		
	0.96 ± 0.12			Day 10		
	0.85 ± 0.13			Day 13		
Plasma Ang II ($[AngII]_{circ}$)	2.94 ± 0.45	SC	40 ng/min	Day 13	V	[184]
	1.49 ± 0.31	SC	200 ng/kg/min	Day 7	F	[13]
	4.34 ± 1.58		350 ng/kg/min			
	5.57 ± 0.85		500 ng/kg/min			
	6.48 ± 1.36	SC	80 ng/min	Day 13	F	[141, 142]*
	2.37 ± 0.55 ($-p$)					
	4.11 ± 0.81 ($-i$)					
	3.45 ± 0.78	IV	10 ng/min	1-hour	F	[118]
9.31 ± 3.72	30 ng/min		V			
22.1 ± 7.09	60 ng/min		F			
Whole kidney Ang II ($[AngII]_T$)	3.58 ± 0.60	SC	80 ng/min	Day 13	F	[141, 142]*
	1.71 ± 0.37 ($-p$)					
	1.88 ± 0.22 ($-i$)					
Peritubular Interstitial Ang II ($[AngII]_{Pt}^{Ext}$)	2.01 ± 0.09	SC	80 ng/min	Day 13	F	[116]
Apical endosomal Ang II ($[AngII]_{Tb}^{Cell} + [AT1R - bound AngII]_{Tb}^{Cell}$)	2.38 ± 0.59	SC	80 ng/min	Day 13	F	[180]
Basolateral endosomal Ang II ($[AngII]_{Pt}^{Cell} + [AT1R - bound AngII]_{Pt}^{Cell}$)	15.5 ± 3.99	SC	80 ng/min	Day 13	F	[180]

Table 3.1: Ang II infusion data used for feedback parameter fitting (F) and validation (V).

*Weighted average of endogenous and exogenous Ang II concentrations reported by Refs. [141] and [142] (weighted by number of rats used in each study).

No changes were made to the parameters identified in Section 2.3 (Tables 2.2 and 2.3) and therefore to the model steady state x_0 given in Table 2.5. The parameters introduced via the incorporation of positive feedback (Section 3.2.1) and to simulate Ang II infusion (Section 3.2.2), hereby referred to as **feedback parameters**, were estimated by simulating the Ang II infusion experiments labelled *fitting (F)* in Table 3.1 from the initial condition x_0 and minimizing the normalized sum of squared errors between the data and the simulation:

$$\sum_j \sum_i \left(\frac{x_i^{true}(t_j) - x_i^{sim}(t_j)}{\sigma_i(t_j)} \right)^2 \quad (3.9)$$

where $x_i^{true}(t_j)$ and $x_i^{sim}(t_j)$ correspond to the i^{th} true and simulated data point collected at time point t_j , respectively and $\sigma_i(t_j)$ corresponds to the standard deviation of $x_i^{true}(t_j)$. MATLAB’s nonlinear programming solver `fmincon` was used for the optimization.

3.3 Results

3.3.1 Model validation

Following the procedure outlined in Section 3.2.4, we minimized Eq. 3.9 to obtain the optimized feedback parameter set shown in Table 3.2. In the cases where time series data was available (Table 3.1), only the last time point (day 13) was used for parameter fitting. All other data points were kept for model validation. Below we compare the model solutions obtained using these parameters and discuss their implications. If not otherwise specified, the results presented were generated using the feedback parameters specific to mechanism (i) (Figure 3.1a), given that they resulted in a much better fit to data (see Section 3.3.1).

The upregulation of hepatic AGT may influence downstream intrarenal, as opposed to systemic, RAS peptide concentrations in Ang II–induced hypertension
 As shown in Figure 3.2, the parameterized model is able to predict the changes in plasma [AGT], PRA, and [Ang I] that accompany 13 days of 40 ng/min subcutaneous Ang II infusion. Although the temporal dynamics are also predicted, only the data on day 13 was used for fitting. The remaining data was used for model validation. In particular, hepatic Ang II-dependent AGT positive feedback fb_{circ}^{AGT} (Eq. 2.10) was found to be required for the simulated fold-increase in plasma [AGT] to match what is reported experimentally [184] (Figure 3.2a). However, given that the Michaelis constant for AGT–renin binding is

Parameter	Description	Value	Unit	Mechanism
k_a	Re-absorption rate from the subcutaneous tissue	3.8×10^{-6}	/min	–
K_{circ}^{AGT}	Strength of positive feedback on hepatic AGT production	450	fmol/mL/ min	–
K_{circ}^{ACE}	Strength of positive feedback on systemic ACE activity	3.9	fmol/mL per min	–
$[AT1R]_{circ}^{Tot}$	Total systemic AT1R concentration	521500	fmol/mL	–
$[AT1R]_{Pv}^{Tot}$	Total post-glomerular blood vasculature AT1R concentration	500	fmol/mL	–
B_{AT1R}	Strength of Ang II–AT1R feedback on renin secretion	2.9	–	–
K_{Pt}^{AT1R}	Strength of positive feedback on peritubular AT1R production	0.66	fmol/mL per min	(i)
K_{Tb}^{AT1R}	Strength of positive feedback on tubular AT1R production	0.05	fmol/mL per min	(i)
K_{Tb}^{AngI}	Strength of positive feedback on tubular endogenous production	7400	fmol/mL per min	(ii)

Table 3.2: Feedback parameters

so large ($K_M = 2.8 \times 10^6$ fmol/mL [43]), fb_{circ}^{AGT} has an inconsequential effect on PRA (Figure 3.2b) and thus, the concentration of plasma peptides downstream in the cascade. We hypothesize that the physiological importance of this feedback is instead specific to the kidney and other local RAS' where the pro-renin receptor is expressed [111, 110, 12, 163]: Indeed, renin binding to the pro-renin receptor (PRR) decreases the Michaelis constant for AGT binding by 85% [111]. As a result, any substantial change in the local [AGT] will impact local renin activity, and thus the local concentrations of downstream peptides such as Ang I and Ang II. Since hepatic AGT is the primary source of AGT in the kidney [98], the upregulation of hepatic (systemic) [AGT] could be one mechanism by which renal renin activity (assumed constant in our model) is maintained following Ang II infusion [141], despite the decrease in PRA that occurs.

Amplification of systemic ACE activity may be required to significantly decrease (increase) the plasma [Ang I] ([Ang II]) in Ang II–induced hypertension
As shown in Figure 3.2c (dark green), the chronic infusion of Ang II significantly reduces the plasma [Ang I]. Simulations suggest that this is the result of i) decreased production from AGT (inhibited renin secretion, see Eq. 2.13) and ii) increased conversion to Ang II (enhanced ACE activity, see Eq. 3.1). Of note, reduced renin activity alone was not found to be sufficient to cause the drop in plasma [Ang I] that is observed experimentally. Without enhanced ACE activity (and thus, more rapid degradation of Ang I), the plasma [Ang I] following 13 days of 40 ng/min subcutaneous infusion plateaus at 73% of its control value (Figure 3.2c, dark green dashed curve), which far exceeds what the data suggests (17%). This provides additional support for the existence of the Ang II-dependent up-regulation of systemic ACE activity (fb_{circ}^{ACE} , Eq. 2.14, 2.16).

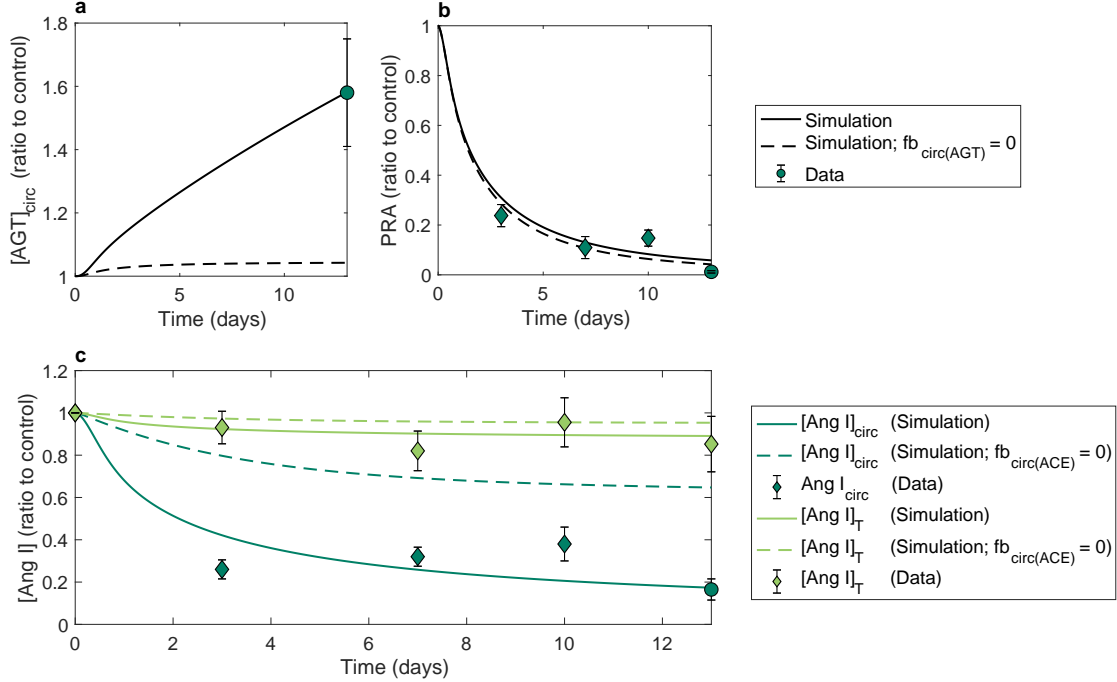


Figure 3.2: Simulated (mechanism (i)) vs. experimental **a** plasma $[AGT]$, **b** PRA, and **c** plasma (dark green) and whole kidney (light green) $[Ang\ I]$ time series following 13 days of 40 ng/min SC Ang II infusion. Circular markers indicate data that was used for fitting; diamond markers indicate data used for validation. Dashed curves indicate simulations made with the specified systemic positive feedback (fb_{circ}^{ACE} or fb_{circ}^{AGT}) removed (set to 0). Data was taken from [184].

Plasma $[Ang\ II]$ dose-response curves for both classes of Ang II infusion (SC: Figure 3.3a and IV: Figure 3.3b) at three different time points (1-hour, 7 days, and 13 days) were also simulated and compared to experimental data (circular markers) to estimate the feedback parameters. As demonstrated in Figure 3.3, the model adequately predicts the relative increase in plasma $[Ang\ II]$ that is observed experimentally. This includes the distribution of endogenously produced vs. exogenously infused plasma $[Ang\ II]$ following 13 days of SC infusion at 80 ng/min (Figure 3.3a, inset). However, the simulations appear to over-estimate the change in plasma $[Ang\ II]$ caused by small SC-infused doses of Ang II. This could indicate that the positive feedback on systemic ACE activity (fb_{circ}^{ACE} , Eq. 3.1) depends non-linearly on the local $[Ang\ II]$. Nevertheless, linearity was assumed to avoid

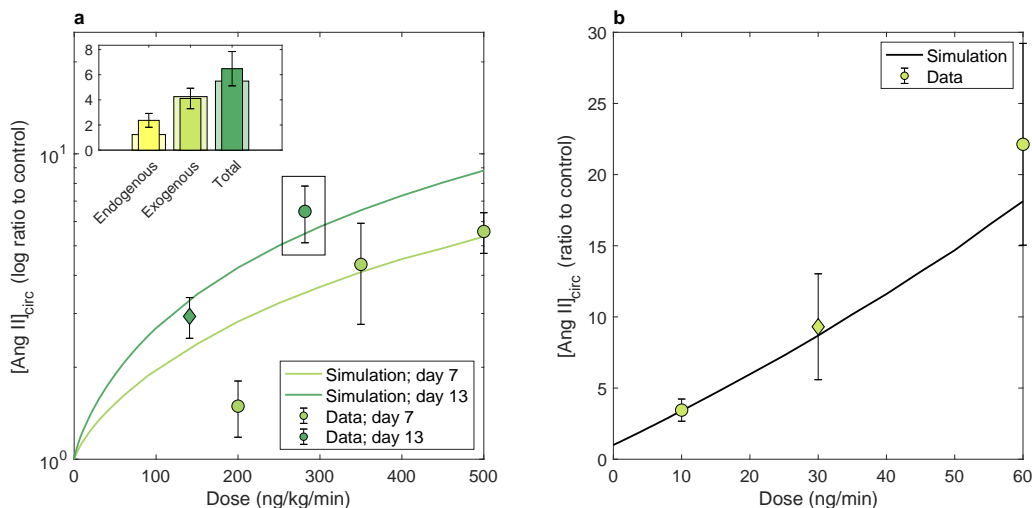


Figure 3.3: Simulated (mechanism (i)) vs. experimental **a** SC and **b** IV Ang II dose–plasma [Ang II]_{circ} response curves. **a**: Dose response following 7 (light green curve) and 13 (dark green curve) days of SC Ang II infusion. Inset: contribution of endogenous vs. exogenous Ang II to the total plasma Ang II concentration at that dose (80 ng/min \approx 282 ng/kg/min assuming a 284 g rat). Narrow bars indicate data used for fitting; wide bars indicate the model simulation. **b**: Dose response following 1-hour of IV Ang II infusion. Circular (diamond) markers indicate data used for fitting (validation). All data is provided in Table 3.1.

issues of parameter identifiability given the lack of data available at small non-vasopressor doses of Ang II. Indeed, most studies infuse large doses of Ang II in order to induce hypertension [14].

Increased intrarenal Ang II production is not required for endogenous Ang II to accumulate in the kidney during Ang II infusion The remaining data points used for parameter identification were specific to Ang II concentrations within kidney. Indeed, feedback parameters were optimized by fitting to the observed fold-change in renal endogenous and exogenous [141, 142], interstitial [116], and intracellular endosome [180] [Ang II] following 13 days of SC Ang II infusion at 80 ng/min. As shown in Figure 3.4, model estimates when mechanism (i) is simulated (dark green bars) are within range of the experimental data (black bars) in each compartment. Of note, the total renal [Ang II] after 13 days of Ang II infusion is comprised of approximately equal parts endogenous and

exogenous Ang II, despite exogenous Ang II making up a larger proportion of the total plasma [Ang II] at this time (Figure 3.3a, inset). Interestingly, the disproportionate renal accumulation of endogenous vs. exogenous Ang II is observed despite the rates of renal Ang II production remaining constant in the model. This suggests that an explicit increase in renal Ang II production is not required for proportionally more endogenous Ang II to accumulate in the kidney in Ang II-induced hypertension.

In fact, if explicit feedback on intrarenal endogenous Ang II production is added to the model in lieu of the feedback on local AT1Rs (i.e. if mechanism (ii) is simulated; Figure 3.4, light green bars), excess endogenous Ang II and not enough exogenous Ang II accumulates in the kidney, resulting in an endogenous-to-exogenous ratio that is significantly greater than what is observed experimentally. Moreover, without the upregulation of basolateral AT1Rs in particular, an excess amount of Ang II ends up in the interstitial space as opposed to tubular epithelial cells which contradicts the experimental findings of Nishiyama et al. [116] and Zhuo et al. [180].

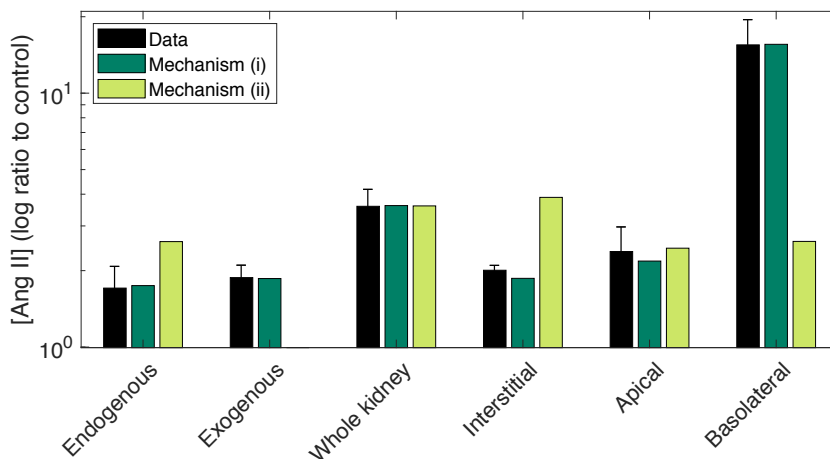


Figure 3.4: Model fit to renal compartmental Ang II data (black bars) following 13 days of SC Ang II infusion (dose: 80 ng/min) when mechanism (i) (dark green bars) vs. mechanism (ii) (light green bars) is simulated. Mechanism (i) is required for the predicted endogenous-, exogenous-, and compartment-specific concentrations to align with their experimentally observed values.

AT1R-mediated uptake of Ang II is the primary mechanism by which Ang II accumulates in the kidney in Ang II-induced hypertension To gain further

insight into the mechanisms underlying the intrarenal accumulation of Ang II during Ang II-induced hypertension, we simulated the Ang II infusion experiment carried out by Zou et al. [184] using both mechanism (i) and (ii) and compared the results to data. In particular, Zou et al. [184] subcutaneously infused Ang II at 40 ng/min for 13 days and observed a rapid, slight decrease in the total renal [Ang I], as well as slow rise in the total renal [Ang II]. When mechanism (i) is simulated, the model is able to closely capture these results, as shown in Figures 3.2c (light green curve) and 3.5 (solid black curve), respectively. In contrast, when mechanism (ii) is simulated, the predicted increase in Ang II (Figure 3.5, dotted black curve) occurs far quicker than is experimentally observed. Indeed, although intrarenal Ang II is within range on day 13, its concentration is significantly over-predicted on day 7 and 10 of the infusion. Given this and the results presented in Section 3.3.1, we conclude that AT1R-mediated uptake of Ang II is the primary mechanism by which Ang II accumulates in the kidney in Ang II-induced hypertension and that increased local expression of AT1Rs, not Ang II, is required.

In the next Section, we examine the experimental results presented by Zou et al. [184] in more detail and use model simulations to offer further insight into the underlying intrarenal and systemic mechanisms.

3.3.2 Model predictions

Renal [Ang I] decreases throughout the development of Ang II-induced hypertension because of a reduction in plasma [Ang I], not renal renin activity As shown in Figure 3.2c, renal [Ang I] decreases significantly less than plasma [Ang I] over the course of the low-dose Ang II infusion. Model simulations can be used to explain this behaviour. Indeed, the large decrease in plasma [Ang I] (Figure 3.2c, dark green curves) that accompanies Ang II infusion was found to be sufficient to cause the small decrease in renal [Ang I] (Figure 3.2c, light green curves) that is observed experimentally; no decrease in local endogenous production (assumed constant in the model) was required. This is consistent with the experimental observation that renal renin activity is conserved during Ang II infusion [141]. Possible mechanisms contributing to the maintenance of kidney renin concentration following Ang II infusion are i) increased renin production in the collecting duct [122, 109, 38, 37] and ii) local pro-renin receptor expression in conjunction with increased [AGT] from elevated hepatic (see Section 3.3.1) [184, 98] and proximal tubule [107, 109, 70, 72] AGT production.

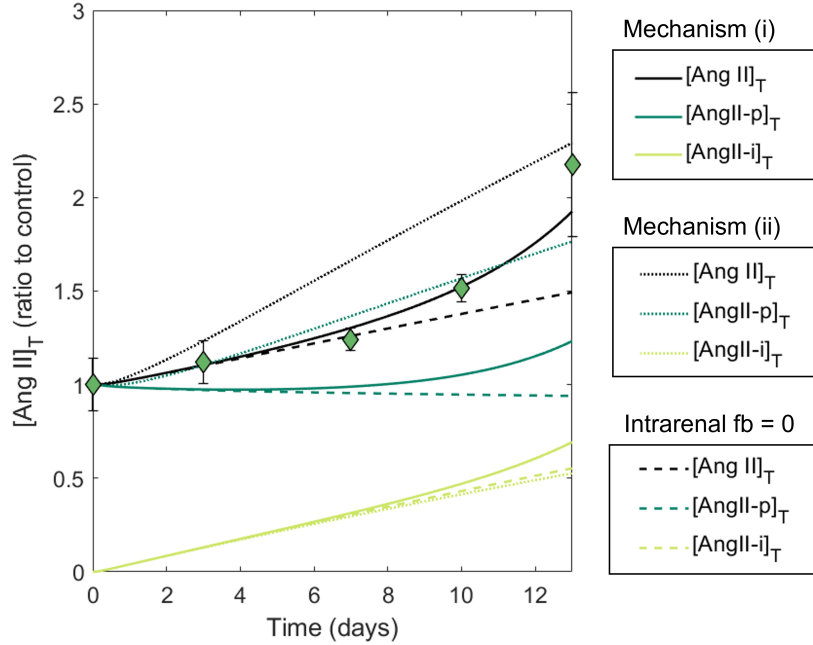


Figure 3.5: Model validation against whole kidney Ang II time series data following SC Ang II infusion (dose: 40 ng/min). Model simulations generated using mechanism (i) (solid curves), mechanism (ii) (dotted curves), and no intrarenal feedback ($fb_{Pt}^{AT1R} = 0$, Eq. A.21; $fb_{Tb}^{AT1R} = 0$, Eq. A.14; $fb_{Tb}^{AngI} = 0$, Eq. A.8; dashed curves) are shown. Mechanism (i) is required to observe a slow-rise in intrarenal [Ang II] (solid black curve) that is consistent with experimental results (Ref. [184]; diamonds).

Enhanced AT1R expression permits the intrarenal accumulation of endogenous Ang II during the second week of low-dose subcutaneous Ang II infusion By simulating the Ang II infusion experiment carried out by Zou et al. [184] in the absence and presence of intrarenal Ang II-dependent AT1R positive feedback, we can gain insight into its role in the development of Ang II-induced hypertension. Indeed, the model predicts that the feedback on AT1R expression is particularly important in the kidney during the second week of low-dose (40 ng/min) SC Ang II infusion: During the first week, exogenously-infused Ang II (Figure 3.5, light green curves) alone accounts for the majority of the increase in total renal [Ang II], even with all renal positive feedback removed (Figure 3.5, dashed curves). This is no longer true in the second week of infusion, where up-regulated AT1R expression is required for a sufficient concentration of endogenous Ang II (Figure

3.5, dark green curves) to accumulate in the kidney.

Given that the renal mechanisms that affect blood pressure are compartment specific, local changes to the distribution of renal angiotensin peptides may lead to blood pressure dis-regulation. Therefore, in the next section we investigate the distributional changes in renal [Ang II] that accompany Ang II infusion to gain insight into the development of Ang II-induced hypertension.

The accumulation of Ang II in tubular epithelial cells is likely crucial to the onset of Ang II-induced hypertension

Figure 3.6 illustrates the predicted temporal change in the renal distribution of [Ang II] during low-dose (40 ng/min) Ang II infusion. In a normotensive rat, the tubular compartment makes up the majority of the total renal [Ang II] (Figure 3.6a, time 0), with the highest concentration of peptides in the luminal fluid (Figure 3.6b, time 0). As shown in Figure 3.6, this does not change significantly over the first 5 days of low-dose SC Ang II infusion. However, at this point the exogenously infused Ang II has sufficiently increased the concentration of apical and basolateral-bound AT1R–Ang II complexes $[AT1R - \text{bound } AngII]_{Tb}^{Mem}$ and $[AT1R - \text{bound } AngII]_{Pt}^{Mem}$ over their steady states to activate the positive feedback on AT1R expression ($fb_{Tb}^{AT1R} > 0$ and $fb_{Pt}^{AT1R} > 0$; Eq.A.14 and A.21). As a result, a feed-forward loop is initiated, whereby increased AT1R expression leads to more AT1R–Ang II binding (Figure 3.6c) which results in more AT1R expression, and so on. Ultimately, more AT1R–Ang II complexes become internalized through both the apical and basolateral membranes of tubular epithelial cells, causing Ang II to accumulate in this intracellular compartment (Figure 3.6d). In particular, since the strength of the positive feedback on basolateral AT1R expression K_{Pt}^{AT1R} is greater than that of apical AT1R expression K_{Tb}^{AT1R} (Table 3.2), a greater proportion of Ang II accumulates via the basolateral membrane i.e. within the peritubular compartment. Interestingly, the time at which Ang II starts accumulating in the peritubular and tubular intracellular compartments of the model, i.e. in tubular epithelial cells, (day 6) coincides exactly with when the rats in Zou et al. [184]’s study started exhibiting a detectable increase in systolic blood pressure. This indicates that the accumulation of Ang II in tubular epithelial cells may play a key role in the development of Ang II-induced hypertension, likely through the stimulation of sodium reabsorption [46, 139, 50, 136].

3.3.3 Local sensitivity analysis

To determine the robustness of the aforementioned results, a local parametric sensitivity analysis was performed after simulating the Ang II infusion experiment performed by

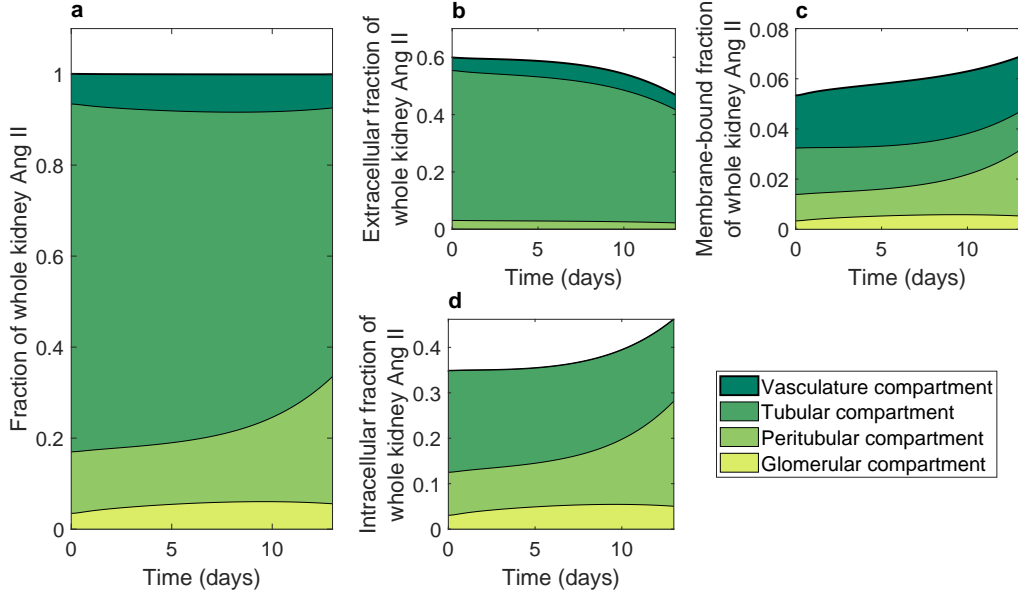


Figure 3.6: Temporal change in the renal distribution of [Ang II] throughout 13 days of SC Ang II infusion at 40 ng/min. Panels depict the relative contribution of each compartment to the: (a) total renal [Ang II], (b) extracellular fraction of renal [Ang II], (c) membrane-bound fraction of renal [Ang II], and (d) intracellular fraction of renal [Ang II].

Zou et al. [184]. Indeed, the percent change in all intrarenal and systemic RAS peptide concentrations on day 13 of the 40 ng/min infusion following a 10% increase in each model parameter were computed.

As shown in Figure 3.7, the model predictions following 13 days of SC 40 ng/min Ang II infusion are most sensitive to changes in the same baseline parameters (parameters that affect the model at steady state) that the model's steady state was (k_{AngI}^{Tb} , c_{ACE}^{Tb} , k_{meg} , k_{diff} ; see Section 2.4.1). Moreover, parameter changes that increase the rate of endogenous Ang II production at baseline (k_{AGT} , c_{chym} , v_{max} , k_{AngI}^{Tb} , and c_{ACE}^{Tb}) often decrease the concentration of tubular epithelial cell-associated Ang II. This is because the same amount of exogenous Ang II is entering these compartments, but there is more endogenous AT1R-bound Ang II at baseline. Hence, any exogenous AT1R-Ang II binding elicits a smaller fold-increase in the AT1R-bound Ang II concentration which blunts the positive feedback on AT1R expression fb_{Tb}^{AT1R} and fb_{Pt}^{AT1R} (Eq. 3.1) and leads to less cell-associated Ang II.

In terms of the feedback parameters, an increase in the rate of Ang II reabsorption from the SC tissue k_a has the most significant impact on the model predictions following Ang

II infusion (Fig 3.7). Indeed, the faster the exogenous Ang II is reabsorbed, the sooner all positive feedback gets activated allowing for greater accumulation of Ang II in the kidney and greater endogenous production in the plasma. The only other feedback parameter that notably affects the accumulation of Ang II in the kidney during infusion is the strength of the positive feedback on AT1R expression along the basolateral membrane of tubular epithelial cells K_{Pt}^{AT1R} . Indeed, a 10% increase in this parameter elicits a 25% increase in cell-associated Ang II in the peritubular compartment. As a result, 7% more Ang II accumulates in the kidney during the Ang II infusion. A similar effect is observed when the strength of the AT1R expression feedback along the apical membrane K_{Tb}^{AT1R} is increased. However, given its smaller original value, a 10% increase in this parameter elicits only a 4% change in cell-associated Ang II in the tubular compartment. This isn't enough to significantly alter the whole kidney [Ang II].

In future work, it would be beneficial to additionally perform a global parametric sensitivity analysis, whereby the impact of concerted parameter changes on the model predictions are examined.

3.4 Discussion

The primary goal of this Chapter was to gain insight into the role of the intrarenal RAS in the development of hypertension induced by Ang II infusion. To accomplish this, the mathematical model of the RAS presented in Chapter 2 was extended to include both intrarenal and systemic positive feedback and then used to simulate Ang II infusion experiments following its validation. In particular, the low dose (40 ng/min), 13 day subcutaneous Ang II infusion experiment carried out by Zou et al. [184] was replicated and the results were examined in detail.

AT1R-mediated uptake of circulating Ang II and enhanced endogenous Ang II generation have both been suggested as key mechanisms contributing to enhanced renal accumulation of Ang II during the development of hypertension [71, 109, 141, 142, 159, 180, 70, 35, 40]. Model simulations suggest that AT1R-mediated uptake of Ang II into **tubular epithelial cells** is the primary mechanism by which Ang II accumulates in the kidney during low-dose Ang II infusion, and that enhanced local Ang II production is not required (see below). This is consistent with the findings of Zhuo et al. [180], who found that blocking AT1R–Ang II binding via **ARB** administration not only prevents the accumulation of Ang II in renal intracellular endosomes, but in the entire kidney itself. We also determined that this effect requires an Ang II–mediated increase in AT1R expression, mainly along the basolateral membrane of these cells. This result is also corroborated by Zhuo et al.

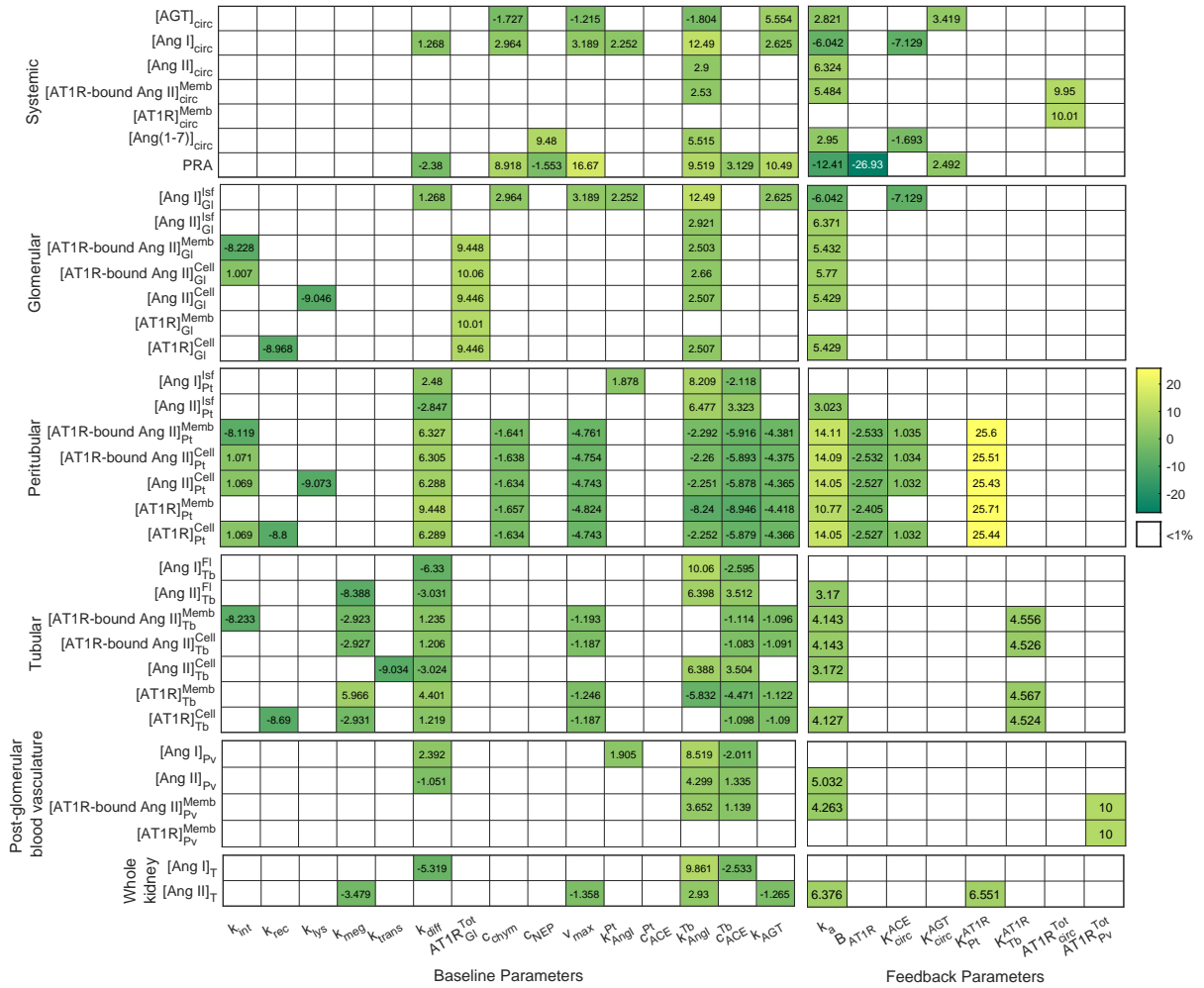


Figure 3.7: Percent change in the predicted systemic and intrarenal RAS concentrations after 13 days of 40 ng/min SC Ang II infusion to a 10% increase in each parameter value.

[180], who found that increased AT1R expression in renal endosomes is, at least in part, responsible for the observed increase in intracellular trafficking of Ang II into renal intracellular endosomes following Ang II infusion. An Ang II-dependent increase in proximal tubule AT1R expression has also been reported by other sources [182, 21], though to our knowledge, its functional role had yet to be discussed until now. Our results suggest that this feedback is likely crucial to the development of hypertension because it permits the intracellular accumulation of Ang II in tubular epithelial cells (see below).

Notably, Ang II was able to accumulate in the simulated kidney without the need to explicitly increase the local endogenous production of Ang II. In fact, more endogenous than exogenous Ang II accumulated in tubular epithelial cells once AT1Rs were up-regulated because the predicted basal rate of endogenous production of Ang II in the kidney exceeded the rate of exogenous Ang II entry into the kidney. An explicit increase to the rate of endogenous Ang II production was not required for this to be true and instead resulted in excess endogenous and insufficient exogenous Ang II accumulation at a rate that far exceeded experimental findings. An assumed constant renal renin activity was instead sufficient because it ensured that the renal [Ang I] and thus the local endogenous production of Ang II decreased only slightly during the infusion, despite the significant decrease in plasma [Ang I]. It is thus likely that the Ang II-dependent AGT amplification mechanism that has been reported in the proximal tubule [107, 109, 70, 40, 72, 138] primarily contributes to the maintenance of renal renin activity [141]. It does not necessarily result in increased endogenous Ang II production above baseline. An elevated renal AGT concentration is able to influence renal renin activity because the kidney expresses pro-renin receptors that reduce the Michaelis constant for renin–AGT binding [111, 110, 12, 163]. This is not the case in the plasma, where we showed that hepatic AGT amplification [91, 138, 106] had an inconsequential effect on PRA and thus, the systemic RAS. We thus hypothesize that this systemic positive feedback mainly influences the intrarenal RAS, since hepatic AGT has been reported as the primary source of AGT in the kidney [98].

In addition to the hepatic AGT positive feedback [91, 138, 106], model simulations suggest that systemic ACE activity is likely also up-regulated by Ang II. Firstly, while sufficient endogenous Ang II was able to accumulate in the kidney without increasing local Ang II production, this was no longer the case in the plasma. Indeed, without enhanced systemic Ang II production, the experimentally measured endogenous concentration of plasma Ang II [141, 142] was under-predicted by the model. Secondly, the reduction in PRA resulting from the Ang II-dependent feedback on renin secretion from the [juxtaglomerular apparatus](#) was not sufficient to cause the drop in plasma [Ang I] that was observed experimentally in Ref. [184]. Indeed, without enhanced ACE activity (and thus, more rapid degradation of Ang I), the plasma [Ang I] far exceeded what the data suggested. While similar feedback has been documented in the kidney [132, 73], future experiments are required to confirm its existence in the systemic circulation.

Finally, we found that the simulated onset of Ang II accumulation in tubular epithelial cells coincided exactly with the experimental inception of hypertension on day 6 of the Ang II infusion experiment performed by [184]. The model thus suggests that the delayed rise in blood pressure is the result of the time it takes for the positive feedback on renal AT1R expression to be sufficiently activated by exogenous Ang II and consequently, for

Ang II to begin accumulating within tubular epithelial cells. Hence, it is likely that the stimulation of sodium reabsorption [46, 50, 139, 136] following the association of Ang II with these cells plays a crucial role in the development of hypertension. This hypothesis will be further explored in Chapter 5 by coupling our intrarenal RAS model to Ahmed and Layton [1]’s whole-body model of blood pressure regulation that considers cardiovascular function, renal hemodynamics, renal sodium and fluid handling, the renal sympathetic nervous system, and the connections between these systems.

3.4.1 Model limitations and future extensions

The main limitation of this model is that it considers the intrarenal and systemic RAS in isolation, when in reality these systems influence and are influenced by many other physiological processes. For example, an increase in renal Ang II is known to affect renal hemodynamic function by increasing afferent and efferent arteriole resistance [1, 173, 25]. This results in an increased filtration fraction (lower renal blood flow, sustained glomerular filtration rate) [154, 25], which will in turn affect the intrarenal distribution of Ang II. This cascade of events is not captured by the present model, which assumes that all renal hemodynamic parameters are known *a priori* and as such are unaffected by Ang II infusion. In future work, the model can be extended to consider all renal hemodynamic flow rates and volumes as variables instead of parameters. In this way, the interplay between Ang II and renal hemodynamics can be incorporated and investigated in detail.

A key consequence of the model’s limited scope is that the downstream effects of altered systemic and renal RAS peptide concentrations are not modelled explicitly. We are thus forced to make assumptions about blood pressure based on prior knowledge of the processes affected by local Ang II concentrations (e.g. sodium reabsorption), without modelling mean arterial pressure directly. As discussed above, this limitation is addressed in Chapter 5 by incorporating the present intrarenal RAS model into Ahmed and Layton’s whole-body blood pressure regulation model [1]. Using the resulting more comprehensive model, the effect of intrarenal Ang II accumulation on mean arterial pressure is studied explicitly.

The effects of anti-hypertensive therapies on the intrarenal RAS can also be studied in the future by creating PK models of various drugs of interest and coupling them to the intrarenal RAS model presented here. In Chapter 4, this is done for the ARB Losartan. However, future work could focus on other classes of anti-hypertensive therapies such as the ACEi.

By fine-tuning its excretory function, the kidney plays a predominant role in blood pressure regulation [44]. Indeed, transplantation studies have demonstrated that hyper-

tension follows the kidney [41]. As such, the mechanisms by which intrarenal RAS regulate blood pressure can be examined by coupling the present model to a kidney function model that simulates epithelial transport of electrolytes and water, such as those by Refs. [77], [75], [140], [29], and [19]. The coupling can be formulated based on the known connections between Ang II, AT1Rs, and ion transport [11, 157]. The RAS-mediated electrolyte transport predicted by the kidney model can modulate glomerular filtration rate via the tubuloglomerular feedback [28, 74], thereby influencing intrarenal RAS distribution.

The current intrarenal RAS model does not consider sex differences, even though it has been long established that the steady state concentrations of most systemic RAS peptides differ between males and females [119], and each sex responds differently to antihypertensive therapies that target the RAS [84]. To account for and explain these disparities, Leete et al. [84] parameterized separate computational models of the systemic RAS for male and female rats. In future work, our intrarenal RAS model could also be extended to account for the known sex differences that exist both at the systemic and intrarenal level using the experimental measurements collected by Pendergrass et al. [119]. A key requirement of this model would be the addition of angiotensin type 2 receptors (AT2Rs), given their lower expression levels in males than females [119] and their hypothesized involvement in sex-specific anti-hypertensive therapy responses [84]. This extension would not only be beneficial for studying sex-differences in the intrarenal RAS, but also the role of AT2Rs in the kidney in hypertension in general. Nevertheless, a sex-specific model could be used to infer sex-differences that exist at the compartmental level (tubular fluid, interstitial space, vasculature, etc.), based on the whole-tissue peptide concentrations that are available [119]. The sex-specific intrarenal RAS models could also later be coupled to a sex-specific blood pressure regulation model [1], a sex-specific epithelial solute transport model [92, 56, 57, 58], or a sex-specific renal blood flow model [20] to study whether the roles of the intrarenal RAS in hypertension and renal function differ between the sexes.

Finally, the present model does not represent the circadian rhythms long observed in the systemic RAS [52] and likely present in the intrarenal RAS. By expanding the present model to incorporate circadian variations in appropriate model parameters, and possibly coupling the resulting RAS model to a kidney function model that represents circadian rhythms [76, 164], the resulting integrative model can be a useful tool for studying the circadian regulation of blood pressure and how its disruption may contribute to the pathogenesis of hypertension [27].

Chapter 4

Angiotensin-receptor blockers and the intrarenal renin angiotensin system in hypertension: A PK/PD modelling study

Abstract

Hypertension is the leading cause of cardiovascular disease and premature death worldwide. Although it is a highly complex and multi-factorial condition, anti-hypertensive therapies that target the RAS are commonly prescribed and often highly effective in restoring normo-tension [60]. However, little is known about how these medications influence the intrarenal RAS. Angiotensin-receptor blockers (ARBs) in particular have been shown to attenuate the rise in intrarenal Ang II observed in various experimental models of hypertension associated with an over-active RAS. The inhibition of all positive feedback loops inherent to the intrarenal RAS, also known as the key point breakdown effect, has been hypothesized to mediate this response. Here, we investigate the validity of this hypothesis using computational modelling. Indeed, a PK/PD model of the ARB Losartan that considers the kidney was developed and used to study how this class of medication influences intrarenal RAS activity, and consequently blood pressure regulation in male rats. Simulations indicate that although the key point break down effect is indeed what prevents intrarenal Ang II levels from rising under concurrent Ang II and Losartan administration,

this alone is likely not responsible for the drug’s blood pressure normalizing effects. Instead, we hypothesize that Losartan administration restores normotension by restricting Ang II to regions of the kidney where the peptide cannot initiate any downstream signalling. Indeed, there was a drastic shift in the intrarenal distribution of Ang II from primarily cell-associated to primarily free (extracellular) peptides following Losartan treatment *in silico*. The results highlight the specific impact of ARBs on intrarenal RAS activity and elucidate the mechanisms underlying their effectiveness as an anti-hypertensive therapy.

4.1 Introduction

Although hypertension is a highly complex and multi-factorial condition, anti-hypertensive therapies that target the RAS are often highly effective treatment strategies [60], due to the long established role of the RAS in blood pressure regulation [36]. Despite the fact that many hypertensive actions of Ang II take place within the kidney (Figure 1.2b), little is known about the impact of these medications on the intrarenal RAS specifically.

The intrarenal accumulation of Ang II that is observed in Ang II-induced hypertensive rats, and whose mechanisms were studied in Chapter 3, is prevented by treatment with ARBs. ARBs are a common anti-hypertensive medication that targets the RAS by binding to and blocking AT1Rs. *How does this class of medication influences the activity of the intrarenal RAS?* Addressing this question would significantly improve our understanding of clinical hypertension, and that can have wide benefits, given the commonality of intrarenal RAS over-activation across pre-clinical hypertensive models and the effectiveness of ARBs as an anti-hypertensive treatment strategy.

It has been hypothesized that ARBs regulate intrarenal Ang II levels by inhibiting all positive feedback loops inherent to the intrarenal RAS, including the up-regulation of proximal tubule angiotensinogen (AGT), collecting duct renin, and tubular epithelial cell AT1R expression. This is also known as the “key point break down effect” [170]. An objective of this Chapter is to investigate the validity of this hypothesis. This is accomplished by coupling our comprehensive model of the rat intrarenal RAS that incorporates each of these feedback loops to a pharmacokinetic model of an ARB. In particular, we simulate and compare Ang II infusion experiments with and without ARB treatment, to study two clinically relevant questions: (i) *Which Ang II accumulation mechanism, enhanced AT1R-mediated uptake (UPTK) or increased endogenous production (PROD), is the primary target of ARB treatment?* (ii) *How does this influence the general activity of the intrarenal RAS, and therefore blood pressure regulation?*

To accomplish the aforementioned goals, we simulate the Ang II infusion experiments of Zou et al. [184], which were performed with and without continuous treatment with [Losartan](#). Losartan was the first ARB prescribed to treat clinical hypertension, and remains an important drug in basic and clinical research today [170]. Following its oral administration, Losartan is reabsorbed from gastrointestinal tract into the systemic circulation where, after entering the liver, it becomes metabolized into EXP3174 by cytochrome p450 enzymes [151]. Both Losartan and its metabolite EXP3174 are competitive antagonists that selectively bind AT1Rs with a high affinity [104, 170].

In published computational models, the effect of Losartan on the RAS is often represented implicitly via a parameter that reduces Ang II-AT1R binding by an arbitrary target amount [84]. However, because we wish to simulate specific Losartan administration experiments, where the change in AT1R-bound Ang II in all compartments (systemic and intrarenal) is not explicitly quantified, the same approach cannot be applied in this case. Instead, a pharmacokinetic model describing Losartan and its metabolite EXP3174 is desirable, as it can be coupled to our RAS model from Chapter 2 via the drug’s known AT1R binding properties. Such a model has previously been developed to study gastric emptying [65]. However, that model simulates a single oral dose of the drug (not continuous treatment with Losartan), and does not consider the kidney as a separate compartment (thus not appropriate for studying intrarenal RAS) .

In this Chapter, we develop a novel pharmacokinetic model of Losartan and its bio-active metabolite EXP3174 in rats and we couple this model to our existing intrarenal RAS model. The combined model is then used to simulate the Losartan administration experiments performed by [184]. Simulation results elucidate the mechanisms by which ARBs effectively target the intrarenal RAS to prevent its dis-regulation and consequently, the development of hypertension following Ang II infusion.

4.2 Methods

4.2.1 Pharmacokinetic model

The PK model considers [Losartan](#) and [EXP3174](#) dynamics in the rat across four compartments: the [gastrointestinal \(GI\)](#) tissue compartment, the systemic vasculature compartment, the peripheral tissue compartment, and the renal tissue compartment. Orally-administered Losartan first enters the GI compartment, before being absorbed into the systemic blood plasma (the systemic vasculature compartment) where a portion is converted into its bio-active metabolite EXP3174 by cytochrome p450 enzyme activity [151].

Both Losartan and its metabolite are then re-distributed into the poorly perfused organs (the peripheral tissue compartment) and the kidney (the renal tissue compartment). The renal compartment is divided into the same tissue sub-compartments as the intrarenal RAS model outlined in Chapter 2: the glomerular sub-compartment, the peritubular sub-compartment, the tubular sub-compartment, and the vasculature sub-compartment (Figure 2.1). The pharmacokinetic model is coupled to that of the intrarenal RAS through Losartan and EXP3174-AT1R-binding in the systemic and intrarenal compartments (see Section 4.2.2). The equations used to model the concentrations of Losartan and EXP3174 in each compartment are described in detail below, with a schematic diagram provided in Figure 4.1.

Gastrointestinal tissue compartment

The rate of change of the amount of Losartan in the GI compartment, Los_{GI} , is determined by the balance between the drug's administration rate K_{Los} and its absorption into the systemic compartment with rate k_a^{Los} :

$$\frac{dLos_{GI}}{dt}(t) = K_{Los}(\text{dose}, t) - k_a^{Los} Los_{GI}(t) \quad (4.1)$$

We simulate two different modes of drug delivery; via a single oral dose and in drinking water. The respective simulations differ in their definition of the source term $K_{Los}(D, t)$ and the initial condition $Los_{GI}(0)$. To simulate a single oral dose D (fmol) of Losartan, we set

$$K_{los}(D, t) = 0 \text{ and } Los_{GI}(0) = D$$

Thus, the given dose of Losartan is absorbed into the systemic compartment upon being administered at $t = 0$. To simulate a dose D (fmol) of Losartan administered in drinking water each day, we set

$$K_{los}(D, t) = \begin{cases} \frac{D}{\Delta t} & \text{if } t \leq \Delta t \\ 0 & \text{if } t > \Delta t \end{cases}$$

where $\Delta t = 12$ hours and $Los_{GI}(0) = 0$. Indeed, the rat is assumed to be awake, constantly drinking water during the first 12 hours of the day and asleep for the remaining 12 hours. In this way, they consume their entire daily dose of Losartan in their awake period. To simulate a drug administered in drinking water over multiple days, we run the model iteratively, using the last time point of the previous iteration as the initial condition for the next iteration.

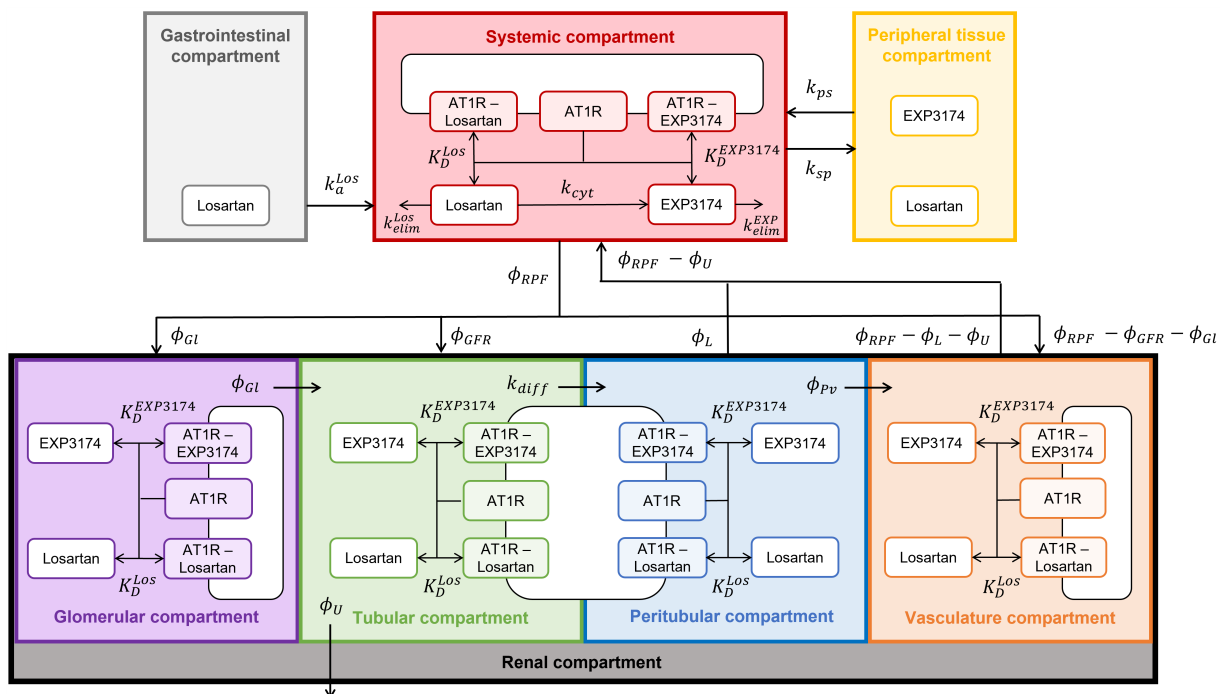


Figure 4.1: Schematic representation of the pharmacokinetic model. The definition of all variables can be found in the text. Orally-administered Losartan enters the circulation (systemic compartment; red) via absorption from the gastrointestinal compartment (light grey) where a portion is converted into its bio-active metabolite EXP3174 by cytochrome p450 enzymes. These molecules are then re-distributed into the poorly perfused organs (the peripheral tissue compartment; yellow) and the kidney (the renal compartment; black). In the kidney, the molecules may either bind to regional AT1Rs, be excreted in urine (at a rate of ϕ_U), or get reabsorbed back into the systemic compartment.

Systemic vasculature compartment

Losartan begins accumulating in the systemic plasma upon being reabsorbed from the GI compartment with rate k_a^{Los} . In plasma, Losartan can be converted to EXP3174 by cytochrome p450 enzymes [151] with rate k_{cyt} , degraded naturally with rate k_{elim}^{Los} , redistributed to the peripheral compartment with rate k_{sp} , or filtered into the kidney (the renal compartment) at a rate proportional to renal plasma flow ϕ_{RPF} (scaled by the ratio of kidney weight W_K to circulating plasma volume V_{circ}). Losartan subsequently returns to the systemic circulation from the peripheral compartment at rate k_{ps} , the peritubular in-

terstitial space at a rate proportional to lymphatic flow ϕ_L , and the renal (post-glomerular) blood vasculature at a rate proportional to $\phi_{RPF} - \phi_L - \phi_U$. Finally, plasma Losartan may to bind to and unbind from systemic AT1Rs (Eq. 4.7) with rates k_{ass}^{Los} and k_{diss}^{Los} , respectively.

$$\begin{aligned}
\frac{d[Los]_{circ}}{dt}(t) &= \frac{k_a^{los}}{V_{circ}} LOS_{GI}(t) - \left(\frac{W_K}{V_{circ}} \phi_{RPF} + k_{sp} + k_{cyt} + k_{elim}^{los} \right) [Los]_{circ}(t) \\
&+ k_{ps}[Los]_{peri}(t) + \frac{W_K}{V_{circ}} \phi_L [Los]_{Pt}^{Ext}(t) \\
&+ \frac{W_K}{V_{circ}} (\phi_{RPF} - \phi_L - \phi_U) [Los]_{Pv}(t) \\
&+ k_{diss}^{Los} [AT1R - bound Los]_{circ}^{Memb}(t) \\
&- k_{ass}^{Los} [AT1R]_{circ}^{Memb}(t) [Los]_{circ}(t)
\end{aligned} \tag{4.2}$$

In the systemic plasma, EXP3174 is produced from Losartan via cytochrome p450 enzyme activity with rate k_{cyt} . Otherwise EXP3174 behaves identically to Losartan in this compartment, differing only in the rate of elimination k_{elim}^{exp} , AT1R binding $k_{elim}^{EXP3174}$, and AT1R unbinding $k_{diss}^{EXP3174}$.

$$\begin{aligned}
\frac{d[EXP3174]_{circ}}{dt}(t) &= k_{cyt}[Los]_{circ}(t) - \left(\frac{W_K}{V_{circ}} \phi_{RPF} + k_{sp} + k_{elim}^{EXP3174} \right) [EXP3174]_{circ}(t) \\
&+ k_{ps}[EXP3174]_{peri}(t) + \frac{W_K}{V_{circ}} \phi_L [EXP3174]_{Pt}^{Ext}(t) \\
&+ \frac{W_K}{V_{circ}} (\phi_{RPF} - \phi_L - \phi_U) [EXP3174]_{Pv}(t) \\
&+ k_{diss}^{EXP3174} [AT1R - bound EXP3174]_{circ}^{Memb}(t) \\
&- k_{ass}^{EXP3174} [AT1R]_{circ}^{Memb}(t) [EXP3174]_{circ}(t)
\end{aligned} \tag{4.3}$$

Peripheral tissue compartment

Both Losartan and EXP3174 are assumed to enter and exit the peripheral compartment at the same rates of k_{sp} and k_{ps} , respectively. Consequently the rate of change of the

peripheral concentration of metabolite X ($X = Los$, EXP3174) is given by:

$$\frac{d[X]_{peri}}{dt}(t) = k_{sp}[X]_{circ}(t) - k_{ps}[X]_{peri}(t) \quad (4.4)$$

Renal tissue compartment

In the kidney, the concentration of Losartan and EXP3174 is described by their redistribution among the extracellular regions of the intrarenal sub-compartments and their association/dissociation with local membrane-bound AT1Rs. The structure of the equations describing the dynamics of each metabolite is similar to that of Ang I and II in the intrarenal RAS model and as such, is similar across all intrarenal sub-compartments. Therefore, as done in Section 2.1, we introduce a general equation describing the rate of change of extracellular Losartan ($X = Los$) and EXP3174 ($X = EXP3174$) in compartment C below, where $C = Gl, Tb, Pt$, or Pv .

$$\begin{aligned} \frac{d[X]_C^{Ext}}{dt}(t) = & \frac{1}{V_C^{Ext}} \left(\sum_j Q_{inj}^{C_{Ext}} [X]_{C_{inj}}^{Ext}(t) - Q_{out}^{C_{Ext}} [X]_C^{Ext}(t) \right) \\ & + k_{diss}^X [AT1R - bound X]_C^{Ext}(t) - k_{ass}^X [X]_C^{Ext}(t) [AT1R]_C^{Ext}(t) \end{aligned} \quad (4.5)$$

The first line represents the balance between the j fluxes into sub-compartment C_{Ext} from sub-compartment C_{inj}^{Ext} with rate $Q_{inj}^{C_{Ext}}$ and the flux out of sub-compartment C_{Ext} with rate $Q_{out}^{C_{Ext}}$. The number of incoming fluxes j differs for each compartment, as summarized in Table 4.1. V_C^{Ext} is a parameter describing the volume of each extracellular sub-compartment. All flux rates and volume parameters are consistent with those of the intrarenal RAS model (Table 2.2). The last line of Eq. 4.5 represents the unbinding and binding of metabolite X to membrane-bound AT1Rs with rates k_{diss}^X and k_{ass}^X , respectively.

For the complete set of model equations in the renal compartment, see Appendix B. For a detailed schematic of the PK model, see Figure 4.1.

4.2.2 Coupling the RAS and pharmacokinetic models

As aforementioned, the PK model is coupled to that of the RAS through Losartan- and EXP3174-AT1R binding in the systemic and renal model compartments. We assume for simplicity that membrane-bound AT1R-Losartan and AT1R-EXP3174 complexes are not

C	$Q_{inj}^{C_{Ext}}$	$[X]_{C_{inj}}^{Ext}(t)$	$Q_{out}^{C_{Ext}}$
Gl	ϕ_L	$[X]_{circ}(t)$	ϕ_L
Tb	ϕ_{GFR} ϕ_{Gl}	$[X]_{circ}(t)$ $[X]_{Gl}^{Ext}(t)$	$k_{diff} + \phi_U$
Pt	k_{diff}	$[X]_{Pt}^{Ext}(t)$	$\phi_{Pv} + \phi_L$
Pv	$\phi_{RPF} - \phi_{GFR} - \phi_{Gl}$ ϕ_{Pv}	$[X]_{circ}(t)$ $[X]_{Pt}^{Ext}(t)$	$\phi_{RPF} - \phi_L - \phi_U$

Table 4.1: Intrarenal sub-compartment-specific parameters corresponding to Eq. 4.5.

internalized. In this way, the dynamics of these complexes are described by substrate-receptor association and dissociation with rates k_{ass}^X and k_{diss}^X , respectively, where $X = Los$ or EXP3174:

$$\begin{aligned} \frac{d[AT1R - \text{bound } X]_C^{Memb}}{dt}(t) &= k_{ass}^X [AT1R]_C^{Memb}(t) [X]_C^{Ext}(t) \\ &\quad - k_{diss}^X [AT1R - \text{bound } X]_C^{Memb}(t) \end{aligned} \quad (4.6)$$

In this general equation, $C = circ, Gl, Pt, Tb$, or Pv . To account for AT1R binding to Losartan and EXP3174 in the RAS model, we update the previous equations describing membrane-bound free AT1R dynamics in all compartments as follows:

$$\begin{aligned} [AT1R]_{circ}^{Memb}(t) &= [AT1R]_{circ}^{Tot} - [AT1R - \text{bound } AngII]_{circ}^{Memb}(t) \\ &\quad - [AT1R - \text{bound } Los]_{circ}^{Memb}(t) \\ &\quad - [AT1R - \text{bound } EXP3174]_{circ}^{Memb}(t) \end{aligned} \quad (4.7)$$

$$\begin{aligned}
V_{Gl}^{Exp}[AT1R]_{Gl}^{Memb}(t) &= AT1R_{Gl}^{Tot} \\
&\quad - V_{Gl}^{Exp}[AT1R - \text{bound } AngII]_{Gl}^{Memb}(t) \\
&\quad - V_{Gl}^{Cell}[AT1R - \text{bound } AngII]_{Gl}^{Cell}(t) \\
&\quad - V_{Gl}^{Cell}[AT1R]_{Gl}^{Cell}(t) \\
&\quad - V_{Gl}^{Exp}[AT1R - \text{bound } Los]_{Gl}^{Memb}(t) \\
&\quad - V_{Gl}^{Exp}[AT1R - \text{bound } EXP3174]_{Gl}^{Memb}(t)
\end{aligned} \tag{4.8}$$

$$\begin{aligned}
[AT1R]_{Pv}^{Memb}(t) &= [AT1R]_{Pv}^{Tot} \\
&\quad - [AT1R - \text{bound } AngII]_{Pv}^{Memb}(t) \\
&\quad - [AT1R - \text{bound } Los]_{Pv}^{Memb}(t) \\
&\quad - [AT1R - \text{bound } EXP3174]_{Pv}^{Memb}(t)
\end{aligned} \tag{4.9}$$

$$\begin{aligned}
\frac{d[AT1R]_C^{Memb}}{dt}(t) &= k_{diss}[AT1R - \text{bound } AngII]_C^{Memb}(t) \\
&\quad - k_{ass}[AT1R]_{Tb}^{Memb}(t)[AngII]_C^{Ext}(t) \\
&\quad + k_{rec} \frac{V_C^{Ext}}{V_{Pt,Tb}^{Cell}} [AT1R]_C^{Cell}(t) \\
&\quad + fb_C^{AT1R} (R_C^{Memb}(t)) \\
&\quad + k_{diss}^{Los}[AT1R - \text{bound } Los]_{Tb}^{Memb}(t) \\
&\quad - k_{ass}^{Los}[AT1R]_{Tb}^{Memb}(t)[Los]_{Tb}^{Ext}(t) \\
&\quad + k_{diss}^{EXP3174}[AT1R - \text{bound } EXP3174]_{Tb}^{Memb}(t) \\
&\quad - k_{ass}^{EXP3174}[AT1R]_{Tb}^{Memb}(t)[EXP3174]_{Tb}^{Ext}(t)
\end{aligned} \tag{4.10}$$

where $C = Tb$ or Pt .

To facilitate running Losartan administration experiments *in silico*, we also modify the secretion of renin from the [juxtaglomerular apparatus](#) such that the strength (B_{AT1R} ; Eq. 4.11) of the AT1R- and Ang II-dependent feedback (ν_{AT1R} ; Eq. 2.13) can differ in a situation where renin is meant to increase or decrease, i.e. when AT1R-bound Ang II decreases or increases, respectively. In the previous formulation, the fitting of B_{AT1R} was restricted to a situation where renin secretion was meant to decrease, i.e. Ang II infusion experiments. In contrast, following Losartan administration renin secretion is expected to increase. Hence, we allow B_{AT1R} to depend on the ratio of $[AT1R - \text{bound } AngII]_{Gl}^{Memb}$ to control ($R_{Gl}^{Memb}(t)$), such that:

$$B_{AT1R}(R_{Gl}^{Memb}(t)) = \begin{cases} B_{AT1R}^+ & \text{if } R_{Gl}^{Memb}(t) \leq 1 \\ B_{AT1R}^- & \text{if } R_{Gl}^{Memb}(t) > 1 \end{cases} \quad (4.11)$$

We take $B_{AT1R}^- = 2.9$, the value previously fit to Ang II infusion data (Table 3.1) in Chapter 3. We determine B_{AT1R}^+ using Losartan administration data (Section 4.2.3).

Finally, we maintain the assumption that renal renin activity k_{AngI}^C remains constant following Losartan administration. This has been observed experimentally in the case of Ang II infusion [141]. However, to our knowledge, similar data is not available following Losartan treatment. We therefore base this assumption on the results presented in Chapter 3, that implicit positive feedback on intrarenal AGT and renin production counteracts the decrease in filtered renin from the systemic circulation. Given this, it seems plausible that any increase in filtered renin (caused by an increase in PRC following Losartan treatment) is also balanced by the inhibition of local intrarenal AGT and renin production.

4.2.3 Model parameter identification

The compartment volume and renal hemodynamic parameters present in the [PK](#) model were taken directly from the RAS model's parameter set (Table 2.2). It was assumed that the rate of association of AT1Rs with Losartan and EXP3174 was the same as Ang II, i.e. that $k_{ass}^{Los} = k_{ass}^{EXP3174} = k_{ass} = 2.4 \times 10^{-5}$ /fmol/mL per min [135]. The dissociation rates for each metabolite X ($X = Los, EXP3174$) were then computed using the expression $k_{diss}^X = k_{ass} K_D^X$, where K_D^X is the dissociation constant of metabolite X reported in the literature ($K_D^{Los} = 10.6\text{nM}$, $K_D^{EXP3174} = 4.7\text{nM}$) [104]. The remaining model parameters

(apart from B_{AT1R}^+) were estimated by simulating a single oral dose (10 mg/kg) of Losartan and minimizing the error (Eq. 3.9) between the simulated and experimental plasma drug concentration time series from Ref. [90]. MATLAB’s nonlinear programming solver `fmincon` was used for the optimization. Lastly, B_{AT1R}^+ was identified by administering 30 mg/kg of Losartan per day in drinking water to the model and comparing the average fold-change in PRA on day 13 to the data from Ref. [184].

4.3 Results

4.3.1 Model parameter identification

Parameter	Description	Value	Unit
k_a^{Los}	Rate constant for Losartan absorption from the GI compartment	0.023	/min
k_{cyt}	Rate of EXP3174 formation from Losartan from cytochrome P450 enzymes	0.602	/min
k_{sp}	Rate of distribution into the peripheral compartment	8.95	/min
k_{ps}	Rate of re-distribution into the systemic compartment	0.060	fmol/g kidney
k_{elim}^{Los}	Rate of Losartan elimination from the systemic compartment	0.00020	/min
$k_{elim}^{EXP3174}$	Rate of EXP3174 elimination from the systemic compartment	0.32	/min
B_{AT1R}^+	Strength of Ang II–AT1R feedback on renin secretion when the [complex] decreases	0.545	–

Table 4.2: Losartan-EXP3174 pharmacokinetic model parameters

As outlined in section 4.2.3, a single oral dose (10 mg/kg) of Losartan was administered to the model and the sum of squared errors (Eq. 3.9) between the true and simulated plasma [Losartan] and plasma [EXP3174] time series was minimized to identify the model parameters. The optimized parameter set is given in Table 4.2, with the simulated (curves) and true time series (markers) shown in Figure 4.2.

Below, fitting results specific to the strength of Ang II-AT1R feedback on renin secretion B_{AT1R}^+ are detailed and the model is validated against the remaining Ang II infusion and Losartan administration experimental data from Ref. [184].

4.3.2 Model validation

In addition to the Ang II infusion experiment (experiment (i): *Ang II*) detailed in Chapter 3, Zou et al. [184] also performed two Losartan administration experiments, where 30

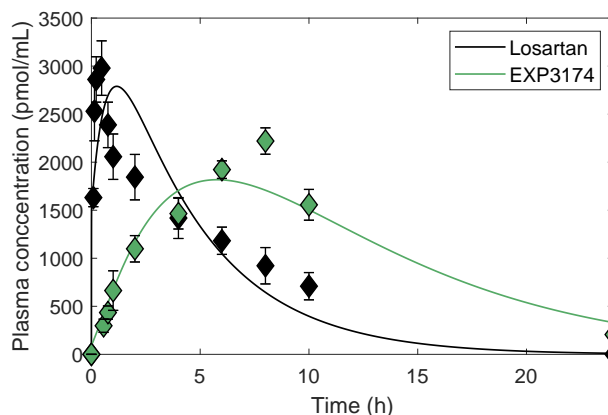


Figure 4.2: Model fit (curves) to plasma Losartan and EXP3174 concentration time series data (markers) following a single oral dose (10 mg/kg) of Losartan.

mg/kg of Losartan was administered per day in drinking water either alone (experiment (ii): *Losartan*) or in conjunction with 40 ng/min of Ang II (experiment (iii): *Ang II + Losartan*). Replicating these experiments *in silico* forms an important step towards the validation of our model.

Figure 4.3 compares the results of each simulated experiment to the data that was collected by Zou et al. [184]. In particular, the average (day 13) simulated (wide bars) and experimental (narrow bars) RAS peptide concentrations are compared to their control values (i.e. the model steady state; Table 2.5). The results of experiment (i) have already been detailed previously in Chapter 3 and are therefore shown for comparison purposes. All data points relating to experiments (ii) and (iii), apart from the increase in PRA under Losartan administration alone (Figure 4.3, starred bar) which was used to fit B_{AT1R}^+ (see Section 4.2.3), were kept for model validation. In general, the simulations show good agreement to data, capturing the experimental trends well. This not only speaks to the robustness of the coupled model, whose PK parameters were identified using data obtained via a different drug administration route (single oral dose vs. in drinking water) and over a different time scale (1 day vs. 2 weeks), but also to the adaptability of the original RAS model, whose parameters (apart from the addition of B_{AT1R}^+) did not need to be modified to accurately predict the variations in systemic and intrarenal RAS peptides that are induced by Losartan.

Model simulations indicate that once administered, Losartan and EXP3174 rapidly bind to systemic and intrarenal AT1Rs, significantly reducing the concentration of AT1R–

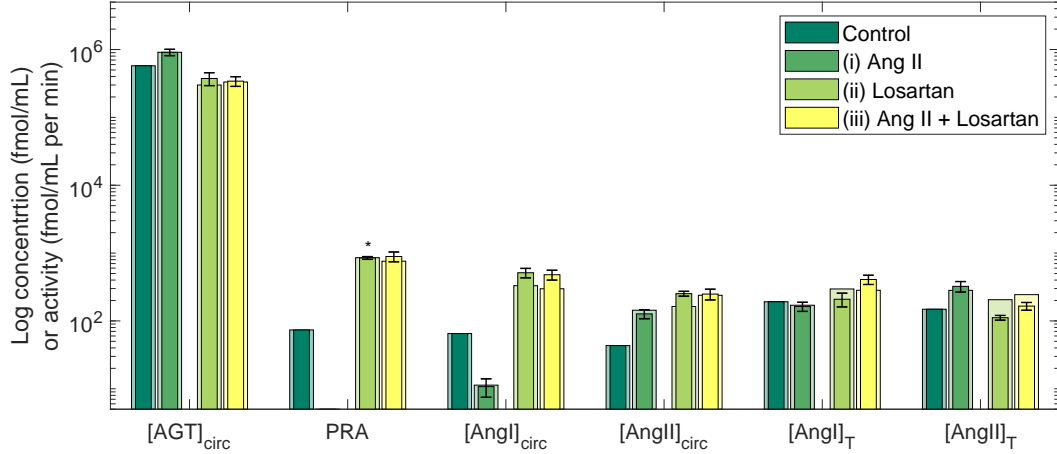


Figure 4.3: Model validation (wide bars) against RAS peptide data (experimental) on day 13 of experiment (i): 40 ng/min subcutaneous Ang II infusion; experiment (ii): 30 kg/mg/day Losartan administration in drinking water; and experiment (iii): 40 ng/min subcutaneous Ang II infusion alongside 30 kg/mg/day Losartan administration in drinking water of Ref. [184]. Control (steady state) concentrations are also provided for comparison.

bound Ang II in all compartments (see Section 4.3.3). With $[AT1R - \text{bound } AngII]_{Gl}^{Mem}$ significantly reduced, the secretion of renin from the juxta glomerular apparatus of the kidney is increased (Eq. 2.13) causing PRA to rise significantly. As a result, plasma [AGT] decreases and plasma [Ang I] increases above control. Model simulations confirm that the observed decrease in plasma [AGT] is the consequence of both enhanced renin activity and a blockage of positive feedback on hepatic AGT production, as was proposed by Ref. [184]. The increase in plasma [Ang I] in conjunction with the unbinding of Ang II from systemic AT1Rs results in a similar fold-increase in plasma [Ang II]. As a result, more Ang I and Ang II get filtered into the kidney, causing the renal [Ang I] and [Ang II] to also increase slightly beyond control. All aforementioned changes in all RAS peptide levels following experiments (ii) and (iii) are summarized in Figure 4.3.

In the next section, we examine the experimental results presented by Ref. [184] in more detail and use model simulations to offer further insight into the impacts of Losartan on both the systemic and intrarenal RAS as well as the inception of hypertension.

4.3.3 Model predictions

Losartan blocks the activation of all systemic and intrarenal positive feedback, resulting in similar regulation of the RAS in the absence and presence of Ang II infusion In their study, Zou and colleagues [184] showed that each RAS peptide varies similarly regardless of whether Ang II is infused concurrently with Losartan or not. In other words, the peptide levels following experiment (ii) and experiment (iii) were similar (Figure 4.3). Model simulations indicate that this is because Losartan inhibits all systemic and intrarenal positive feedback loops by blocking AT1R-Ang II binding: With AT1Rs blocked by Losartan, excess Ang II from the infusion cannot initiate any downstream signalling, and thus the intrinsic regulation of all endogenous RAS peptides remains approximately the same as if an infusion were not taking place. As a result, the only peptide whose concentration significantly differs following Ang II infusion under concurrent Losartan administration is that that is being exogenously infused, i.e. Ang II itself. Indeed, by separating the endogenously produced Ang II from the exogenously infused Ang II (see Section 3.2.3), we show that exogenous Ang II is the primary contributor to the increased plasma [Ang II] (Figure 4.4A) and intrarenal [Ang II] (Figure 4.4B) observed in experiment (iii) relative to experiment (ii). In particular, the overall fold-increase in plasma [Ang II] is larger than the fold-increase in intrarenal [Ang II] because the kidney accumulates comparatively less exogenous Ang II than the systemic compartment. The mechanisms governing this disparity are outlined below.

Losartan has differential effects on the accumulation of exogenous and endogenous Ang II in the plasma and the kidney because of their independent regulation As outlined in the previous Chapter, less exogenous Ang II accumulates in the kidney than in the plasma during a normal Ang II infusion (experiment (i)). However, this disparity is significantly enhanced by concurrent Losartan administration (experiment (iii)). Indeed, model simulations indicate that Losartan reduces the accumulation of exogenous Ang II in the kidney, but not the systemic circulation following Ang II infusion (Figure 4.4, dark green bars (i) vs. bars (iii)). In particular, its administration resulted in a 47% decrease in the simulated intrarenal exogenous [Ang II] with no change in the systemic exogenous [Ang II]. These results are qualitatively consistent with those of Ref. [183], who observed a marked decrease in the exogenous intrarenal, but not plasma, [Ang II] following concurrent Ang II infusion and Losartan administration. This also supports the hypothesis presented in Chapter 3, that intrarenal Ang II accumulation relies primarily on *UPTK* (AT1R-mediated uptake of Ang II) during Ang II infusion. Because the accumulation of exogenous Ang II in the plasma does not rely on AT1Rs (occurs extracellularly), Losartan

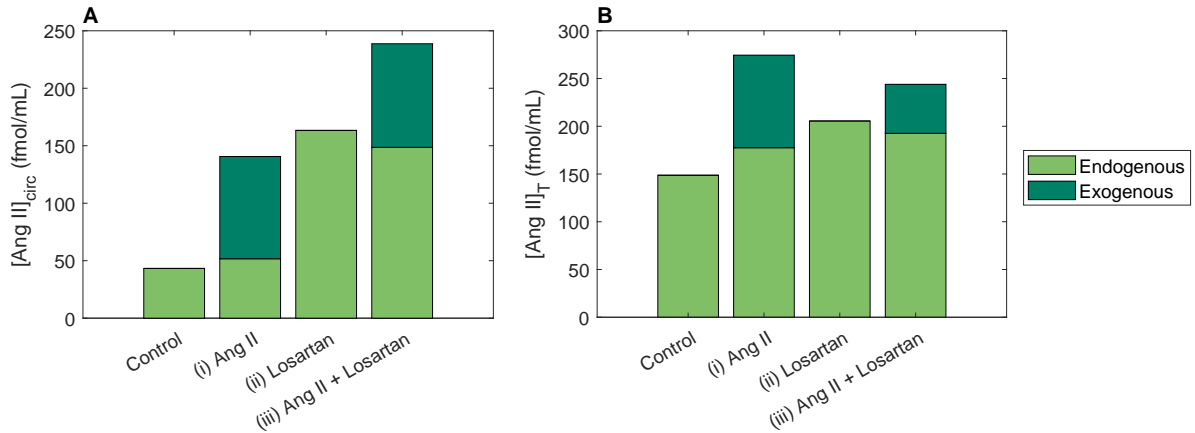


Figure 4.4: Average (simulated) **A** plasma and **B** intrarenal exogenous (dark green) and endogenous (light green) [Ang II] on day 13 of experiment (i): 40 ng/min subcutaneous Ang II infusion; experiment (ii): 30 kg/mg/day Losartan administration in drinking water; and experiment (iii) 40 ng/min subcutaneous Ang II infusion alongside 30 kg/mg/day Losartan administration in drinking water of Ref. [184].

has little impact on this concentration.

In contrast, the endogenous concentration of plasma Ang II, but not intrarenal Ang II is greatly enhanced by Losartan following Ang II infusion (Figure 4.4, light green bars (i) vs. (iii)). This effect was also reported in Ref. [183], who observed little change in intrarenal endogenous [Ang II] alongside a significant increase in plasma endogenous [Ang II] when Losartan was administered concurrently with Ang II. Model simulations indicate that the increase in endogenous plasma [Ang II] arises as a result of Losartan displacing all endogenous Ang II peptides that were initially bound to AT1Rs, and therefore not included in the free [Ang II]. Although this displacement also happens in the kidney, $[AngII]_T$ depends on the concentration of AT1R-bound Ang II in all sub-compartments (Eq. 2.9), and therefore **Losartan** has a smaller impact on the endogenous intrarenal [Ang II].

Losartan likely prevents Ang II-induced hypertension by restricting Ang II to extracellular regions where the peptide cannot initiate downstream signalling

By examining the effects of Losartan on the intrarenal distribution of Ang II, we can gain insight into the mechanisms by which this anti-hypertensive therapy mitigates the consequences of sustained Ang II infusion. In particular, Figure 4.5 compares the temporal

change in the intrarenal distribution of [Ang II] following Ang II infusion alone (panels X.i.) and in conjunction with Losartan administration (panels X.iii.). As outlined above, Losartan administration significantly reduces the amount of exogenous Ang II (dark green) that accumulates in the kidney during sustained Ang II infusion (Figure 4.5A). It does this by rapidly binding to all AT1Rs within the kidney, displacing the previously AT1R-bound endogenous Ang II (light green) and preventing any subsequent AT1R-Ang II binding because of its (and EXP3174's) high receptor affinity [104]. Indeed, the membrane-bound fraction of intrarenal Ang II rapidly decreases 0 within the first 5 hours of Losartan administration (Figure 4.5B). This blockage occurs before any exogenously infused Ang II even has a chance to bind to these receptors. As a result, Ang II no longer accumulates within the tubular epithelium (Figure 4.5C). In fact, the intracellular fraction of intrarenal Ang II decreases by approximately 69% following Losartan administration, from 0.35 to 0.11. This small intracellular fraction is entirely sustained by megalin-dependent uptake, which is unaffected by Losartan administration. With intracellular uptake severely limited, Ang II is forced to accumulate in the extracellular regions of the kidney (Figure 4.5D). The forced shift from intracellular to extracellular Ang II accumulation explains Losartan's effectiveness as an anti-hypertensive therapy: Although the total intrarenal [Ang II] still increases slightly beyond control, Losartan importantly restricts Ang II to compartments where the peptide cannot activate any downstream signalling cascades, such as the stimulation of sodium reabsorption. As a result, blood pressure does not increase [184].

In a real-world scenario, the ARB Losartan is prescribed once a patient has already developed hypertension, and not as a preventative measure. Therefore we use the model to simulate the effect of Losartan on an already hypertensive rat, whose high blood pressure has been induced by a 40 ng/min 13-day SC Ang II infusion (experiment (i) from Ref. [184]). Figure 4.6 illustrates the effect of Losartan treatment on the intrarenal concentration (panel A) and distribution (panels B-F) of Ang II. All observations are consistent with those of experiment (iii): Losartan inhibits the uptake of circulating (exogenous) Ang II within the kidney, but does not fully return intrarenal Ang II levels to control (Figure 4.6A,B). Nevertheless, Losartan drastically alters the intrarenal distribution of Ang II such that the vast majority becomes restricted to extracellular compartments (Figure 4.6C, D, E). Since the accumulated Ang II can no longer act as a signalling molecule in these regions, blood pressure is likely to decrease as a result of the Losartan administration.

4.3.4 Local sensitivity analysis

To determine the robustness of the aforementioned results, a local parametric sensitivity analysis was performed after simulating experiment (iii) from Ref. [184] (40 ng/min subcu-

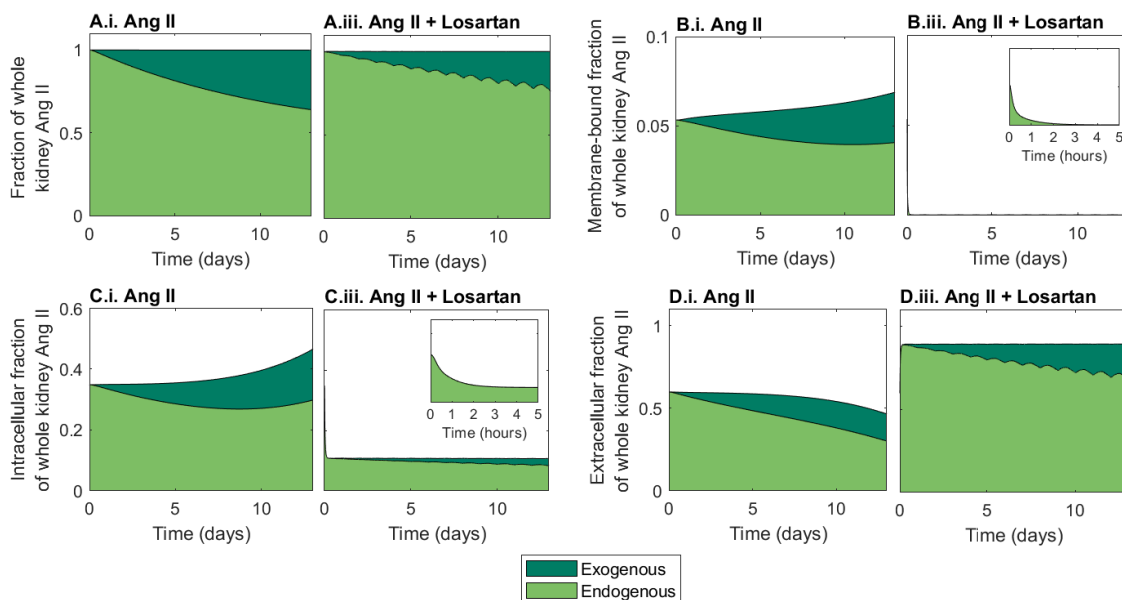


Figure 4.5: Temporal change in the intrarenal distribution of Ang II throughout 13 days of SC Ang II infusion (40 ng/min) alone (panels **X.i**) or in conjunction with 30mg/kg/day Losartan administration in drinking water (panels **X.iii**). Panels depict the relative contribution of endogenous (light green) and exogenous (dark green) Ang II to the: **(A)** total renal [Ang II], **(B)** membrane-bound fraction of renal [Ang II], **(C)** intracellular fraction of renal [Ang II], and **(D)** extracellular fraction of renal [Ang II].

taneous Ang II infusion plus 30 mg/kg/day Losartan administration in drinking water). Indeed, the percent change in the average drug (Figure 4.7) and RAS peptide (Figure 4.8) concentrations on the final day of the experiment (day 13) following a 10% increase in each model parameter was computed in each model compartment.

As shown in Figure 4.7, the effects of the parametric perturbations on the concentrations of Losartan and EXP3174 in all compartments were as expected. When the Losartan dose is reabsorbed more rapidly from the gastrointestinal tract (i.e. k_a^{Los} is increased), the drug's average concentration in the GI tissue compartment on day 13 of treatment is lower than control. When the activity of systemic cytochrome p450 enzymes k_{cyt} is increased, and therefore the conversion of Losartan to EXP3174 is increased, the Losartan concentration in all downstream compartments (systemic, renal, and peripheral) decreases. An increased rate of uptake k_{sp} or release k_{ps} of Losartan from the peripheral tissue compartment results

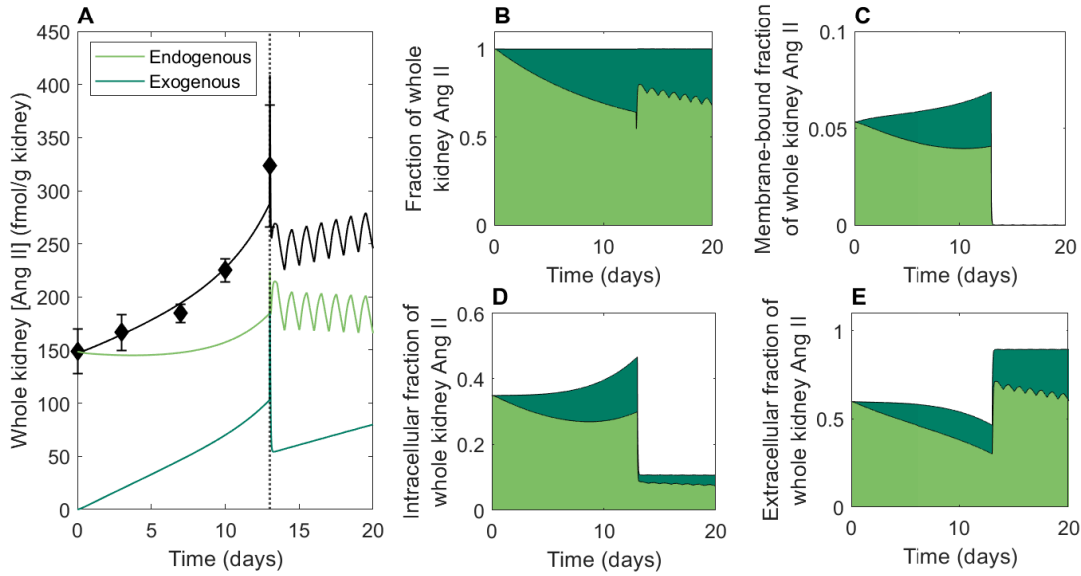


Figure 4.6: The effect of Losartan on the intrarenal (**A**) concentration and (**B–E**) distribution of Ang II in a hypertensive rat. Hypertension was induced via 13 days of subcutaneous Ang II infusion at 40 ng/min (experiment (i) from Ref. [184]; diamonds) and subsequently treated with Losartan (30 mg/kg/day) for 7 days. Panels **B–E** depict the relative contribution of endogenous (light green) and exogenous (dark green) Ang II to the: (**B**) total renal [Ang II], (**C**) membrane-bound fraction of renal [Ang II], (**D**) intracellular fraction of renal [Ang II], and (**E**) extracellular fraction of renal [Ang II].

in a higher or lower Losartan concentration in these tissues, respectively. When EXP3174 is systemically degraded at a more rapid rate (i.e. $k_{elim}^{EXP3174}$ increases), its concentration in all downstream compartments decreases. Systemically, this frees up more AT1Rs for Losartan to bind to, thereby increasing the concentration of AT1R-bound Losartan in this vasculature compartment. Unlike EXP3174 however, increasing the rate of Losartan degradation k_{elim}^{Los} does not affect significantly affect the drugs concentration. Given this, and the fact that its optimized value is very close to 0, we can stipulate that Losartan degradation is primarily mediated by its conversion to EXP3174. Finally, increasing the drinking water duration Δt , and therefore the time over which the rat consumes the drug dose does not impact its average concentration in any compartment as the amount of drug that is consumed overall remains unchanged. Moreover, the strength of the feedback on renin secretion B_{AT1R}^+ does not impact the pharmacokinetic model itself, only the intrarenal RAS model that it is coupled to.

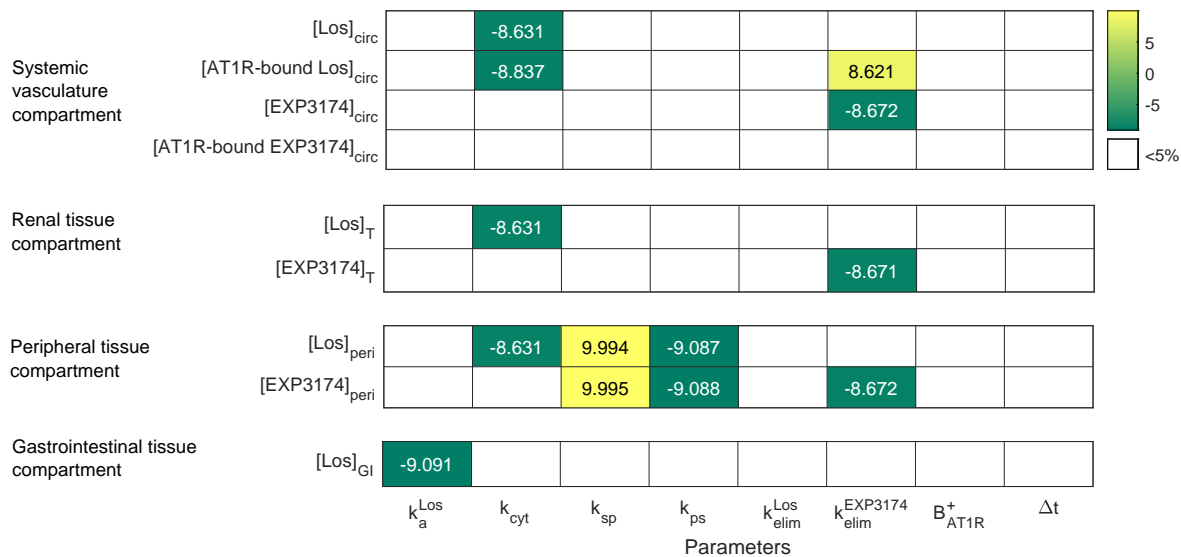


Figure 4.7: Percent change in the predicted average compartmental **Losartan** and **EXP3174** concentrations following 13 days of 40 ng/min SC Ang II infusion alongside 30 mg/kg/day Losartan administration in drinking water when each parameter value is increased by 10%.

In fact, as shown in Figure 4.8, the intrarenal RAS model predictions are most sensitive to increases in B_{AT1R}^+ . With the feedback loop's strength increased, the same fold-decrease in AT1R-bound Ang II elicits a larger secretion of renin from the kidney and therefore a larger production of all endogenous peptides downstream in the cascade (Ang I and Ang II). As a result, more endogenous Ang II also gets filtered into the kidney which raises the total intrarenal $[\text{Ang II}]$ in all regions. As expected, changes to B_{AT1R}^+ do not affect exogenous Ang II levels. The only other parameter that impacts intrarenal RAS model predictions is the rate of EXP3174 degradation in the systemic compartment $k_{\text{elim}}^{\text{EXP3174}}$. Since EXP3174 is much more potent than Losartan, it mediates the majority of its AT1R-blocking effects [129]. Therefore, when its degradation rate is increased (and therefore, its concentration is decreased), less AT1Rs are blocked by the metabolite, allowing for more AT1R-Ang II binding. However, the resulting increase in both systemic and intrarenal AT1R-bound Ang II, though proportionally large, are minute in absolute value (on the order of 10^{-3}). Therefore, these changes do not influence the rest of the system significantly.

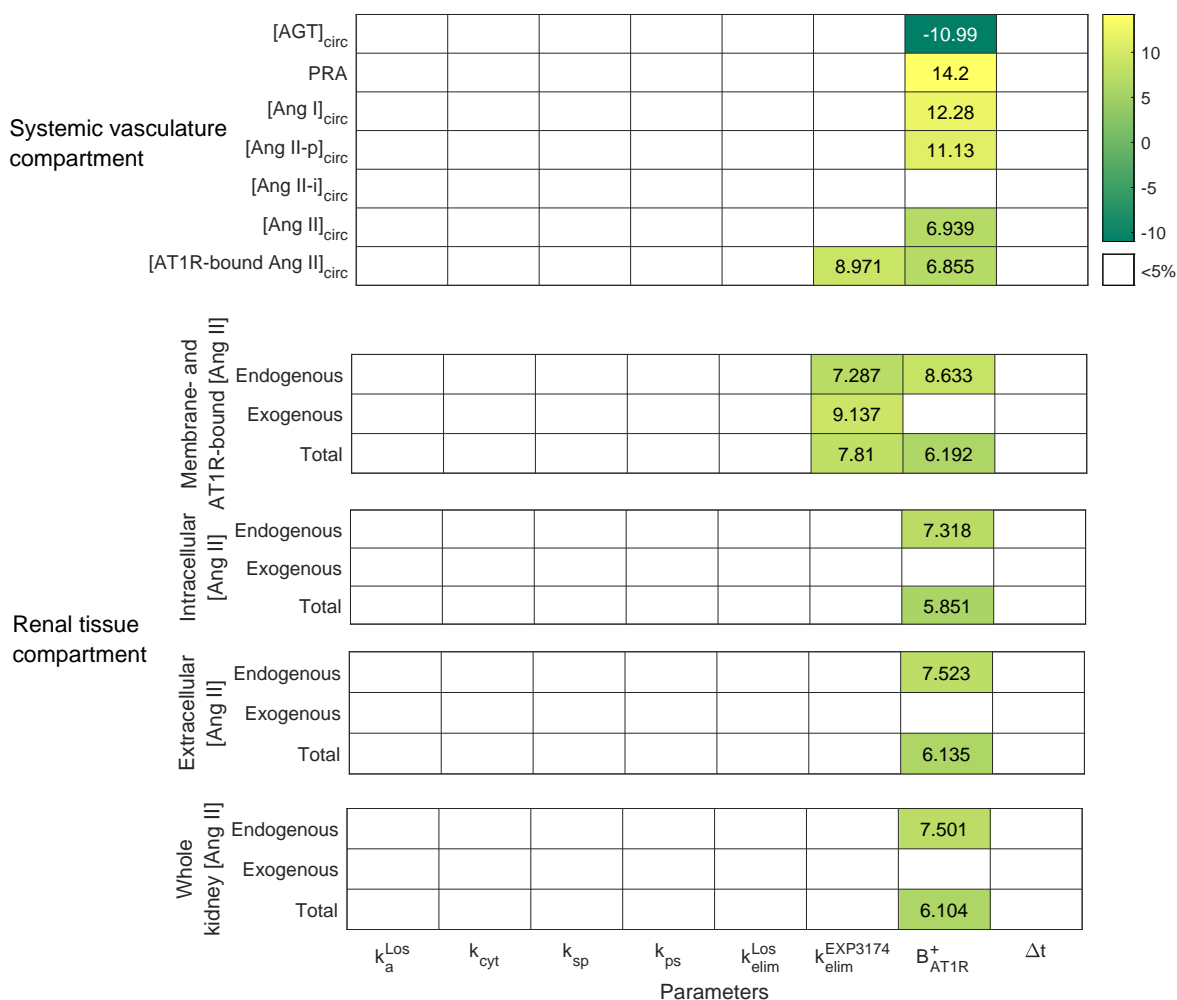


Figure 4.8: Percent change in the predicted average systemic and intrarenal RAS peptide concentrations following 13 days of 40 ng/min SC Ang II infusion alongside 30 mg/kg/day Losartan administration in drinking water when each parameter value is increased by 10%.

4.4 Discussion

In this Chapter, we aimed to study the effects of antihypertensive therapy Losartan on the activity of the intrarenal RAS in both control and hypertensive conditions. To do so, a robust PK model of Losartan and its bio-active metabolite EXP3174 was developed and coupled to that of the intrarenal and systemic RAS presented in Chapter 2. The coupled

PK/PD model was then used to replicate the various Losartan administration experiments from Ref. [184]. In particular, Losartan (30 mg/kg/day) was administered in drinking water either alone or in conjunction with sustained low dose (40 ng/min) Ang II infusion and the results were examined in detail.

Many studies have shown that Losartan helps prevent intrarenal Ang II levels from rising during Ang II infusion experiments and other experimental models of hypertension [184, 183, 170]. Model simulations indicate that this is mainly mediated by a reduced uptake of circulating (exogenous) Ang II into tubular epithelial cells. Endogenous peptide levels in the kidney remain relatively unchanged despite significantly increased plasma concentrations. We propose that this is due to Losartan’s inhibition of all positive feedback on endogenous Ang II production in the kidney (which is implicit in the assumption of a constant renal renin activity, see Section 4.2.1; renal tissue compartment). These observations are qualitatively consistent with those of Ref. [183] and provide further support to the conclusions drawn in Chapter 3. Indeed, it is likely that enhanced AT1R-mediated uptake, facilitated by increased AT1R expression, is the primary mechanism by which Ang II accumulates in the kidney during Ang II infusion; Positive feedback on local AGT and renin production acts secondarily to conserve basal Ang II production rates despite significantly reduced plasma, and therefore filtered, peptide levels. The significant differences in endogenous and exogenous peptide accumulation in the plasma and the kidney speak to the independent regulation of the systemic and intrarenal RAS and explain their de-coupling in experimental models of hypertension.

In general, model simulations confirm that Losartan attenuates the rise intrarenal Ang II levels during the development of hypertension via the “key point break-down effect” (blocking all positive feedback within the kidney), as was suggested by [170]. However, we hypothesize that this is not the primary mechanism by which Losartan acts to normalize blood pressure. Instead, model simulations suggest that it’s Losartan’s blockage of the main intracellular uptake path (AT1R binding and internalization) that contributes to the drug’s blood pressure regulating effects. Indeed, with this pathway still intact exogenous Ang II would continue to accumulate intrarenally, and more importantly, intracellularly as any infusion progressed, causing blood pressure to rise. This is not observed experimentally. Therefore, we hypothesize that it is actually the shift from intracellular to extracellular Ang II localization within the kidney that prevents blood pressure from rising under Losartan administration: Without being able to bind to or enter renal (or systemic) cells, Ang II cannot regulate sodium reabsorption, vessel tone, initiate secondary hormone secretion, or perform any signalling that would lead to increases in blood pressure. The same principal would likely hold for other ARBs.

4.4.1 Model limitations and future extensions

A key limitation of the proposed model was the necessary assumption that renal renin activity remains constant following Losartan administration. While the computational results of the previous Chapter were used to justify this choice (see Section 4.2.1; renal tissue compartment), future work should focus on gathering experimental measurements of renal renin activity before and after Losartan treatment in both control and hypertensive rats.

In addition, the model does not account for the effects of Ang II, and thus of Losartan and EXP3174, on renal hemodynamic function. As mentioned previously, intrarenal Ang II influences renal blood flow and glomerular filtration rate via various AT1R-dependent mechanisms. Indeed, afferent arteriole resistance, efferent arteriole resistance, the structure of the glomerular filtration barrier, and renal autoregulatory mechanisms such as tubuloglomerular feedback and the myogenic response are all affected by AT1R-bound Ang II, and therefore by Losartan administration [170, 1, 25, 154, 173]. Given that so many mechanisms are at play, the effect of Losartan on glomerular filtration rate is variable, often depending on whether blood pressure falls in or out of the renal autoregulatory range [170]. As a result, including a direct link between Losartan and the current model's renal hemodynamic parameters would be intractable. In future work, this could be overcome by incorporating the present model into Ahmed and Layton's whole-body blood pressure regulation model [1], which already considers renal autoregulatory mechanisms and afferent/efferent arteriole resistance as variables. By simulating Losartan administration under different autoregulatory conditions, the mechanisms contributing to the drug's variable effect on renal hemodynamics could be investigated. The resulting more comprehensive Losartan-blood pressure regulation model could also be used to study how the Losartan-mediated shift from intracellular to extracellular intrarenal Ang II localization influences the stimulation of sodium reabsorption and mean arterial pressure (also variables in Ahmed and Layton's model [1]).

To more comprehensively examine the effect of Losartan administration on sodium reabsorption along the nephron, the present model could also be coupled to a kidney function model that stimulates epithelial transport of electrolytes and water [77, 75, 140, 29, 19]. As was mentioned previously, the coupling can be formulated based on the many known connections between Ang II, AT1Rs, and ion transport along the nephron [11, 157, 170]. Such a model could then be used to elucidate which transporters and nephron segments most greatly influence Losartan's normalization of renal excretory function [170].

It has been long established that males and females respond differently to anti-hypertensive therapies, including ARBs like Losartan [84]. The current model is limited in that it does

not consider sex differences, and therefore our results are specific to a male rat’s response to Losartan treatment. This limitation could be overcome in future work by parameterizing sex-specific intrarenal and systemic model compartments using the procedure discussed in Chapter 3 (section 3.4.1). The sex differences in the response of various RAS peptides to ARB treatment, which to our knowledge has not been well characterized in experiments, could then be simulated. These results could shed light on why male hypertensive rats tend to exhibit a greater reduction in blood pressure following Losartan administration than females [172]. The sex-specific PK models could also be coupled to a sex-specific blood pressure regulation model [1], a sex-specific epithelial solute transport model [92, 56, 57, 58], or a sex-specific renal blood flow model [20] to study the sex-specific effects of Losartan on blood pressure, sodium reabsorption, and renal hemodynamics in more detail, respectively.

Another natural extension of this work would be the creation of a pharmacokinetic model of a common ACEi. In this way, the effects of the two classes of anti-hypertensive therapies on the intrarenal RAS could be compared. Coupling can be achieved through systemic and renal ACEi-based inhibition of ACE activity c_{ACE}^C in all model compartments C . We hypothesize that ACEis, like ARBs, will prevent Ang II-induced hypertension, at least in part, by blocking the AT1R-mediated accumulation of Ang II in tubular epithelial cells. However, this class of drug will achieve this via a different mechanism: ACEi will reduce the endogenous production of Ang II in the kidney and thus, the pool of Ang II that can be internalized. We expect ARBs to be more effective than ACEi at preventing hypertension induced by Ang II infusion. This is because ACEi would not prevent the accumulation of exogenous Ang II in tubular epithelial cells following Ang II infusion, but ARBs do (as demonstrated above).

Finally, the present model still does not represent the circadian rhythms long observed in the systemic RAS [52] and likely present in the intrarenal RAS. By expanding the present model to incorporate circadian variations in appropriate model parameters, the resulting integrative model could be used to explore whether the timing of Losartan administration influences its effectiveness as an anti-hypertensive therapy.

Chapter 5

A mathematical model of slow-pressor hypertension: The impact of the intrarenal RAS and impaired pressure natriuresis

Abstract

Hypertension is a highly complex, multi-factorial disease associated with many patho-physiological changes. To investigate clinical hypertension stemming from the impairment of each contributing factor, different animal experimental models can be used. Many of these models, particularly those associated with an over-active RAS, produce slowly progressive increases in both intrarenal Ang II and blood pressure. However, little is known about how the former response, intrarenal RAS over-activation, contributes to the latter effect, slow-pressor hypertension. Rats exposed to these experimental protocols also display an impaired pressure natriuresis response, but whether this is causal or a consequence of the observed hypertension remains openly debated. Here, we investigate these two clinically relevant open questions using computational modelling. In particular, we develop the first computational model of long-term blood pressure regulation in the rat that considers the intrarenal RAS and simulate various *in silico* Ang II infusion experiments with the intrarenal effects of Ang II turned on/off. Simulations suggest that the resetting of the pressure natriuresis response necessitates increased blood pressure to maintain

sodium and fluid homeostasis: Blood pressure must increase enough to offset Ang II's indirect (aldosterone-mediated) and direct effects on sodium reabsorption. Furthermore, these effects must be initiated sequentially to observe slow-pressor hypertension. This is facilitated by systemic and intrarenal RAS de-coupling. Our results thus shed light on the functional importance of both impaired pressure natriuresis and the progressive rise in intrarenal Ang II that has been observed in various experimental models of hypertension. It is likely that these mechanisms are also involved in pathogenesis of clinical hypertension associated with an over-active RAS.

5.1 Introduction

Hypertension is a highly complex, multi-factorial disease associated with many pathophysiological changes, including; arterial stiffening, impaired [pressure natriuresis](#), and an over-active [RAS](#). Since many of these systems interact with one another, it is difficult, and in many cases impossible, to narrow the conditions inception to a single cause. One clinically relevant open question relates to whether abnormal pressure natriuresis is a cause or consequence of chronic hypertension. Moreover, given the many intrarenal actions of Ang II, and the discovery that the kidney not only expresses, but independently regulates all components of the RAS, the significance of the local intrarenal RAS to the pathogenesis and progression of hypertension is also of interest. To answer these questions, experimental models of hypertension that target each of these systems – the kidney and the RAS – have been devised [[88](#), [134](#)]. Here, we examine clinical hypertension associated with an overactive RAS through the lens one such experimental model – hypertension induced by [Ang II](#) infusion.

Chronic Ang II infusions consistently result in slowly progressive increases in both intrarenal Ang II and blood pressure. In previous Chapters, a novel mathematical model of the RAS was devised to examine the mechanisms that mediate the former response, i.e. rising intrarenal Ang II levels in Ang II-induced hypertension. While at the time hypotheses were made regarding how this response might contribute to the slow development of hypertension (slow-pressor hypertension) in these rats, they could not be substantiated because the model did not consider sodium balance nor blood pressure explicitly.

Many whole-body long-term blood pressure regulation models have been created previously (see Chapter 1 for a thorough review) [[45](#), [49](#), [64](#), [85](#), [1](#)]. However, none include an intrarenal RAS. This includes Ahmed and Layton's long-term blood pressure regulation model in the rat which was developed to help interpret the results of various animal

experiments, including Ang II infusion experiments. Like all other existing blood pressure regulation models, it falsely assumes that the intrarenal effects of Ang II are mediated by systemic Ang II. Although the systemic and intrarenal RASs are connected and often vary in tandem, this is no longer true during Ang II-induced hypertension (or any experimental model of hypertension stemming from an overactive RAS). In these cases, a more comprehensive blood pressure model that distinguishes between the systemic and the intrarenal RASs is desirable.

In this Chapter, we thus create the first whole-body long-term blood pressure regulation model in the rat that considers the intrarenal RAS. Using this model, we aim to: (i) *delineate the mechanisms that mediate slow-pressor hypertension* and (ii) *quantify the role of the intrarenal RAS and of impaired pressure natriuresis in this response*. In particular, we couple a simplified version of Ahmed and Layton [1]’s blood pressure regulation model to that of the intrarenal and systemic RASs presented in Chapter 2. After parameterizing and validating the model against data collected from various Ang II infusion experiments, we use it to make predictions regarding the mechanisms of slow-pressor hypertension. In particular, we suggest answers to the following questions: (i) *Does the resetting of the pressure natriuresis response necessitate increased blood pressure to maintain solute and fluid homeostasis in Ang II-induced hypertensive rats?*, and (ii) *Do progressively rising intrarenal Ang II levels functionally contribute to slow-pressor hypertension? If so, how?* Our results shed light on the pathogenesis of slow-pressor hypertension induced by Ang II infusion, and thus the development of clinical hypertension associated with an overactive RAS.

5.2 Methods

5.2.1 Blood pressure regulation model

The long-term blood pressure regulation model presented in this Chapter is adopted from Ahmed and Layton’s [1] male rat model with various modifications. Firstly, the model was re-parameterized to represent a Sprague Dawley, as opposed to a Munich Wister, male rat (see Section 5.2.3). This is because the majority of Ang II infusion experiments, including all those replicated in this work, are performed in Sprague Dawley rats [102, 184, 133, 117]. Sprague Dawley differ from Munich Wistar rats in that they are much larger and have different baseline hemodynamics [105]. Size affects blood volume, and therefore all RAS peptide concentrations. Hence, this re-parameterization also ensured that all RAS and hemodynamic variables were consistent with those of the RAS model outlined in Chapter 2.

Secondly, because our primary goal was to study the effects of the intrarenal RAS on renal sodium and fluid handling during the development of Ang II-induced hypertension, many of the other original model components were removed or simplified: Indeed, all renal hemodynamic variables (renal blood flow and glomerular filtration rate) were assumed constant and all feedback relating to autonomic and sympathetic nervous activity, atrial natriuretic peptide, and water intake (anti-diuretic hormone) were fixed. The assumed constant glomerular filtration rate is a reasonable simplification given that this variable has not been observed to change drastically following non-pressor doses of Ang II [167, 25, 154].

Finally, various novel variables were added to the model, including an indirect and chronic effect of Ang II on vascular resistance as well as an updated representation of renal sodium handling. Moreover, the original systemic-only RAS model was replaced with the novel systemic and intrarenal RAS model described in Chapter 2. Coupling was achieved via the effects of intrarenal Ang II on sodium reabsorption along the nephron and the effects of renal fluid handling on both systemic and intrarenal RAS concentrations.

The subsections below detail the changes made to each model component – cardiovascular function, renal sodium and fluid handling, and the RAS – in greater detail. A schematic diagram of the resulting blood pressure regulation model is shown in Figure 5.1. Model equations and parameters not described in detail here can be found in Appendix C.

Cardiovascular function

Angiotensin II (Ang II) is a potent vasoconstrictor. However, since its direct effects on the vasculature are acute (1-2 mins) [64], they are not considered in Ahmed and Layton’s long-term blood pressure regulation model [1] nor any of its prior iterations [45, 64, 49, 85, 1]. While this assumption is well-founded, a chronic, indirect effect of Ang II on total peripheral resistance, R_{tp} , has been observed experimentally. Indeed, chronic Ang II infusions are associated with a delayed increase in R_{tp} [117, 113] which contributes significantly to the delayed rise in blood pressure that is observed [125]. Hence, this indirect effect must be added to the model to enable the study of slow-pressor hypertension induced by Ang II infusion.

Multiple factors contribute to the delayed rise in R_{tp} in slow-pressor hypertension [155], including inflammation, reduced nitric oxide signalling, and the stimulation of oxidative stress [2, 67, 113, 125, 127, 128]. Since these vascular effects are intimately connected and their individual contributions to this response are not known, we instead introduce a simplified intermediate variable, $OXST$, that represents their combined effect on R_{tp} .

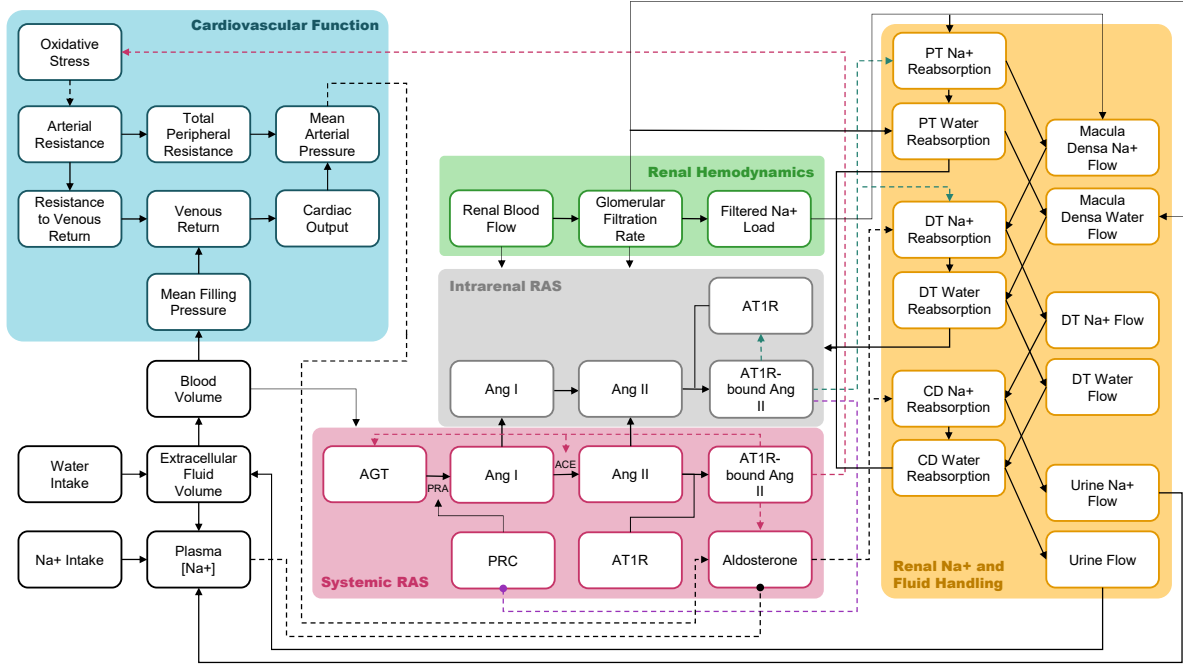


Figure 5.1: Schematic model of blood pressure regulation. Nodes within the grey compartment denote variables that describe the intrarenal RAS; pink, the systemic RAS; green, renal hemodynamics; yellow, renal sodium Na^+ and fluid handling; blue, cardiovascular function. Solid arrows indicate direct connections between variables. Dashed pointed and dotted connections indicate positive and negative indirect connections, respectively. Effects of AT1R-bound Ang II are colour-coated based on the RAS compartment from which they originate: Pink connections denote the effects of systemic AT1R-bound Ang II; purple connections, glomerular AT1R-bound Ang II; green connections, tubular-epithelial cell-associated (tubular and peritubular) AT1R-bound Ang II. The schematic representation of the intrarenal RAS model component (grey) has been simplified for readability. Please see Figure 2.2 for a detailed representation of all intrarenal variables.

The production of $OXST$ is assumed to be both AT1R-bound Ang II (via R_{circ} , Eq. 3.2) and time-dependent (via ρ_{OXST} , Eq. 5.2). This is based on the consensus that there is a time requirement for AT1R-bound Ang II to activate the additional vasoconstrictor processes that lead to elevated R_{tp} and blood pressure [125]. In particular, we assume that it takes 12 hours for $OXST$ production to commence following Ang II infusion, after which its production rate increases linearly before reaching its maximum on (and after)

day 5. The piece-wise formalism for ρ_{OXST} (Eq. 5.2) is based on the observation that “slow pressor responses need 5 to 10 hours to develop and reach a maximal peak 3 to 5 days after the onset of the infusion” [128]. To account for the slower time scale of $OXST$ dynamics, we also introduce a time constant τ_{OXST} to be fit to available peripheral resistance data [117] following the chronic infusion of a sub-pressor dose of Ang II. Taken together, we obtain the following formalism for $OXST$ dynamics:

$$\frac{dOXST}{dt}(t) = \frac{1}{\tau_{OXST}} (\rho_{OXST}(t) \times R_{circ}(t) - OXST(t)) \quad (5.1)$$

where

$$\rho_{OXST}(t) = \begin{cases} 0 & t < \frac{1}{2} \text{ days} \\ \frac{2}{9} (t - \frac{1}{2}) & \frac{1}{2} \leq t < 5 \text{ days} \\ 1 & t \geq 5 \text{ days} \end{cases} \quad (5.2)$$

$OXST$ affects the model by modifying arterial resistance R_a , and thus R_{tp} (Eq. 5.4). In particular, R_a is taken to be the basic arterial resistance R_{ba} (Table C.1) multiplied by the effect of the additional vascular changes ϵ_{OXST} where $\epsilon_{OXST}(t) = 1 + OXST(t)$.

$$R_a(t) = R_{ba} \times \epsilon_{OXST}(t) \quad (5.3)$$

Total peripheral resistance R_{tp} is then computed as the sum of the arterial resistance R_a and the basic venous resistance R_{bv} (Table C.1):

$$R_{tp}(t) = R_a(t) + R_{bv} \quad (5.4)$$

Renal sodium and fluid handling

As in Ref. [1], the nephron is divided into three segments; the proximal tubule (pt), distal tubule (dt), and the collecting duct (cd). Anatomically, the pt segment is comprised of the proximal tubule and the loop of Henle. Various changes were made with regards to the handling of sodium in each segment, as described below.

pt sodium handling Once filtered into the tubule, a fraction $\eta_{pt-sodreab}$ of the sodium load ϕ_{filsod} is reabsorbed by the pt , resulting in an absolute pt sodium reabsorption rate of $\phi_{pt-sodreab}$. Fractional pt sodium reabsorption $\eta_{pt-sodreab}$ is modified by Ang II and

perfusion pressure. These effects are represented by the functions γ_{AT1R} (Eq. 5.7) and γ_{hyp} (Eq. 5.10), respectively (see below).

$$\phi_{pt-sodreab}(t) = \phi_{filsod}(t) \times \eta_{pt-sodreab}(t) \quad (5.5)$$

$$\eta_{pt-sodreab}(t) = \eta_{pt-sodreab}^{eq} \times \gamma_{AT1R}(t) \times \gamma_{hyp}(t) \quad (5.6)$$

A limitation of previous versions of this model was the assumption that *pt* sodium reabsorption is affected by the systemic, as opposed to the local [AT1R-bound Ang II]. This simplification becomes particularly problematic during an investigation of hypertension, given that the systemic and intrarenal [Ang II] become decoupled [184, 18, 168, 150]. Therefore, in this Chapter we allow fractional sodium reabsorption (in all applicable segments, see below) to depend on tubular epithelial cell-associated AT1R-bound Ang II, denoted *AT1R – bound Ang II*_{Tb, Pt}^{Memb, Cell} (Eq. 5.9). In this way, AT1R-Ang II binding along either membrane of tubular epithelial cells impacts sodium reabsorption. This assumption is consistent with the observation that in the proximal tubule in particular, Ang II modulates sodium transporters on both membranes, basolateral (Na⁺/HCO₃⁻ and Na⁺/K⁺ATPase) and apical (Na⁺/H⁺ exchanger) [124].

$$\gamma_{AT1R}(R_{Tb, Pt}^{Memb, Cell}(t)) = \gamma_{AT1R}^c + \frac{\gamma_{AT1R}^a}{1 + \exp\left(-\gamma_{AT1R}^b \left(R_{Tb, Pt}^{Memb, Cell}(t) - 1\right)\right)} \quad (5.7)$$

$$R_{Tb, Pt}^{Memb, Cell}(t) = \frac{AT1R - \text{bound } AngII_{Tb, Pt}^{Memb, Cell}(t)}{AT1R - \text{bound } AngII_{Tb, Pt}^{Memb, Cell, eq}}, \quad (5.8)$$

$$\begin{aligned} AT1R - \text{bound } AngII_{Tb, Pt}^{Memb, Cell}(t) &= V_{Tb}^{Ext}[AT1R - \text{bound } AngII]_{Tb}^{Memb}(t) \\ &+ V_{Pt}^{Ext}[AT1R - \text{bound } AngII]_{Pt}^{Memb}(t) \\ &+ V_{Pt, Tb}^{Cell}([AT1R - \text{bound } AngII]_{Tb}^{Cell}(t) \\ &+ [AT1R - \text{bound } AngII]_{Pt}^{Cell}(t)) \end{aligned} \quad (5.9)$$

Also affecting sodium reabsorption in this segment is the [pressure natriuresis](#) mechanism, whereby increases in renal perfusion pressure result in decreased sodium reabsorption and thus, increased sodium excretion. In previous model iterations, filtered sodium load

ϕ_{filsod} was used as the determinant of this mechanism: increases in filtered load led to reductions in fractional pt sodium reabsorption. However, changes in filtered sodium load do not necessarily mirror those of renal perfusion pressure. Moreover, although incompletely understood, the mechanisms currently believed to mediate pressure natriuresis do not depend on filtered sodium load [5]. Instead, it is believed that pressure natriuresis is driven by the high renal interstitial hydrostatic pressures that result from high perfusion pressures [5]. Indeed, high interstitial pressures alter the permeability of proximal tubule tight junctions to sodium, lead to the release of various autocoids, and cause the re-distribution of apical Na^+ transporters [5]. Given this, we allow fractional pt sodium reabsorption to instead depend directly on renal perfusion pressure (assumed to be the same as mean arterial pressure P_{ma} [1]) and replace γ_{filsod} in Ref. [1] with γ_{hyp} :

$$\gamma_{hyp}(P_{ma}(t)) = \gamma_{hyp}^c - \frac{\gamma_{hyp}^a}{1 + \exp(-\gamma_{hyp}^b (P_{ma}(t)/P_{ma}^{eq} - \gamma_{hyp}^d))} \quad (5.10)$$

where P_{ma}^{eq} is the baseline (steady state) mean arterial pressure.

dt sodium handling As in Ref. [1], the portion of the sodium load that is not reabsorbed at the level of the proximal tubule passes by the **macula densa**. A fraction $\eta_{dt-sodreab}$ of this macula densa sodium flow ϕ_{md-sod} is reabsorbed by the distal tubule to give an absolute distal tubule sodium reabsorption rate of $\phi_{dt-sodreab}$. Fractional distal tubule sodium reabsorption is affected both directly and indirectly (via aldosterone) by Ang II. These effects are represented by the functions ψ_{AT1R} (Eq. 5.15) and ψ_{ALD} (Eq. 5.14), respectively. ψ_{ALD} is taken directly from Ref. [1]. The direct effect of Ang II on distal tubule sodium reabsorption was not considered in previous model iterations. However, it is well documented that Ang II increases distal tubule sodium reabsorption independently of aldosterone by stimulating ENaC expression and activity [177, 97]. Hence, we introduce the function ψ_{AT1R} to represent this effect. As in the proximal tubule, we assume that distal tubule fractional sodium reabsorption depends on tubular epithelial cell-associated [AT1R-bound Ang II]. This is because the AT1R-bound Ang II signalling mechanisms in this segment are not membrane restricted [177, 97].

$$\phi_{md-sod}(t) = \phi_{filsod}(t) - \phi_{pt-sodreab}(t) \quad (5.11)$$

$$\phi_{dt-sodreab}(t) = \phi_{md-sod}(t) \times \eta_{dt-sodreab}(t) \quad (5.12)$$

$$\eta_{dt-sodreab}(t) = \eta_{dt-sodreab}^{eq} \times \psi_{ALD}(t) \times \psi_{AT1R}(t) \quad (5.13)$$

$$\psi_{ALD}([ALD]_{circ}(t)) = \frac{\psi_{al}^a}{1 + \psi_{al}^b \exp(-\psi_{al}^c [ALD]_{circ}(t))} - \psi_{al}^d \quad (5.14)$$

$$\psi_{AT1R}\left(R_{Tb,Pt}^{Mem b, Cell}(t)\right) = \psi_{AT1R}^c + \frac{\psi_{AT1R}^a}{1 + \exp\left(-\psi_{AT1R}^b \left(R_{Tb,Pt}^{Mem b, Cell}(t) - 1\right)\right)} \quad (5.15)$$

cd sodium handling Whatever sodium load remains at the end of the distal tubule ϕ_{dt-sod} enters the *cd*, where a fraction $\eta_{dt-sodreab}$ is reabsorbed to give an absolute *cd* sodium reabsorption rate of $\phi_{cd-sodreab}$. The sodium flow that remains, ϕ_{u-sod} , gets excreted in urine. Here, we adopt a simplified model of *cd* sodium handling, such that reabsorption is only affected by this segment's sodium inflow rate ϕ_{dt-sod} via the function λ_{dt} (taken directly from [1]). Although direct and indirect (aldosterone-mediated) effects of Ang II on sodium reabsorption are documented in this segment, we did not include either in the model for simplicity. The former assumption is based on reports by Wu and colleagues [169] that Ang II had a much lower stimulatory effect on ENaC in the collecting duct than the distal tubule. The latter was required to ensure that sodium and water balance were maintained simultaneously in the absence of the effects of anti-diuretic hormone on water reabsorption. Furthermore, given the formalism adopted by Ref. [1], whereby a 10% increase in serum aldosterone results in only a 0.6% increase in fractional collecting duct sodium reabsorption, a zeroing assumption is reasonable.

$$\phi_{dt-sod}(t) = \phi_{md-sod}(t) - \phi_{dt-sodreab}(t) \quad (5.16)$$

$$\phi_{cd-sodreab}(t) = \phi_{dt-sod}(t) \times \eta_{cd-sodreab}(t) \quad (5.17)$$

$$\eta_{cd-sodreab}(t) = \eta_{cd-sodreab}^{eq} \times \lambda_{dt}(t) \quad (5.18)$$

$$\lambda_{dt}(t) = \lambda_{dt}^a + \frac{\lambda_{dt}^b}{1 + \exp(\lambda_{dt}^c (\phi_{dt-sod}(t)/SF_S - \lambda_{dt}^d))} \quad (5.19)$$

Finally, the fluid reabsorption model adopted in this work does not differ significantly from Ref. [1] and closely mirrors that of sodium reabsorption in all segments. For details, please see the Appendix C.3.

The renin-angiotensin system

As aforementioned, the original systemic-only RAS model outlined in Ref. [1] was replaced with the systemic and intrarenal RAS model described in Chapter 2, barring a few modifications (described below).

In Chapter 3, the functions describing positive feedback on tubular epithelial cell AT1R expression, f_{Pt} and f_{Tb} , were assumed linear for simplicity (Eq. 3.1). However, when simulating the model over longer time scales (> 2 weeks), this simplification results in unphysiological concentrations of intrarenal AT1Rs and Ang II. To correct for this, in this Chapter we assume that the positive feedback desensitizes once the total intrarenal expression of AT1Rs, $AT1R_T$ (Eq. 5.21), reaches a threshold, denoted $AT1R_T^*$. In particular, we impose the following piece-wise representation of the positive feedback fb_C in the tubular ($C = Tb$) and peritubular compartments ($C = Pt$).

$$fb_C^{AT1R}(R_C^{Memb}(t)) = \begin{cases} 0 & \text{if } R_C^{Memb}(t) \leq 1 \\ K_C^{AT1R}(R_C^{Memb}(t) - 1) & \text{if } R_C^{Memb}(t) > 1 \text{ and } AT1R_T(t) < AT1R_T^* \\ fb_C^{AT1R}(t^*)e^{-(t-t^*)} & \text{if } R_C^{Memb}(t) > 1 \text{ and } AT1R_T(t) \geq AT1R_T^* \end{cases} \quad (5.20)$$

$$\begin{aligned} AT1R_T(t) = & V_{Pt,Tb}^{Cell} ([AT1R]_{Pt}^{Cell}(t) + [AT1R - bound AngII]_{Pt}^{Cell}(t)) \\ & + V_{Pt,Tb}^{Cell} ([AT1R]_{Tb}^{Cell}(t) + [AT1R - bound AngII]_{Tb}^{Cell}(t)) \\ & + V_{Gl}^{Cell} ([AT1R]_{Gl}^{Cell}(t) + [AT1R - bound AngII]_{Gl}^{Cell}(t)) \\ & + V_{Pt}^{Ext} ([AT1R]_{Pt}^{Memb}(t) + [AT1R - bound AngII]_{Pt}^{Memb}(t)) \\ & + V_{Tb}^{Ext} ([AT1R]_{Tb}^{Memb}(t) + [AT1R - bound AngII]_{Tb}^{Memb}(t)) \\ & + V_{Gl}^{Ext} ([AT1R]_{Gl}^{Memb}(t) + [AT1R - bound AngII]_{Gl}^{Memb}(t)) \\ & + V_{Pv} ([AT1R]_{Pv}(t) + [AT1R - bound AngII]_{Pv}^{Memb}(t)) \end{aligned} \quad (5.21)$$

where $R_C^{Memb}(t)$ is given by Eq. 3.2 and t^* is the time at which the AT1R expression threshold $AT1R_T^*$ is reached.

In previous Chapters, we also assumed that all terms related to intrarenal fluid handling were known *a priori*. In this Chapter, we correct for this by replacing these parameters

with their dynamic-variable counterparts (with the exception of renal blood flow and the glomerular filtration rate). In particular, since urine flow ϕ_U is considered in both models, we do a direct replacement of the parameter from Chapter 2 with the variable (Eq. C.13) from the blood pressure model (scaled by kidney weight W_K). This allows us to compute the flow from the peritubular [interstitial space](#) into the renal blood vasculature ϕ_{P_v} (Eq. C.15). We also compute the RAS model’s total plasma volume V_{circ} from the blood pressure model’s blood volume V_b variable (Eq. C.28), assuming a fixed hematocrit Hct of 0.42 [105]. Finally, we compute the renal lymphatic flow rate ϕ_L (Eq. C.14) from the sum of the dynamic pt , dt , and cd water reabsorption rates, maintaining the assumption that ϕ_L accounts for 2% of the total fluid reabsorption from the kidney [146].

5.2.2 Simulating Ang II infusion experiments

All *in silico* subcutaneous Ang II infusion experiments are simulated similarly to Chapter 3. However, in this Chapter we assume that subcutaneously-infused Ang II has a low bioavailability. In other words, we assume that only a fraction of the Ang II entering the subcutaneous tissue actually reaches the systemic circulation. In practice, we simulate this by multiplying the original subcutaneous infusion term $K_{inf}^{SC}(t)$ (Eq. 3.8) by a bioavailability parameter F ($0 < F < 1$). Given that the subcutaneous tissue is predominantly adipose tissue which expresses its own local RAS [89], pre-systemic degradation, AT1R-binding, and uptake of Ang II into adipocytes could all contribute to the peptide’s low subcutaneous bioavailability [33, 126, 156]. Introducing a bioavailability parameter was required to see the plasma [Ang II] plateau by the second week of subcutaneous Ang II infusion, as is observed experimentally [184]. Indeed, without F the fitted subcutaneous Ang II absorption rate k_a had to be so low that the plasma [Ang II] continued to increase for greater than 4 week-long infusions, which is unphysiological.

5.2.3 Parameter identification

The majority of the model’s parameters, including all those that impact the system at steady state, were either taken directly from the RAS model outlined in Chapter 2 (Tables 2.2) or derived from Ahmed and Layton’s blood pressure model [1] using hemodynamic and volumetric data for male Sprague Dawley rats. The remaining minority that needed calibration were specific to the RAS and to renal sodium handling. The parameters related to the RAS were identified first by fitting to various Ang II infusion studies [117, 184, 179], keeping sodium (and thus, water) reabsorption fixed in all segments. Then, the parameters specific to sodium handling in the pt and dt were identified by simulating the Ang II

infusion experiment of Minas et al. [102] while imposing various physiological constraints on sodium and water balance. Details are provided below.

Reparameterization for the Sprague Dawley rat Ahmed and Layton’s original male rat model [1] was created by reparameterizing the human models from Ref. [64, 49] to Munich Wistar male rat renal hemodynamic data from [105] and the systemic RAS hormone levels from Ref. [84]. However, given that we aimed to: i) couple this model to the intrarenal RAS model outlined in Chapter 2, which was parameterized to Sprague Dawley data; and ii) simulate in-silico Ang II infusion experiments, which are predominantly performed on Sprague Dawley rats, we needed to re-parameterize the model from Ref. [1] to Sprague Dawley male rat renal hemodynamic and volumetric data. This was done using the data from Ref. [105], following the same steps outlined in Ref. [1]. The baseline values of all model parameters and variables are given in Tables C.1 and C.2, respectively. Those that differ between the two models relate to blood flow, vascular resistance, urine flow, urine sodium flow, fluid volume, and the RAS.

RAS parameters *Ang II bioavailability and subcutaneous absorption* Both the bioavailability F and the subcutaneous absorption rate k_a of Ang II were fit to plasma [Ang II] time series data from [184]. Moreover, to ensure the updated coupled model simulations remained consistent with those of Chapter 3 and with the data that was used to fit the uncoupled RAS model (Table 3.1, *fitting*), the RAS model’s feedback parameters K_C^x (Eq. 3.1, 5.20) were also updated. *Vascular effects of Ang II* The time constant τ_{OXST} of $OXST$ (Eq. 5.1) dynamics was obtained by minimizing the error between the simulated and experimental change in total peripheral resistance R_{tp} (Eq. 5.4) following 10 days of 200 ng/kg/min subcutaneous Ang II infusion [117]. *Intrarenal AT1R-feedback desensitization* The threshold for AT1R feedback desensitization $AT1R_T^*$ was fit to ensure that $AT1R_T$ (Eq. 5.21) matched receptor expression data from Ref. [179] following 21 days of Ang II infusion.

Renal sodium transport parameters The remaining unidentified parameters were those that regulate pt and dt sodium reabsorption via the effector functions γ_{AT1R} (Eq. 5.7), γ_{hyp} (Eq. 5.10), and ψ_{AT1R} (Eq. 5.15). We first reduced the total number of unknowns by fixing each of these effects at steady state, i.e. imposing that $\gamma_{AT1R}(1) = \gamma_{hyp}(P_{ma}^{eq}) = \psi_{AT1R}(1) = 1$. In doing so, we obtained the following relationships:

$$\gamma_{AT1R}^c = 1 - \frac{\gamma_{AT1R}^a}{2}$$

$$\gamma_{hyp}^c = 1 + \frac{\gamma_{hyp}^a}{1 + \exp(-\gamma_{hyp}^b(1 - \gamma_{hyp}^d))}$$

$$\psi_{AT1R}^c = 1 - \frac{\psi_{AT1R}^a}{2}$$

To simplify the parameter space even further, we took advantage of the computational results of Edwards and McDonough [30]. In this study, a steady state model of solute transport was used to examine the impact of prolonged Ang II infusion on sodium transport along the nephron. In particular, their simulations suggest that prolonged (14 day) Ang II (400 ng/kg/min) infusion causes proximal tubule sodium flux to decrease by 3% (relative to control). To best make use of this estimation, we re-formulate the strength of the pressure natriuresis response γ_{hyp}^a in terms of γ_{AT1R}^a such that as $P_{ma}, R_{Tb,Pt}^{Mem b, Cell} \rightarrow \infty$, $\gamma_{hyp} \times \gamma_{AT1R} \rightarrow 0.96$, where $0.96 < 0.97$ was chosen because we do not expect these functions to be fully saturated at a dose of 400 ng/kg/min. Taken together, we obtain:

$$\gamma_{hyp}^a = \left(1 - \frac{0.96}{1 + \gamma_{AT1R}^a/2}\right) \left(1 + \frac{1}{\exp(-\gamma_{hyp}^b(1 - \gamma_{hyp}^d))}\right)$$

To fit the remaining 6 parameters: γ_{AT1R}^a , γ_{AT1R}^b , γ_{hyp}^b , γ_{hyp}^d , ψ_{AT1R}^a , and ψ_{AT1R}^b , we simulate the non-pressor (80 ng/min) subcutaneous Ang II infusion experiment of Minas et al. [102]. In particular, we minimize the error between the predicted and experimental 28-day blood pressure time series while imposing several physiology-based constraints on key variables related to sodium and fluid homeostasis. In particular, we ensure: i) that blood volume remains within $\pm 8\%$ of control throughout the experiment [69], and ii) that sodium and fluid balance is restored at the new hypertensive steady state [48]. In other words, sodium and water intake should match urinary excretion, and blood volume, extracellular fluid volume, and plasma sodium concentration should return to baseline.

5.2.4 Systemic RAS-only blood pressure regulation model

As a primary goal of this Chapter was to unravel the specific impact of the intrarenal RAS on slow-pressor hypertension, we slightly modify the blood pressure model described above to create a version, hereby referred to as the *systemic model*, where all intrarenal effects of Ang II are falsely assumed to depend on systemic Ang II. In this way, we can directly compare simulations made with the two models (and previous work [1]) to determine the distinct effect(s) of intrarenal Ang II on blood pressure regulation.

In the *systemic model*, we impose that γ_{AT1R} (Eq. 5.7) and ψ_{AT1R} (Eq. 5.15) depend on R_{circ} as opposed to $R_{Tb, Pt}^{Memb, Cell}$ (Eq. 5.8). In addition, we re-fit γ_{AT1R}^a (Eq. 5.7) to ensure that sodium and fluid balance is still being restored following all infusions simulated with *systemic model*. All other parameters remain consistent between the two models. Unless otherwise specified, all references to the model hereunder refer to the blood pressure model that considers the intrarenal RAS, i.e. the *intrarenal model*.

5.3 Results

5.3.1 Model parameter identification and validation

As detailed in Section 5.2.3, after reparameterizing the model to represent a male Sprague Dawley rat, the remaining RAS- and renal sodium transport-related parameters were identified sequentially by fitting to data obtained from various Ang II infusion studies. The resulting parameter set and steady state variable values are shown in Tables C.1 and C.2, respectively.

RAS parameters Figure 5.2 summarizes the model’s fit to plasma [*AngII*] (panel a), total peripheral resistance (panel b), and intrarenal AT1R expression (panel c) data collected by Zou et al. [184], Pasquie et al. [117], and Zhu et al. [179], respectively. As shown in Figure 5.2a, introducing a bioavailability parameter ($F = 0.056$, solid curve) permitted the plasma [Ang II] to plateau by the end of a prolonged (> 2 week) infusion experiment and improved the model’s fit to experimental data. Moreover, this assumption did not effect the model’s ability to replicate the change in systemic and intrarenal RAS peptide levels resulting from a 40 ng/min subcutaneous Ang II infusion experiment (Figure 5.3). Indeed, simulations remain consistent with all experimental data [184] that was previously used to fit (dark green circular markers) and validate (light green diamond markers) the uncoupled RAS model.

With F and k_a optimized, two subsequent *in silico* Ang II infusion experiments were then performed to calibrate the effect of Ang II on vascular resistance (Figure 5.2b) and intrarenal AT1R feedback desensitization (Figure 5.2c). Indeed, it was found that a chronic, indirect effect of Ang II on vascular resistance ϵ_{OXST} was necessary for R_{tp} to increase beyond control to the levels observed experimentally by Pasquie et al [117]. A time constant τ_{OXST} of 9.86 days for the intermediate variable $OXST$ provided the best fit to experimental data [117]. Similarly, allowing intrarenal AT1R feedback, i.e. f_{Pt} and f_{Tb} , to desensitize

once the total amount of intrarenal AT1Rs exceeded a certain threshold value ($AT1R_T^*$, dotted line) was necessary to prevent the unreasonable activation of the intrarenal RAS following high dose and/or prolonged (greater than 2 week long) Ang II infusion experiments. A threshold of $AT1R_T^*/AT1R_T^{eq} = 4.2$ was found to fit the expression data from Zhu et al. [179] most optimally.

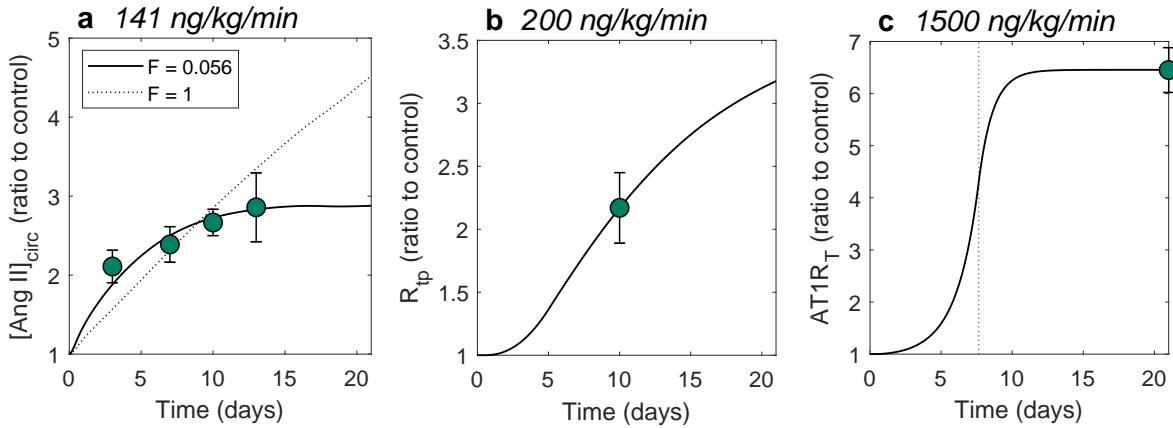


Figure 5.2: Simulated vs. experimental **a** plasma [Ang II], **b** total peripheral resistance R_{tp} , and **c** intrarenal AT1R levels following 141 ng/kg/min (40 ng/min) [184], 200 ng/kg/min [117], and 1500 ng/kg/min [179] Ang II infusions, respectively. **a** Introducing a bioavailability parameter ($F = 0.056$, solid curve) permitted the plasma [Ang II] to plateau after 2 weeks of Ang II infusion, as was observed by Zou and colleagues [184]. **b** A time constant τ_{OXS} of 9.86 days provided the best fit to available total peripheral resistance data from Ref. [117]. **c** A threshold intrarenal AT1R ratio of 4.3 over control provided the best fit to expression data from Ref. [179]. This threshold was achieved after approximately 7 days (vertical dotted line) for a subcutaneous dose of 1500 ng/kg/min.

Renal sodium transport parameters As detailed in Section 5.2.3, parameters related to sodium handling in the pt and dt were identified by simulating the 28-day, 80 ng/min Ang II infusion experiment of Minas et al. [102], minimizing the difference between the simulated and experimental blood pressure response curve, and imposing several constraints on sodium and water balance. In particular, blood volume could not exceed $\pm 8\%$ of baseline [69] and sodium and fluid balance had to be restored at the new hypertensive steady state. As shown in Figure 5.4, these constraints were satisfied not just for Minas et al. [102]’s 80 ng/min (≈ 282 ng/kg/min for a 284g rat) dose of Ang II, but for all non-

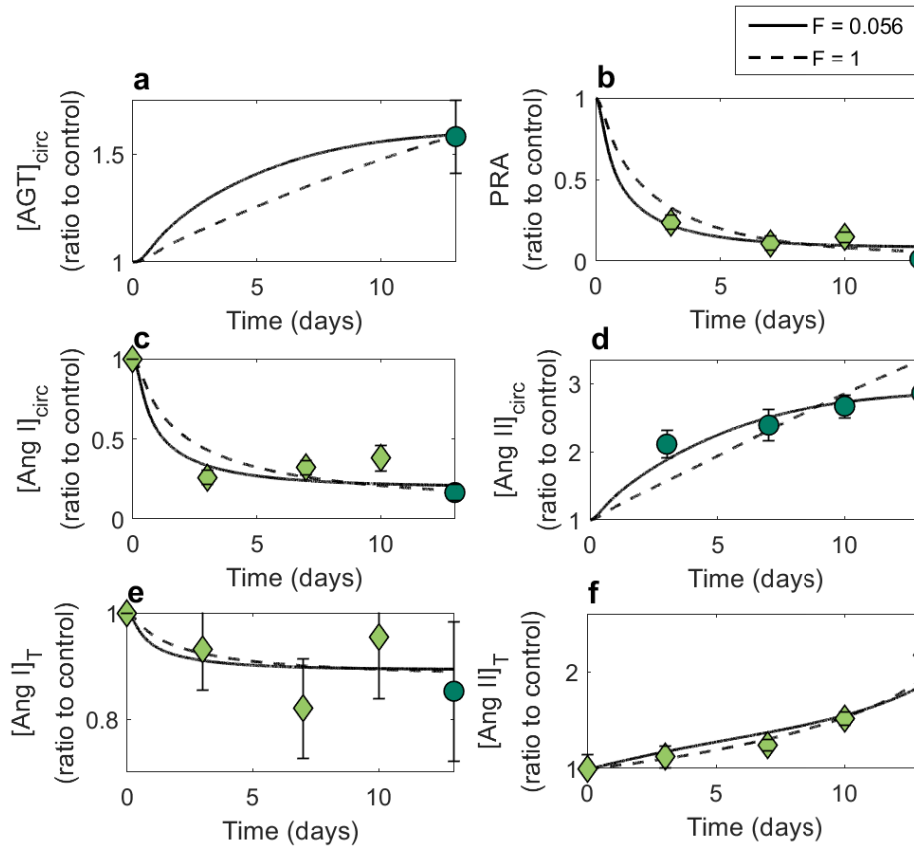


Figure 5.3: Impact of Ang II bioavailability on intrarenal and systemic RAS peptide time series following Ang II infusion. Simulations are compared to data collected by Zou et al. [184] during a 13-day, 40 ng/min Ang II infusion experiment. Dark green circular markers reflect the data points used for fitting. Light green diamond markers reflect the data points used for validation. Introducing a bioavailability parameter ($F = 0.056$; solid curves) improves the model’s fit to measured circulating plasma concentrations (panel D) and does not significantly effect any time series previously used for model validation (see Chapter 3).

pressor doses of Ang II from 40-400 ng/kg/min. The mechanisms by which such balance is restored are discussed in the Sections that follow (Section 5.3.2).

Figure 5.5 compares the predicted blood pressure responses of the *systemic model* (dashed curves) and the *intrarenal model* (solid curves) to data collected from two infusion experiments with different doses. In panel a, the two models fits to the data collected by

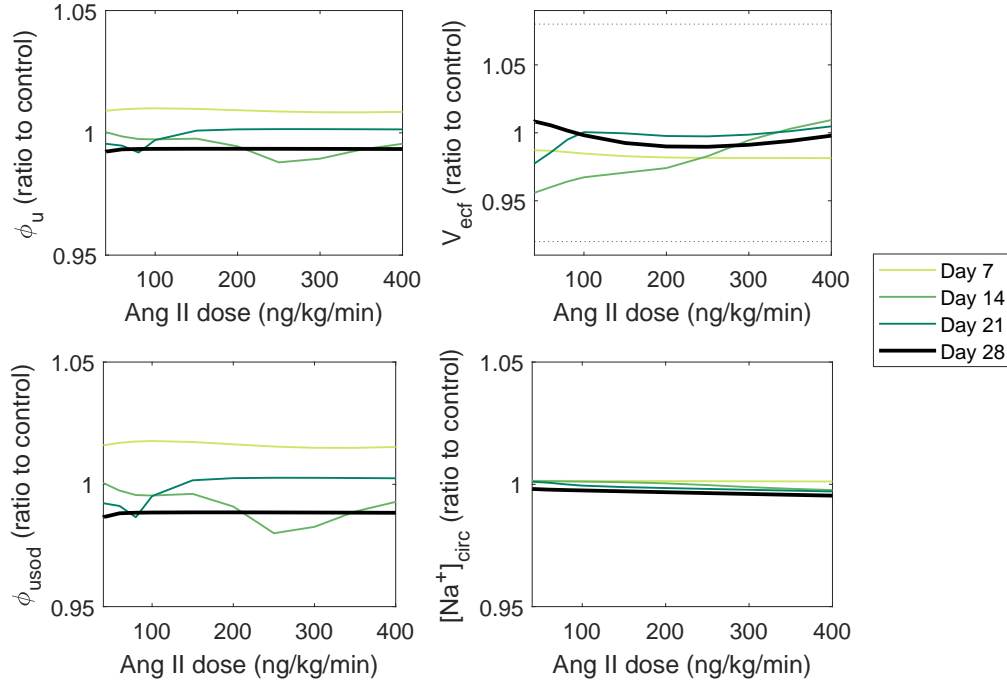


Figure 5.4: Impact of Ang II dosage on sodium and fluid balance after 7, 14, 21, and 28 days of subcutaneous infusion. With water and sodium intake fixed, **a** urine flow, **b** extracellular fluid volume, **c** sodium excretion, and **d** plasma sodium concentration should all return to baseline (ratio to control ≈ 1) by day 28 of each infusion. For the duration of each experiment, extracellular fluid volume does not exceed $\pm 4\%$ of control, which is consistent with the $\pm 8\%$ experimental bound (panel b, dotted lines) reported by King and Fink [69].

Minas et al. [102] are provided. In panel **b**, the two models are validated against the data collected by Sampson et al. [133] over the course of their 14 day, 400 ng/kg/min Ang II infusion experiment. At both doses, the *intrarenal model* (solid curves) shows excellent agreement to data. The *systemic model* (dashed curves) does not, despite sodium and fluid balance being restored in both cases (see below).

It is evident that the intrarenal RAS is essential to the development of slow-pressor hypertension: Although blood pressure rises to the same hypertensive steady state in both cases, it does so far too rapidly when a systemic-only RAS module is considered. To effectively replicate the slow-rise in blood pressure that follows the administration of sub-

pressor doses of Ang II, the intrarenal concentration of Ang II and its effects on sodium reabsorption need to be explicitly considered. Below, we discuss why this is the case and elaborate on the mechanisms involved in the development of slow-pressor hypertension.

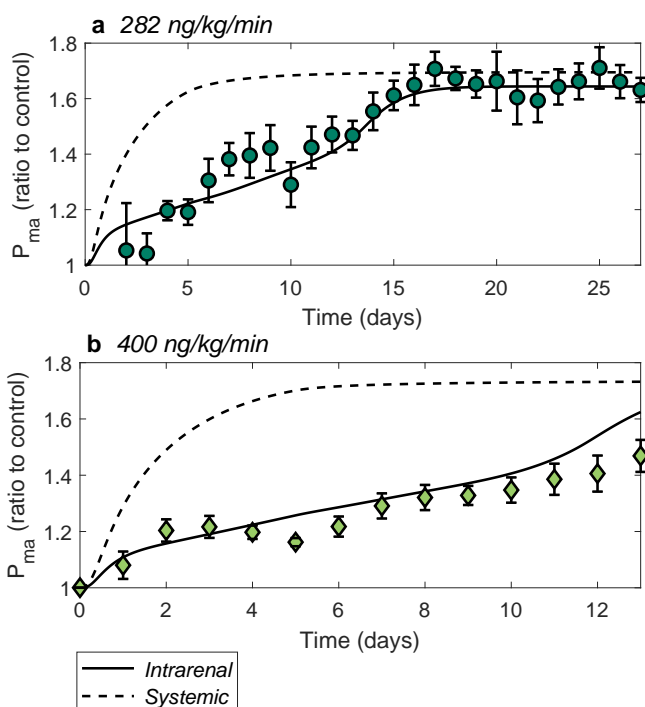


Figure 5.5: Impact of the intrarenal RAS on the blood pressure response induced by **a** 282 ng/kg/min (80 ng/min) [102] and **b** 400 ng/kg/min [133] Ang II infusion. Dark green circular markers reflect the data points used for fitting. Light green diamond markers reflect the data points used for validation. Dashed curves were simulated with the *systemic* model.

5.3.2 Model predictions

The development of Ang II-induced hypertension is mediated by the balance between pressure natriuresis and Ang II's direct and indirect effects on sodium reabsorption

To unravel the mechanisms that mediate the development of Ang II-induced hypertension, we extend the 400 ng/kg/min Ang II infusion experiment of Sampson et al. [133] to 28 days

and examine key model variables, such as; blood pressure, sodium balance, fluid volume, and vascular resistance when various Ang II-driven effects are turned on/off. Figure 5.6 summarizes the results. We begin by describing the results of the wild-type *intrarenal model* (solid curves), before delving in to the results of each *in silico* knockout experiment (dashed/dotted curves) to justify our conclusions. Furthermore, we divide the response into four Phases (white and grey shaded regions) based on whether the wild-type model is exhibiting net sodium reabsorption ($\phi_{usod} < \phi_{usodin}$) or excretion ($\phi_{usod} > \phi_{usodin}$):

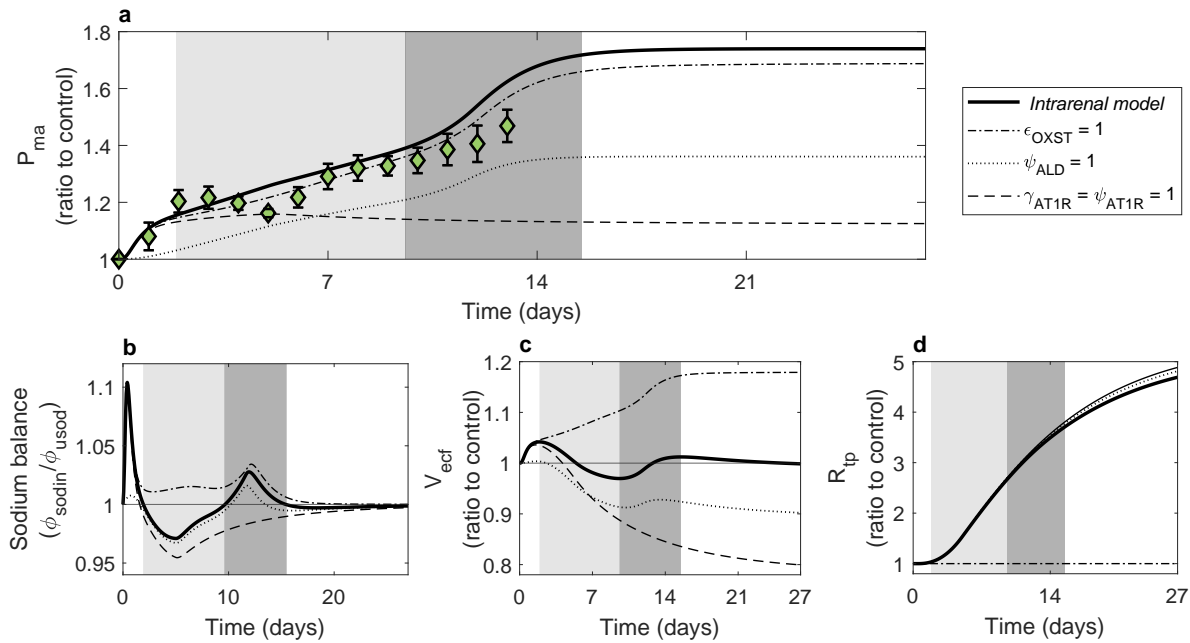


Figure 5.6: Mechanisms that mediate slow-pressor hypertension induced by Ang II infusion. The response of key model variables to a 400 ng/kg/min Ang II infusion are shown, including: **a** blood pressure (P_{ma}), **b** sodium balance ($\phi_{usod}/\phi_{usodin}$), **c** extracellular fluid volume (V_{ecf}), and **d** total peripheral resistance (R_{tp}). Wild-type *intrarenal model* simulations (solid curves) are compared to *in silico* knockout experiments, where the indirect aldosterone-mediated (dotted curves) and direct effects of Ang II on sodium reabsorption (dashed curves) and vascular resistance (dash-dotted curves) are removed. The first two weeks of the wild-type blood pressure response (panel **a**) are compared to validation data (markers) from Sampson et al. [133].

Phase 1 (Figure 5.6, first unshaded (white) region) begins with the rapid release of aldosterone from the adrenal gland shortly after the Ang II infusion begins. Aldosterone

acts on the kidney to increase sodium reabsorption (panel b) leading to an increase in extracellular fluid volume V_{ecf} (panel c) and blood pressure P_{ma} (panel a). This volume-induced increase in P_{ma} feeds back to inhibit *pt* sodium reabsorption via the pressure natriuresis response γ_{hyp} (Eq. 5.10). This negative feedback restores sodium balance by the end of Phase 1 and prevents V_{ecf} from rising any further.

At the start of **Phase 2** (Figure 5.6, light grey shaded region), the chronic effects of Ang II on vascular resistance R_{tp} (panel d) have begun to take effect. As a result, P_{ma} (panel a) continues to rise despite the fact that blood volume (panel c) is now decreasing (because of the pressure-natriuresis effect). Blood volume does not decrease indefinitely however due to the progressive rise in intrarenal Ang II that has been occurring alongside each of these processes: Indeed, at approximately mid-way through Phase 2 (day 6 of the infusion), the AT1R-mediated effects of Ang II on *pt* and *dt* sodium reabsorption have sufficiently activated and begin to overpower the pressure natriuresis response. This brings sodium balance back to baseline (and causes V_{ecf} to hit a local minimum) by the end of Phase 2.

The direct effects of Ang II on sodium reabsorption remain in full effect at the start of **Phase 3** (Figure 5.6, dark grey shaded region). Indeed, there is a net reabsorption of sodium and water (panel b) that causes V_{ecf} (panel c) to increase. However, after a few more days of Ang II infusion, the positive feedback on intrarenal AT1Rs (Eq. 5.21) starts to desensitize (Eq. 5.20) and tubular epithelial cell-associated Ang II levels level off. With all sodium reabsorption-enhancing effects now saturated and P_{ma} (panel a) still rising, the pressure natriuresis effect takes over once again which brings sodium excretion back to baseline by the end of Phase 3.

In **Phase 4** (Figure 5.6, second unshaded (white) region), P_{ma} equilibrates such that the value of γ_{hyp} (Eq. 5.10) at the new hypertensive steady state balances the combined effect of all sodium reabsorption-inducing functions that have since saturated. In other words, after approximately 15 days of prolonged infusion the pressure natriuresis response has shifted to a higher set point in order to maintain sodium and fluid balance. This supports experimental findings that the *resetting of the pressure natriuresis response necessitates increased blood pressure to maintain solute and fluid homeostasis*: Blood pressure must rise sufficiently for its feedback on *pt* sodium reabsorption to balance the combined stimulatory effects of aldosterone and Ang II along the nephron.

These findings are confirmed by the results of various *in silico* knockout studies: Firstly, When the effect of aldosterone on sodium reabsorption ψ_{ALD} (Eq. 5.14) is removed (Figure 5.6, dotted curves), the initial increase in sodium reabsorption (panel b), V_{ecf} (panel c), and P_{ma} (panel a) are all significantly inhibited. Secondly, when the vascular effects of

Ang II are inhibited ($\epsilon_{O_{XST}} = 1$; Figure 5.6, dash-dotted curves), P_{ma} never rises to the extent required to bring ϕ_{usod} above and thus, V_{ecf} back to baseline. Instead, the model remains in a state of net sodium reabsorption for the remainder of the infusion, leading to an unphysiological volume-induced increase in P_{ma} . Lastly, when the direct effects of intrarenal Ang II on sodium reabsorption are inhibited ($\gamma_{AT1R} = \psi_{AT1R} = 1$; Figure 5.6, dashed curves), the model no longer shifts from a state of net excretion to net reabsorption as it enters Phase 3 of the response. As a result, there is net loss of volume and hypertension is no longer observed.

The relative low blood pressure in the previous knockout experiment speaks to the importance of Ang II-mediated sodium handling in the development of hypertension: With this effect removed, hypertension is no longer observed. To determine whether the timing of the activation is equally as significant, next we compare these findings to those of the *systemic model*, where all effects of intrarenal Ang II are replaced with systemic Ang II (which has more rapid dynamics). Results are shown in Figure 5.7.

Aldosterone and Ang II must act at distinct time scales within the kidney to observe slow-pressor hypertension

As demonstrated in Figure 2.2, both the *systemic model* and the *intrarenal model* produce the same degree of hypertension (panel a) and adequately restore sodium and water balance (panels b and c) following prolonged Ang II infusions. However, the *systemic model* is incapable of producing slow-pressor hypertension. Indeed, P_{ma} rises far too rapidly when the concentration and the effects of intrarenal Ang II are not considered. Simulations suggest that this is because the hypertensive mechanism differs (Figure 5.8): With aldosterone and Ang II acting simultaneously on the kidney in the *systemic model*, Phase 1 of the response is significantly exaggerated, i.e. the initial increase in sodium reabsorption, V_{ecf} , and P_{ma} are much larger. Furthermore, since systemic Ang II does not progressively rise during the infusion like intrarenal Ang II, there is no Phase 2 or Phase 3 of the response. Instead, Phase 1 is followed directly by Phase 4 and there is no slow rise in P_{ma} .

In summary, our results suggest that the slow development of hypertension following Ang II infusion is dictated by the timing of Ang II's actions within the kidney. In particular, the indirect (aldosterone-mediated) and direct actions of Ang II on sodium reabsorption must occur sequentially. This is facilitated by the de-coupling of the systemic and intrarenal RASs. Our results, illustrated in Figure 5.8, therefore shed light on the functional importance of the progressive rise in intrarenal Ang II that has been observed in various experimental models of slow-pressor hypertension.

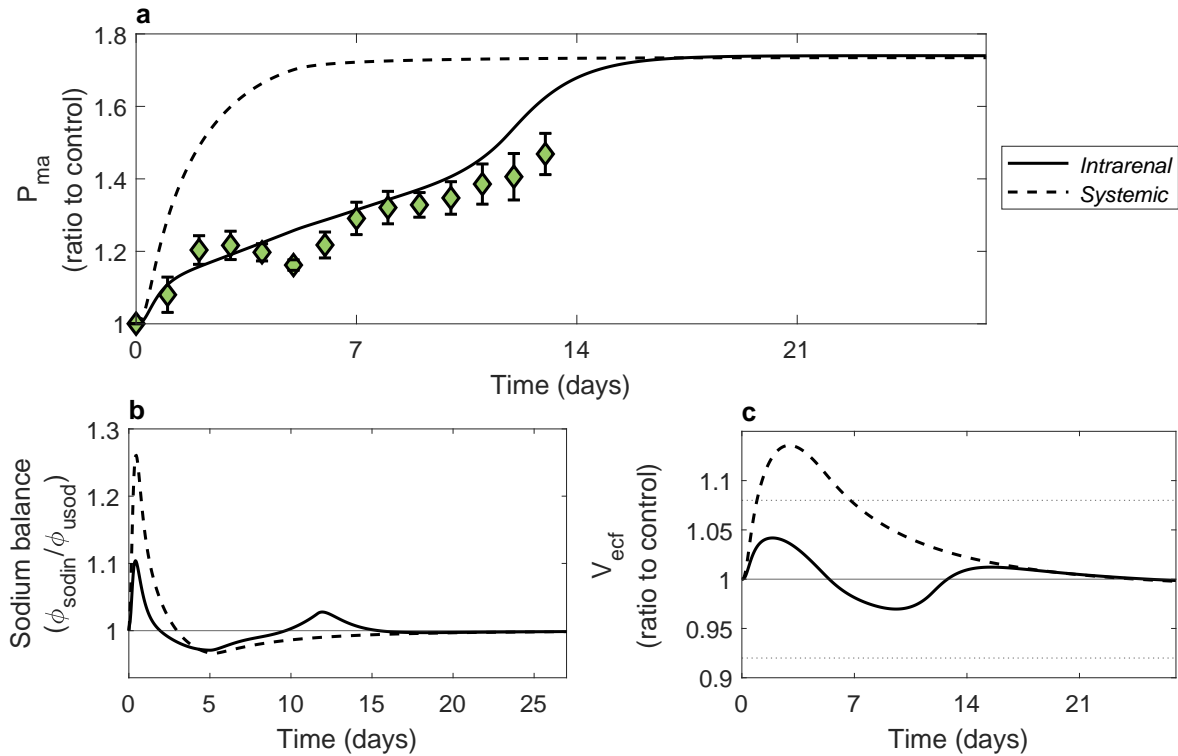


Figure 5.7: Impact of intrarenal Ang II on the development of slow-pressor hypertension. The response of key model variables to a 400 ng/kg/min Ang II infusion are shown, including: **a** blood pressure (P_{ma}), **b** sodium balance (ϕ_{usod}/ϕ_{sodin}), and **c** extracellular fluid volume (V_{ecf}), when the *intrarenal model* (solid curves) vs. the *systemic model* (dashed curves) is simulated. To effectively replicate the slow-rise in blood pressure that follows the administration of sub-pressor doses of Ang II, the intrarenal concentration of Ang II and its effects on sodium reabsorption need to be explicitly considered.

5.4 Discussion

The primary goal of this Chapter was to identify the role of the intrarenal RAS in the development of hypertension induced by Ang II infusion. To accomplish this, Ahmed and Layton [1]’s male rat long-term blood pressure regulation model was updated and coupled to the intrarenal and systemic RAS model presented in Chapter 2. After parameterizing and validating the coupled model against data collected from various Ang II infusion experiments, simulations were conducted to gain insight into the mechanisms that mediate

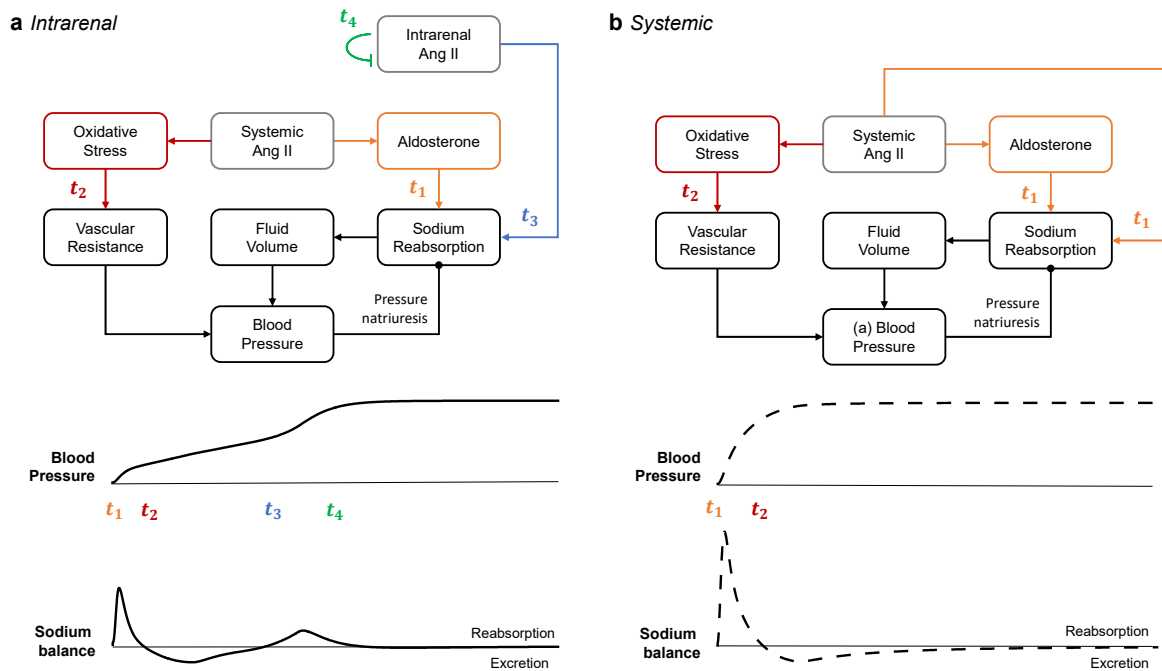


Figure 5.8: Schematic representation of the mechanisms governing Ang II-induced hypertension when the **a** *intrarenal model* or the **b** *systemic model* is simulated. Aldosterone and Ang II must act at distinct time scales (t_1 and t_3 , respectively) within the kidney to observe slow-pressor hypertension.

slow-pressor hypertension. By comparing the findings of this *intrarenal model* to those of a *systemic model* where all intrarenal effects of Ang II were (falsely) assumed to be mediated by systemic Ang II, the particular importance of the intrarenal RAS in producing such blood pressure responses was elucidated. Below, we discuss the answers to the research questions outlined in Section 5.1.

Does the resetting of the pressure natriuresis mechanism necessitate increased blood pressure to maintain solute and fluid homeostasis in Ang II-induced hypertensive rats? Yes. Simulations suggest that in Ang II-induced hypertension in particular, a higher set point for the pressure natriuresis mechanism (i.e. its resetting) is required to maintain sodium balance. In other words, impaired pressure natriuresis is not a consequence of, but rather a cause of the observed hypertension. With Ang II acting both directly and indirectly to stimulate sodium reabsorption along the nephron, blood pressure

must increase to an extent that produces an equally-strong inhibitory effect on *pt* sodium reabsorption to restore sodium balance. Indeed, when either the indirect (aldosterone-mediated; Figure 5.6, dotted curves) or the direct (Figure 5.6, dashed curves) effects of Ang II on the kidney were removed from the model, blood pressure (Figure 5.6a) did not increase nearly as significantly relative to the wild-type simulations. This conclusion is consistent with the experimental studies of Hall et al. in Ang II-induced hypertensive dogs [47] and has also been observed in other experimental models of hypertension, such as aldosterone, adrenocorticotrophic hormone, and norepinephrine hypertension [48].

Do progressively rising intrarenal Ang II levels functionally contribute to slow-pressor hypertension? Yes. Not only must Ang II accumulate in the kidney to observe hypertension following Ang II infusion (as illustrated by the aforementioned *in silico* knockout experiments; Figure 5.6, dashed curves), but the speed at which intrarenal Ang II levels rise also dictates the dynamics of the conditions progression. In particular, our results suggest that aldosterone and Ang II must act at distinct time scales within the kidney to observe slow-pressor hypertension (Figure 5.8a). When the two peptides act simultaneously (as was the case in the *systemic model*; Figure 5.8b), blood pressure rises far faster than is experimentally predicted. The successive activation of sodium transport by aldosterone and Ang II was also necessary to ensure that extracellular fluid volume did not exceed the experimental bounds reported by King and Fink [69] ($\pm 8\%$) during each Ang II infusion experiment. Indeed, extracellular fluid volume remained within $\pm 4\%$ of control throughout all *intrarenal* infusion experiments (Figure 5.7c, solid curve), but increased to over 13% of control during the *systemic* experiments (Figure 5.7c, dashed curve).

In practice, the sequential activation of sodium transport by Ang II is facilitated by the de-coupling of the systemic and intrarenal RASs. Indeed, systemic Ang II levels (Figure 5.3d) rise far more rapidly than intrarenal Ang II levels (Figure 5.3f) during the development of Ang II-induced hypertension. As discussed in Chapter 3, this is because Ang II accumulates extracellularly in the plasma, but intracellularly in the kidney. Indeed, intrarenal Ang II levels do not rise significantly until the positive feedback on intrarenal AT1R expression has sufficiently activated to facilitate enhanced AT1R-mediated uptake of circulating Ang II into tubular epithelial cells.

5.4.1 Model limitations and future extensions

The model presented in this Chapter has several limitations. Firstly, all renal hemodynamic variables (renal blood flow and glomerular filtration rate) are assumed constant. Although,

the latter is consistent with experimental findings [4, 167, 32], an increase in intrarenal Ang II is known to lower renal blood flow by increasing afferent and efferent arteriole resistance [167, 4]. This increase in filtration fraction is not captured by the present model. In future work, the effects of Ang II on afferent and efferent arteriole resistance [176] can be re-introduced to the model, along with the effects of tubuloglomerular feedback [10] and the myogenic response [96]. Having calibrated an accurate dose-dependent formalism to simulate Ang II infusion experiments in this Chapter, these effects can be compared to *in vivo* hemodynamic data from Ref's [32] and [166] for the purposes of fitting and/or validation.

Secondly, when calibrating the present model, we were limited in the amount of data that was available to fit the renal sodium transport parameters. While the impact of Ang II on tubular sodium transporter expression has been measured experimentally [112], the downstream effect of these changes on sodium flux along the nephron remains unknown. Therefore, to fit our model we used computational estimates of these fluxes [30]. In future work, we could instead replace the current sodium and fluid handling component of the blood pressure regulation model with the kidney function model of Edwards et al. [30] directly. In this way, the measured effects of Ang II on sodium transporters could be considered explicitly.

Another avenue for future work would be to couple the PK model of Losartan presented in Chapter 4 to the blood pressure regulation model described here. Coupling can be achieved via the drug's known AT1R binding properties and the impact of blood volume on its systemic concentration. Coupling may also require that some solute transport effector functions be re-calibrated, as each were only fit to data where the local AT1R-bound Ang II concentration increased above control. When Losartan is administered, we expect these concentrations to decrease. Moreover, since the glomerular filtration rate is often not conserved following Losartan administration [170], the renal hemodynamic component of the model must also first be updated as described above. Nevertheless, once complete the resultant PK/PD model would allow us to study the downstream effects of inhibited intrarenal Ang II accumulation on blood pressure explicitly. Furthermore, by simulating Losartan administration under different autoregulatory conditions, the mechanisms contribution to the drug's variable effect on renal hemodynamics could also be investigated.

A similar approach could also be taken to study the effects of ACEis on blood pressure regulation. Indeed, a PK model of a common ACEi could be created and coupled to that of blood pressure regulation via the inhibition of systemic and intrarenal ACE activity. By comparing its findings to those of the comprehensive Losartan model outlined above, the differential effects of ARBs and ACEis could be quantified. In Chapter 4, we hypothesized that ARBs would be more effective than ACEis in preventing hypertension induced by Ang

II because the latter class of drugs would not prevent the intracellular uptake of exogenous Ang II in the kidney. This hypothesis could be substantiated should these two PK/PD models be developed.

Like all models developed in this thesis, this blood pressure regulation model and its results are specific to male rats. However, many regulators of blood pressure, including both the RAS and kidney function, are different between the sexes. Ahmed and Layton [1] previously created sex-specific models of blood pressure regulation in the rat by accounting for differences in size, renal hemodynamics, and systemic RAS hormone concentrations. In future work, a similar re-parameterization could be applied to the model presented in this Chapter to create versions that include an intrarenal RAS. Once developed, the resulting sex-specific blood pressure regulation models could be used to explain why blood pressure increases more in male rats than female rats chronically infused with the same dose of Ang II [133]. These models could also be coupled to that of Losartan (Chapter 4) to examine why males and females respond differently to anti-hypertensive therapies that target the RAS.

Finally, the current model does not represent the circadian pattern of blood pressure nor its regulators. By extending the model to incorporate these rhythms in appropriate model parameters, and possibly coupling it to a kidney function model that represents circadian rhythms [76, 164], it can be used to examine how circadian disruption may contribute to the pathogenesis of hypertension. Indeed, disruption of the circadian pattern of blood pressure is associated with increased risk of cardiovascular disease [27].

Chapter 6

Conclusions

Hypertension is the leading cause of cardiovascular disease and premature death world-wide [8, 101]. Despite the many social and pharmacological efforts aimed at hypertension prevention and control, its prevalence continues to increase. In 2015, 1.52 billion adults were impacted globally; 137 million (9%) more than in 2010 [8, 101]. Hypertension is rapidly becoming a world-wide epidemic. Thus, it is imperative that we fully understand blood pressure physiology and the etiology of its dis-regulation.

Hypertension is a multi-factorial condition associated with multiple risk factors and patho-physiological changes. The interconnected nature of the systems involved makes it difficult, and in many cases impossible, to link its inception to a single cause. Animal experimental models have proved useful in reducing the complexity of the problem, allowing researchers to focus on how the impairment of one system may affect the others and lead to hypertension. By building off of these experimental results, computational models can be developed and used to run *in silico* experiments that may be difficult or impossible to perform in practice. Historically, such computational efforts have proved particularly useful when studying systems that are multi-factorial in nature, such as blood pressure regulation, because once a model has been developed that includes all components of interest, they can be turned on/off to examine their impact on the network as a whole.

In the Chapters presented in this thesis, we developed various computational models to study the intrarenal RAS in hypertension by building off the results of one experimental model of interest; chronic Ang II infusions. Our contributions to the field include: a novel model of the intrarenal and systemic RAS in the male rat (*model 1*); the first PK/PD model of the ARB Losartan that considers the kidney (*model 2*); and the first whole-body long-term blood pressure regulation model that includes an intrarenal RAS (*model 3*).

Below, we discuss how these models were used to answer our initial research questions and summarize our key findings:

What mechanisms mediate the progressive rise in intrarenal Ang II that accompanies hypertension induced by Ang II infusion? Enhanced AT1R-mediate uptake of circulating Ang II (*UPTK*) is the primary mechanism by which Ang II accumulates in the kidney in Ang II-induced hypertension: Previously, both *UPTK* and increased endogenous Ang II production (*PROD*) had been suggested as mechanisms contributing to intrarenal Ang II accumulation following chronic Ang II infusions. However, their individual contributions to this response had yet to be delineated. Since each mechanism relies on a distinct source of intrarenal positive feedback (*UPTK*; enhanced tubular epithelial AT1R expression, *PROD*; enhanced proximal tubule AGT and collecting duct renin production), we took a computational approach to unravel their effects: By simulating *model 1* in the absence and presence of the different positive feedback loops, we showed that *UPTK* is the primary mechanism by which Ang II accumulates in the kidney. *PROD* acts secondarily to conserve basal Ang II production rates despite significantly reduced plasma, and therefore filtered, peptide levels. Indeed, the vast majority of Ang II accumulates intracellularly after positive feedback on intrarenal AT1R expression has been sufficiently activated.

How does this over-activation contribute to blood pressure dis-regulation? An over-active intrarenal RAS increases blood pressure via Ang II's direct effects on sodium reabsorption in the kidney: While hypothesized in Chapter 3, this was confirmed in Chapter 5 by running simulations using *model 3*. Indeed, with Ang II acting directly (and indirectly) to increase sodium reabsorption along the nephron, blood pressure must increase to an extent that produces an equally-strong inhibitory effect on proximal tubule transport such that sodium balance is restored via pressure natriuresis. When the direct effects of Ang II on the kidney were removed *in silico*, hypertension was not observed. Hypertension was also inhibited when Ang II's indirect (aldosterone-mediated) effects on sodium reabsorption were removed, though to a lesser extent. In summary, our results suggest that in Ang II-induced hypertension, Ang II initiates the resetting of the pressure natriuresis mechanism by stimulating sodium reabsorption. Since impaired pressure natriuresis is observed in all cases of hypertension, it is likely that the same is true for cases of clinical hypertension stemming from an over-active RAS.

Another key model insight was the discovery that the timing of intrarenal RAS over-activation affects the dynamics of the blood pressure response. Indeed, slow pressor hypertension is a consequence of systemic and intrarenal RAS decoupling: The progressive accumulation of Ang II in the kidney permits the sequential activation of sodium reabsorption by aldosterone, then Ang II. This decoupling also allows fluid volume to remain within normal physiological limits over the course of the infusion. Our findings explain why

previous model iterations, which only consider the systemic RAS, were unable to replicate the slow rise in blood pressure that accompanies Ang II infusion [1].

How are these responses altered by treatment with RAS-modulating anti-hypertensive therapies? ARBs prevent intrarenal Ang II levels from rising by blocking all positive feedback in the kidney, but likely prevent blood pressure from rising by blocking the peptide's main intracellular uptake pathway: The key point break-down effect, i.e. the inhibition of all intrarenal positive feedback, had previously been proposed as the mechanism by which Losartan prevents both intrarenal Ang II and blood pressure from rising following Ang II infusion [170]. While model simulations confirm that the former is true, we propose that the latter is not. Indeed, we observed that Losartan administration inhibits both *UPTK* and *PROD*. The former, driven by a lack of positive feedback on AT1R expression, prevented circulating (exogenous) Ang II from accumulating in tubular epithelial cells. The latter, driven by a lack of positive feedback on local AGT and renin production, helped to maintain intrarenal endogenous peptide concentrations despite their significantly higher plasma concentrations. These two effects successfully prevented intrarenal Ang II levels from rising significantly during each infusion. Perhaps more importantly however, we also observed a shift in Ang II localization from mainly intracellular to mainly extracellular compartments. We hypothesize that it is actually this effect that primarily contributes to Losartan's blood pressure normalizing effects. Indeed, regardless of its intrarenal concentration, if Ang II cannot bind to or enter renal cells, it cannot effect sodium reabsorption and thus blood pressure. Below, we elaborate on this hypothesis in greater detail.

How does this explain the effectiveness of these treatment strategies in preventing clinical hypertension associated with an overactive RAS? We hypothesize that by blocking AT1Rs, ARBs effectively remove all previous sodium reabsorption enhancing stimuli which allows pressure natriuresis to return to its initial set point: With all Ang II restricted to extracellular compartments and unable to bind to AT1Rs, both its indirect and direct effects on sodium reabsorption become inhibited. Indeed, systemic Ang II is no longer able to stimulate the release of aldosterone and intrarenal Ang II is no longer able to act on the kidney directly. Without these stimuli present to increase sodium reabsorption, an elevated blood pressure is no longer required to maintain sodium balance via pressure natriuresis. In fact, if blood pressure were to remain at its previous hypertensive set point, we hypothesize that the body would be put in a state of negative sodium balance and volume would decrease to unphysiological levels. In essence, ARBs trigger yet another resetting of the pressure natriuresis mechanism where blood pressure now decreases to restore sodium balance. As discussed below, in future work this hypothesis could be substantiated by coupling the [PK](#) model of Losartan outlined in [Chapter 4](#) to the blood pressure model presented in [Chapter 5](#).

6.1 Model limitations and future extensions

In this thesis, we produced three novel computational models to study the role of the intrarenal RAS in hypertension. Beginning with the development of an isolated RAS model (*model 1*), we zoomed in to unravel the mechanisms mediating the progressive rise in intrarenal Ang II that accompanies Ang II infusion. Then, by extending the model to include a PK representation of the ARB Losartan (*model 2*), we examined the impact of this RAS-modulating anti-hypertensive therapy on the general activity of the intrarenal RAS. Lastly, by coupling our model to one of blood pressure regulation and creating the first model of long-term blood pressure regulation that considers an intrarenal RAS (*model 3*), we zoomed back out to determine how the aforementioned effects actually contribute to blood pressure dis-regulation. In general, with these models we were able to analyze the mechanisms contributing to both the development of and the prevention of hypertension at multiple scales. Below, we discuss the multiple ways that our models and results could be extended in future work.

Modelling sex-differences The models presented in this thesis are specific to male rats. Because the majority of physiological research has been conducted in males, this choice was made to maximize the amount of data that could be used for model calibration and validation. However, it has been long established that the steady state concentrations of most RAS peptides differ between males and females [119], and that each sex responds differently to anti-hypertensive therapies that target the RAS [84]. Moreover, in multiple experimental models of hypertension, including spontaneously hypertensive rats, salt-sensitive rats, and Ang II hypertensive rats, males develop an earlier and more severe hypertension than females [79, 133]. It is important that future work address these differences. Not only will this ensure an equal understanding of the mechanisms governing the development of and the prevention of hypertension in females, but hopefully improve our understanding of why young males appear to be more at risk for clinical hypertension than females [79]. In practice, a sex-specific investigation of the intrarenal RAS in hypertension and renal function would begin with the re-calibration of our intrarenal RAS model to the systemic and whole-kidney experimental measurements collected by [119]. This model could be subsequently coupled to our PK model of Losartan (or a different RAS-modulating anti-hypertensive therapy), a sex-specific blood pressure regulation model [1], a sex-specific epithelial solute transport model [92, 56, 57, 58], or a sex-specific renal blood flow model [20] to study how sex affects kidney function and blood pressure (dis-)regulation.

Modelling anti-hypertensive therapies In Chapter 4 we created the first PK/PD model of the ARB Losartan that considers the kidney. In doing so, we gained key insight into how this medication modulates the activity of the intrarenal RAS in hypertensive male

rats. However, because blood pressure was not represented explicitly, we could not quantify the downstream impact of these changes on blood pressure regulation. In future work, this could be overcome by coupling the model's PK component to the model of long term blood pressure regulation presented in Chapter 5. A similar approach could be taken to study other RAS-modulating anti-hypertensive therapies such as ACEis. Given the multifactorial nature of hypertension, there is no one way to treat it. Different patients respond differently to different classes of medication. By improving our understanding of how each medication targets each regulator of blood pressure, computational modelling can be used to inform and suggest more tailored treatment regimens based on a patient's history, sex, and co-morbidities. With multiple PK models calibrated, the effect of polytherapeutic treatment regimens (simultaneous treatment with 2 or more medications) could also be investigated; Polytherapy is common and often required to get blood pressure under control [26].

Modelling other experimental models of hypertension Here we have discussed the role of the intrarenal RAS in the pathogenesis of hypertension induced by Ang II infusion. However, Ang II infusion is an experimental model which relies on the constant administration of non physiological doses of Ang II [174]. As a result, it has a limited scope in terms of its relevance to clinical hypertension. Nevertheless, the conclusions drawn from this work may have broader implications to other forms of hypertension that are associated with an overactive RAS. Indeed, the decoupling of the systemic and intrarenal RAS has been observed in many other experimental models of hypertension that better represent clinical hypertension, such as: two-kidney, one-clip Goldblatt hypertension [18], salt-sensitive rats [168], and spontaneously hypertensive rats [150]. Hence, it is expected that the systemic and intrarenal RAS become de-coupled in cases of clinical hypertension that are associated with an overactive RAS. Furthermore, the mechanisms mediating this effect are likely the same as those that contribute to Ang II-induced hypertension. These hypotheses can be further explored in future work, by using the presented models to study the functional role of the intrarenal RAS in other experimental models of hypertension that do not involve the exogenous infusion of Ang II.

Modelling other (patho-)physiological systems While the studies presented in this thesis were specific to hypertension, the intrarenal RAS is also known to be involved and exhibit notable changes in various other conditions, such as: pregnancy [145], nephrectomy [75, 34, 81], and SGLT2 inhibition and diabetes [80, 55, 82, 148]. By integrating our model of the RAS into existing computational models of these other physiological and pathophysiological systems, we can begin to unravel the many and diverse ways in which the intrarenal RAS influences our physiology and health.

Historically, mathematical physiology has been an invaluable tool to unravel the com-

plex systems involved in a wide range of biological and physiological phenomenon [68]. Here, we demonstrated its effectiveness in studying the intricacies of blood pressure physiology and the etiology of its dis-regulation. It is our hope that future studies can continue moving the needle towards a more comprehensive understanding of hypertension, so that more effective treatment and prevention strategies may be devised.

References

- [1] Sameed Ahmed and Anita T Layton. Sex-specific computational models for blood pressure regulation in the rat. *American Journal of Physiology-Renal Physiology*, 318(4):F888–F900, 2020.
- [2] Toru Aizawa, Nobukazu Ishizaka, Shin-Ichi Usui, Noriko Ohashi, Minoru Ohno, and Ryozo Nagai. Angiotensin ii and catecholamines increase plasma levels of 8-epi-prostaglandin f2 α with different pressor dependencies in rats. *Hypertension*, 39(1):149–154, 2002.
- [3] SA Al-Merani, DP Brooks, BJ Chapman, and KA Munday. The half-lives of angiotensin II, angiotensin II-amide, angiotensin III, Sar1-Ala8-angiotensin II and renin in the circulatory system of the rat. *The Journal of physiology*, 278(1):471–490, 1978.
- [4] Shuji Arima, Kentaro Kohagura, Michiaki Abe, and Sadayoshi Ito. Mechanisms that control glomerular hemodynamics. *Clinical and experimental nephrology*, 5:55–61, 2001.
- [5] Eun Ji Baek and Sejoong Kim. Current understanding of pressure natriuresis. *Electrolytes & Blood Pressure: E & BP*, 19(2):38, 2021.
- [6] Edwin J Baldelomar, Jennifer R Charlton, Scott C Beeman, and Kevin M Bennett. Measuring rat kidney glomerular number and size in vivo with MRI. *American Journal of Physiology-Renal Physiology*, 314(3):F399–F406, 2018.
- [7] Nidia Basso and Norberto A Terragno. History about the discovery of the renin-angiotensin system. *Hypertension*, 38(6):1246–1249, 2001.
- [8] Emelia J Benjamin, Paul Muntner, Alvaro Alonso, Marcio S Bittencourt, Clifton W Callaway, April P Carson, Alanna M Chamberlain, Alexander R Chang, Susan Cheng, Sandeep R Das, et al. Heart disease and stroke statistics—2019 update: a report from the american heart association. *Circulation*, 139(10):e56–e528, 2019.

- [9] Marie Briet and Ernesto L Schiffrin. Aldosterone: effects on the kidney and cardiovascular system. *Nature Reviews Nephrology*, 6(5):261–273, 2010.
- [10] JOSEPHINE P Briggs, GISELA Schubert, and JURGEN Schnermann. Quantitative characterization of the tubuloglomerular feedback response: effect of growth. *American Journal of Physiology-Renal Physiology*, 247(5):F808–F815, 1984.
- [11] Kevin D Burns and Ningjun Li. The role of angiotensin II-stimulated renal tubular transport in hypertension. *Current hypertension reports*, 5(2):165–171, 2003.
- [12] Duncan J Campbell. Critical review of prorenin and (pro) renin receptor research. *Hypertension*, 51(5):1259–1264, 2008.
- [13] Duncan J Campbell. Do intravenous and subcutaneous angiotensin II increase blood pressure by different mechanisms? *Clinical and Experimental Pharmacology and Physiology*, 40(8):560–570, 2013.
- [14] Duncan J Campbell, Anne C Lawrence, Amanda Towrie, Athena Kladis, and Anthony J Valentijn. Differential regulation of angiotensin peptide levels in plasma and kidney of the rat. *Hypertension*, 18(6):763–773, 1991.
- [15] Statistics Canada. Blood pressure of adults, 2016-2019. Health fact sheets, Statistics Canada, 2021.
- [16] Statistics Canada. Table 13-10-0801-01 leading causes of death, total population (age standardization using 2011 population). Data table, Statistics Canada, 2022.
- [17] Dulce Elena Casarini, Mirian Aparecida Boim, RC Stella, MH Krieger-Azzolini, Jose Eduardo Krieger, and Nestor Schor. Angiotensin I-converting enzyme activity in tubular fluid along the rat nephron. *American Journal of Physiology-Renal Physiology*, 272(3):F405–F409, 1997.
- [18] Ludek Cervenka, Chi-Tarng Wang, Kenneth D Mitchell, and L Gabriel Navar. Proximal tubular angiotensin II levels and renal functional responses to at1 receptor blockade in nonclipped kidneys of Goldblatt hypertensive rats. *Hypertension*, 33(1):102–107, 1999.
- [19] Jing Chen, Ioannis Sgouralis, Leon C Moore, Harold E Layton, and Anita T Layton. A mathematical model of the myogenic response to systolic pressure in the afferent arteriole. *American Journal of Physiology-Renal Physiology*, 300(3):F669–F681, 2011.

- [20] Ying Chen, Jennifer C Sullivan, Aurélie Edwards, and Anita T Layton. Sex-specific computational models of the spontaneously hypertensive rat kidneys: factors affecting nitric oxide bioavailability. *American Journal of Physiology-Renal Physiology*, 313(2):F174–F183, 2017.
- [21] Hui-Fang Cheng, Bryan N Becker, Kevin D Burns, Raymond C Harris, et al. Angiotensin II upregulates type-1 angiotensin II receptors in renal proximal tubule. *The Journal of clinical investigation*, 95(5):2012–2019, 1995.
- [22] Steven D Crowley, Susan B Gurley, Maria J Herrera, Phillip Ruiz, Robert Griffiths, Anil P Kumar, Hyung-Suk Kim, Oliver Smithies, Thu H Le, and Thomas M Coffman. Angiotensin II causes hypertension and cardiac hypertrophy through its receptors in the kidney. *Proceedings of the National Academy of Sciences*, 103(47):17985–17990, 2006.
- [23] Chantal Csajka, Thierry Buclin, Hans R Brunner, and Jérôme Biollaz. Pharmacokinetic-pharmacodynamic profile of angiotensin ii receptor antagonists. *Clinical pharmacokinetics*, 32:1–29, 1997.
- [24] Chantal Csajka, Thierry Buclin, Karin Fattinger, Hans R Brunner, and Jérôme Biollaz. Population pharmacokinetic-pharmacodynamic modelling of angiotensin receptor blockade in healthy volunteers. *Clinical pharmacokinetics*, 41:137–152, 2002.
- [25] Kate M Denton, Warwick P Anderson, and Raja Sinniah. Effects of angiotensin II on regional afferent and efferent arteriole dimensions and the glomerular pole. *American Journal of Physiology-Regulatory, Integrative and Comparative Physiology*, 279(2):R629–R638, 2000.
- [26] Catherine G Derington, Jordan B King, Jennifer S Herrick, Daichi Shimbo, Ian M Kronish, Joseph J Saseen, Paul Muntner, Andrew E Moran, and Adam P Bress. Trends in antihypertensive medication monotherapy and combination use among us adults, national health and nutrition examination survey 2005–2016. *Hypertension*, 75(4):973–981, 2020.
- [27] Lauren G Douma and Michelle L Gumz. Circadian clock-mediated regulation of blood pressure. *Free radical biology and medicine*, 119:108–114, 2018.
- [28] Aurélie Edwards, Hayo Castrop, Kamel Laghmani, Volker Vallon, and Anita T Layton. Effects of nkcc2 isoform regulation on nacl transport in thick ascending limb and macula densa: a modeling study. *American Journal of Physiology-Renal Physiology*, 307(2):F137–F146, 2014.

- [29] Aurélie Edwards and Anita T Layton. Calcium dynamics underlying the myogenic response of the renal afferent arteriole. *American Journal of Physiology-Renal Physiology*, 306(1):F34–F48, 2014.
- [30] Aurélie Edwards and Alicia A McDonough. Impact of angiotensin ii-mediated stimulation of sodium transporters in the nephron assessed by computational modeling. *American Journal of Physiology-Renal Physiology*, 317(6):F1656–F1668, 2019.
- [31] Brianne Ellis, Xiao C Li, Elisa Miguel-Qin, Victor Gu, and Jia L Zhuo. Evidence for a functional intracellular angiotensin system in the proximal tubule of the kidney. *American Journal of Physiology-Regulatory, Integrative and Comparative Physiology*, 302(5):R494–R509, 2012.
- [32] Tonja W Emans, Daniela Patinha, Jaap A Joles, Maarten P Koeners, Ben J Janssen, and CT Paul Krediet. Angiotensin ii-induced hypertension in rats is only transiently accompanied by lower renal oxygenation. *Scientific reports*, 8(1):16342, 2018.
- [33] Anas M Fathallah and Sathy V Balu-Iyer. Anatomical, physiological, and experimental factors affecting the bioavailability of sc-administered large biotherapeutics. *Journal of pharmaceutical sciences*, 104(2):301–306, 2015.
- [34] Hadi Fattah, Anita Layton, and Volker Vallon. How do kidneys adapt to a deficit or loss in nephron number? *Physiology*, 34(3):189–197, 2019.
- [35] Fernanda M Ferrão, Lucienne S Lara, and Jennifer Lowe. Renin-angiotensin system in the kidney: What is new? *World journal of nephrology*, 3(3):64, 2014.
- [36] Frej Fyhrquist, K Metsärinne, and I Tikkanen. Role of angiotensin II in blood pressure regulation and in the pathophysiology of cardiovascular disorders. *Journal of human hypertension*, 9:S19–24, 1995.
- [37] Alexis A Gonzalez, Liu Liu, Lucienne S Lara, Dale M Seth, L Gabriel Navar, and Minolfa C Prieto. Angiotensin II stimulates renin in inner medullary collecting duct cells via protein kinase C and independent of epithelial sodium channel and mineralocorticoid receptor activity. *Hypertension*, 57(3):594–599, 2011.
- [38] Alexis A Gonzalez and Minolfa C Prieto. Renin and the (pro) renin receptor in the renal collecting duct: role in the pathogenesis of hypertension. *Clinical and Experimental Pharmacology and Physiology*, 42(1):14–21, 2015.

- [39] Romer Gonzalez-Villalobos, R Bryan Klassen, Patricia L Allen, LG Navar, and Timothy G Hammond. Megalin binds and internalizes angiotensin ii. *American Journal of Physiology-Renal Physiology*, 288(2):F420–F427, 2005.
- [40] Romer A Gonzalez-Villalobos, Dale M Seth, Ryousuke Satou, Heather Horton, Naro Ohashi, Kayoko Miyata, Akemi Katsurada, Duy V Tran, Hiroyuki Kobori, and L Gabriel Navar. Intrarenal angiotensin II and angiotensinogen augmentation in chronic angiotensin II-infused mice. *American Journal of Physiology-Renal Physiology*, 295(3):F772–F779, 2008.
- [41] Ettore Guidi, Daniela Menghetti, Silvano Milani, Giuseppe Montagnino, Paola Palazzi, and Giuseppe Bianchi. Hypertension may be transplanted with the kidney in humans: a long-term historical prospective follow-up of recipients grafted with kidneys coming from donors with or without hypertension in their families. *Journal of the American Society of Nephrology*, 7(8):1131–1138, 1996.
- [42] François Guillaud and Patrick Hannaert. A computational model of the circulating renin-angiotensin system and blood pressure regulation. *Acta biotheoretica*, 58:143–170, 2010.
- [43] Jolanta Gutkowska, Pierre Corvol, Amintas FS Figueiredo, Tadashi Inagami, Jacob Bouhnik, and Jacques Genest. Kinetic studies of rat renin and tonin on purified rat angiotensinogen. *Canadian Journal of Biochemistry and Cell Biology*, 62(2-3):137–142, 1984.
- [44] Arthur C Guyton. Blood pressure control—special role of the kidneys and body fluids. *Science*, 252(5014):1813–1816, 1991.
- [45] Arthur C Guyton, Thomas G Coleman, and Harris J Granger. Circulation: overall regulation. *Annual review of physiology*, 34(1):13–44, 1972.
- [46] JE Hall. Control of sodium excretion by angiotensin II: intrarenal mechanisms and blood pressure regulation. *American Journal of Physiology-Regulatory, Integrative and Comparative Physiology*, 250(6):R960–R972, 1986.
- [47] JE Hall, AC Guyton, MJ Smith Jr, and TG Coleman. Blood pressure and renal function during chronic changes in sodium intake: role of angiotensin. *American Journal of Physiology-Renal Physiology*, 239(3):F271–F280, 1980.

- [48] John E Hall, H Leland Mizelle, Drew A Hildebrandt, and Michael W Brands. Abnormal pressure natriuresis. a cause or a consequence of hypertension? *Hypertension*, 15(6_pt.1):547–559, 1990.
- [49] K Melissa Hallow, Arthur Lo, Jeni Beh, Manoj Rodrigo, Sergey Ermakov, Stuart Friedman, Hector de Leon, Anamika Sarkar, Yuan Xiong, Ramesh Sarangapani, et al. A model-based approach to investigating the pathophysiological mechanisms of hypertension and response to antihypertensive therapies: extending the Guyton model. *American Journal of Physiology-Regulatory, Integrative and Comparative Physiology*, 306(9):R647–R662, 2014.
- [50] PJ Harris and JA Young. Dose-dependent stimulation and inhibition of proximal tubular sodium reabsorption by angiotensin II in the rat kidney. *Pflügers Archiv*, 367(3):295–297, 1977.
- [51] V Hegedüs, P Faarup, T Nørgaard, and C Lønholdt. Volume changes in the rat renal cortex during urography. *The British journal of radiology*, 51(610):793–798, 1978.
- [52] M Hilfenhaus. Circadian rhythm of the renin-angiotensin-aldosterone system in the rat. *Archives of toxicology*, 36(3):305–316, 1976.
- [53] Ulrich Hilgenfeldt. Half-life of rat angiotensinogen: influence of nephrectomy and lipopolysaccharide stimulation. *Molecular and cellular endocrinology*, 56(1-2):91–98, 1988.
- [54] Y Hong, J Dingemans, and DE Mager. Pharmacokinetic/pharmacodynamic modeling of renin biomarkers in subjects treated with the renin inhibitor aliskiren. *Clinical Pharmacology & Therapeutics*, 84(1):136–143, 2008.
- [55] Rui Hu and Anita Layton. A computational model of kidney function in a patient with diabetes. *International journal of molecular sciences*, 22(11):5819, 2021.
- [56] Rui Hu, Alicia A McDonough, and Anita T Layton. Functional implications of the sex differences in transporter abundance along the rat nephron: modeling and analysis. *American Journal of Physiology-Renal Physiology*, 317(6):F1462–F1474, 2019.
- [57] Rui Hu, Alicia A McDonough, and Anita T Layton. Sex differences in solute transport along the nephrons: effects of Na⁺ transport inhibition. *American Journal of Physiology-Renal Physiology*, 319(3):F487–F505, 2020.

- [58] Rui Hu, Alicia A McDonough, and Anita T Layton. Sex differences in solute and water handling in the human kidney: Modeling and functional implications. *iScience*, page 102667, 2021.
- [59] László Hunyady, Kevin J Catt, Adrian JL Clark, and Zsuzsanna Gáborik. Mechanisms and functions of at1 angiotensin receptor internalization. *Regulatory peptides*, 91(1-3):29–44, 2000.
- [60] M Mohsen Ibrahim. RAS inhibition in hypertension. *Journal of Human Hypertension*, 20(2):101–108, 2006.
- [61] Noriaki Ikeda, Fumiaki Marumo, Masuo Shirataka, and Toshiro Sato. A model of overall regulation of body fluids. *Annals of Biomedical Engineering*, 7:135–166, 1979.
- [62] John D Imig, Gabriel L Navar, Li-Xian Zou, Katie C O’Reilly, Patricia L Allen, James H Kaysen, Timothy G Hammond, and L Gabriel Navar. Renal endosomes contain angiotensin peptides, converting enzyme, and AT1A receptors. *American Journal of Physiology-Renal Physiology*, 277(2):F303–F311, 1999.
- [63] Jessica R Ivy and Matthew A Bailey. Pressure natriuresis and the renal control of arterial blood pressure. *The Journal of physiology*, 592(18):3955–3967, 2014.
- [64] Fatih Karaaslan, Yagmur Denizhan, Abidin Kayserilioglu, and H Ozcan Gulcur. Long-term mathematical model involving renal sympathetic nerve activity, arterial pressure, and sodium excretion. *Annals of biomedical engineering*, 33(11):1607–1630, 2005.
- [65] Eleni Karatza and Vangelis Karalis. Modelling gastric emptying: A pharmacokinetic model simultaneously describing distribution of losartan and its active metabolite exp-3174. *Basic & Clinical Pharmacology & Toxicology*, 126(3):193–202, 2020.
- [66] Avi Katz, Maria Luiza A Caramori, Susan Sisson-Ross, Thomas Groppoli, John M Basgen, and Michael Mauer. An increase in the cell component of the cortical interstitium antedates interstitial fibrosis in type 1 diabetic patients. *Kidney international*, 61(6):2058–2065, 2002.
- [67] Noritaka Kawada, Enyu Imai, Aleksander Karber, William J Welch, and Christopher S Wilcox. A mouse model of angiotensin ii slow pressor response: role of oxidative stress. *Journal of the American Society of Nephrology*, 13(12):2860–2868, 2002.

- [68] James Keener and James Sneyd. Mathematical physiology, volume 8 of interdisciplinary applied mathematics. *Springer-Verlag, New York*, 200:400, 1998.
- [69] Andrew J King and Gregory D Fink. Chronic low-dose angiotensin ii infusion increases venomotor tone by neurogenic mechanisms. *Hypertension*, 48(5):927–933, 2006.
- [70] Hiroyuki Kobori, Lisa M Harrison-Bernard, and L Gabriel Navar. Enhancement of angiotensinogen expression in angiotensin II-dependent hypertension. *Hypertension*, 37(5):1329–1335, 2001.
- [71] Hiroyuki Kobori, Masaomi Nangaku, L Gabriel Navar, and Akira Nishiyama. The intrarenal renin-angiotensin system: from physiology to the pathobiology of hypertension and kidney disease. *Pharmacological reviews*, 59(3):251–287, 2007.
- [72] Hiroyuki Kobori, Minolfa C Prieto-Carrasquero, Yuri Ozawa, and L Gabriel Navar. AT1 receptor mediated augmentation of intrarenal angiotensinogen in angiotensin II-dependent hypertension. *Hypertension*, 43(5):1126–1132, 2004.
- [73] Vijay Koka, Xiao Ru Huang, Arthur CK Chung, Wansheng Wang, Luan D Truong, and Hui Yao Lan. Angiotensin II up-regulates angiotensin I-converting enzyme (ACE), but down-regulates ACE2 via the AT1-ERK/p38 MAP kinase pathway. *The American journal of pathology*, 172(5):1174–1183, 2008.
- [74] Anita T Layton. Feedback-mediated dynamics in a model of a compliant thick ascending limb. *Mathematical biosciences*, 228(2):185–194, 2010.
- [75] Anita T Layton, Aurélie Edwards, and Volker Vallon. Adaptive changes in gfr, tubular morphology, and transport in subtotal nephrectomized kidneys: modeling and analysis. *American Journal of Physiology-Renal Physiology*, 313(2):F199–F209, 2017.
- [76] Anita T Layton and Michelle L Gumz. Sex differences in circadian regulation of kidney function of the mouse. *American Journal of Physiology-Renal Physiology*, 2022.
- [77] Anita T Layton and Harold E Layton. A computational model of epithelial solute and water transport along a human nephron. *PLoS computational biology*, 15(2):e1006108, 2019.

- [78] Anita T Layton, Leon C Moore, and Harold E Layton. Multistable dynamics mediated by tubuloglomerular feedback in a model of coupled nephrons. *Bulletin of mathematical biology*, 71(3):515, 2009.
- [79] Anita T Layton and Jennifer C Sullivan. Recent advances in sex differences in kidney function. *American Journal of Physiology-Renal Physiology*, 316(2):F328–F331, 2019.
- [80] Anita T Layton and Volker Vallon. Cardiovascular benefits of sglt2 inhibition in diabetes and chronic kidney diseases. *Acta physiologica (Oxford, England)*, 222(4):e13050, 2018.
- [81] Anita T Layton and Volker Vallon. Sglt2 inhibition in a kidney with reduced nephron number: modeling and analysis of solute transport and metabolism. *American Journal of Physiology-Renal Physiology*, 314(5):F969–F984, 2018.
- [82] Anita T Layton, Volker Vallon, and Aurélie Edwards. Predicted consequences of diabetes and sglt inhibition on transport and oxygen consumption along a rat nephron. *American Journal of Physiology-Renal Physiology*, 310(11):F1269–F1283, 2016.
- [83] Hyo B Lee and M Donald Blaufox. Blood volume in the rat. *Journal of Nuclear Medicine*, 26(1):72–76, 1985.
- [84] Jessica Leete, Susan Gurley, and Anita T Layton. Modeling sex differences in the renin angiotensin system and the efficacy of antihypertensive therapies. *Computers & chemical engineering*, 112:253–264, 2018.
- [85] Jessica Leete and Anita T Layton. Sex-specific long-term blood pressure regulation: Modeling and analysis. *Computers in biology and medicine*, 104:139–148, 2019.
- [86] Kevin V Lemley and Wilhelm Kriz. Anatomy of the renal interstitium. *Kidney international*, 39(3):370–381, 1991.
- [87] KV Lemley, M Elger, I Koeppen-Hagemann, M Kretzler, M Nagata, T Sakai, S Uiker, and W Kriz. The glomerular mesangium: capillary support function and its failure under experimental conditions. *The clinical investigator*, 70(9):843–856, 1992.
- [88] Lilach O Lerman, Alejandro R Chade, Vincenzo Sica, and Claudio Napoli. Animal models of hypertension: an overview. *Journal of Laboratory and Clinical Medicine*, 146(3):160–173, 2005.
- [89] Po Sing Leung. Local ras. *The Renin-Angiotensin System: Current Research Progress in The Pancreas: The RAS in the Pancreas*, pages 69–87, 2010.

- [90] Hong Li, Lu Liu, Lei Xie, Dongmei Gan, and Xiaoqing Jiang. Effects of berberine on the pharmacokinetics of losartan and its metabolite exp3174 in rats and its mechanism. *Pharmaceutical biology*, 54(12):2886–2894, 2016.
- [91] Junyi Li and Allan R Brasier. Angiotensinogen gene activation by angiotensin II is mediated by the rel A (nuclear factor-kappaB p65) transcription factor: one mechanism for the renin angiotensin system positive feedback loop in hepatocytes. *Molecular Endocrinology*, 10(3):252–264, 1996.
- [92] Qianyi Li, Alicia A McDonough, Harold E Layton, and Anita T Layton. Functional implications of sexual dimorphism of transporter patterns along the rat proximal tubule: modeling and analysis. *American Journal of Physiology-Renal Physiology*, 315(3):F692–F700, 2018.
- [93] Xiao C Li, Ana Paula de Oliveira Leite, Xu Chen, Chunling Zhao, Xiaowen Zheng, Jianfeng Zhang, and Jia L Zhuo. The intratubular and intracrine renin-angiotensin system in the proximal tubules of the kidney and its roles in angiotensin II-induced hypertension. In *Selected Chapters from the Renin-Angiotensin System*. IntechOpen, London, UK, 2019.
- [94] Xiao C Li, Dongmin Zhu, Xiaowen Zheng, Jiangfeng Zhang, and Jia L Zhuo. Intratubular and intracellular renin–angiotensin system in the kidney: a unifying perspective in blood pressure control. *Clinical Science*, 132(13):1383–1401, 2018.
- [95] Arthur Lo, Jennifer Beh, Hector De Leon, Melissa K Hallow, Ramprasad Ramakrishna, Manoj Rodrigo, Anamika Sarkar, Ramesh Sarangapani, and Anna Georgieva. Using a systems biology approach to explore hypotheses underlying clinical diversity of the renin angiotensin system and the response to antihypertensive therapies. In *Clinical trial simulations*, pages 457–482. Springer, 2011.
- [96] Rodger Loutzenhiser, Anil Bidani, and Lisa Chilton. Renal myogenic response: kinetic attributes and physiological role. *Circulation research*, 90(12):1316–1324, 2002.
- [97] Mykola Mamenko, Oleg Zaika, Daria V Ilatovskaya, Alexander Staruschenko, and Oleh Pochynyuk. Angiotensin ii increases activity of the epithelial na+ channel (enac) in distal nephron additively to aldosterone. *Journal of biological chemistry*, 287(1):660–671, 2012.
- [98] Taiji Matsusaka, Fumio Niimura, Akihiro Shimizu, Ira Pastan, Akihiko Saito, Hiroyuki Kobori, Akira Nishiyama, and Iekuni Ichikawa. Liver angiotensinogen is the

- primary source of renal angiotensin II. *Journal of the American Society of Nephrology*, 23(7):1181–1189, 2012.
- [99] Bernd Meibohm and H Derendorf. Basic concepts of pharmacokinetic/pharmacodynamic (pk/pd) modelling. *International journal of clinical pharmacology and therapeutics*, 35(10):401–413, 1997.
- [100] Alfred F Michael, William F Keane, Leopoldo Raij, Robert L Vernier, and S Michael Mauer. The glomerular mesangium. *Kidney international*, 17(2):141–154, 1980.
- [101] Katherine T Mills, Andrei Stefanescu, and Jiang He. The global epidemiology of hypertension. *Nature Reviews Nephrology*, 16(4):223–237, 2020.
- [102] Jacqueline N Minas, Max A Thorwald, Debra Conte, Jose-Pablo Vázquez-Medina, Akira Nishiyama, and Rudy M Ortiz. Angiotensin and mineralocorticoid receptor antagonism attenuates cardiac oxidative stress in angiotensin ii-infused rats. *Clinical and Experimental Pharmacology and Physiology*, 42(11):1178–1188, 2015.
- [103] Kenneth D Mitchell, Severina M Jacinto, and John J Mullins. Proximal tubular fluid, kidney, and plasma levels of angiotensin II in hypertensive ren-2 transgenic rats. *American Journal of Physiology-Renal Physiology*, 273(2):F246–F253, 1997.
- [104] Shin-ichiro Miura, Sadashiva S Karnik, and Keijiro Saku. Angiotensin II type 1 receptor blockers: class effects versus molecular effects. *Journal of the Renin-Angiotensin-Aldosterone System*, 12(1):1–7, 2011.
- [105] KAREN Munger and CHRISTINE Baylis. Sex differences in renal hemodynamics in rats. *American Journal of Physiology-Renal Physiology*, 254(2):F223–F231, 1988.
- [106] A Nakamura, Hiroshi Iwao, Kiyoshi Fukui, Shoji Kimura, Toshiaki Tamaki, Shigetada Nakanishi, and Youichi Abe. Regulation of liver angiotensinogen and kidney renin mrna levels by angiotensin II. *American Journal of Physiology-Endocrinology And Metabolism*, 258(1):E1–E6, 1990.
- [107] L Gabriel Navar, Hiroyuki Kobori, and Minolfa Prieto-Carrasquero. Intrarenal angiotensin II and hypertension. *Current hypertension reports*, 5(2):135–143, 2003.
- [108] L Gabriel Navar, Lynn Lewis, Anka Hymel, Branko Braam, and Kenneth D Mitchell. Tubular fluid concentrations and kidney contents of angiotensins I and II in anesthetized rats. *Journal of the American Society of Nephrology*, 5(4):1153–1158, 1994.

- [109] L Gabriel Navar, Minolfa C Prieto, Ryousuke Satou, and Hiroyuki Kobori. Intrarenal angiotensin II and its contribution to the genesis of chronic hypertension. *Current opinion in pharmacology*, 11(2):180–186, 2011.
- [110] G Nguyen. Renin/prorenin receptors. *Kidney international*, 69(9):1503–1506, 2006.
- [111] Genevieve Nguyen, Françoise Delarue, Céline Burcklé, Latifa Bouzhir, Thomas Giller, Jean-Daniel Sraer, et al. Pivotal role of the renin/prorenin receptor in angiotensin II production and cellular responses to renin. *The Journal of clinical investigation*, 109(11):1417–1427, 2002.
- [112] Mien TX Nguyen, Donna H Lee, Eric Delpire, and Alicia A McDonough. Differential regulation of na⁺ transporters along nephron during ang ii-dependent hypertension: distal stimulation counteracted by proximal inhibition. *American Journal of Physiology-Renal Physiology*, 305(4):F510–F519, 2013.
- [113] Akira Nishiyama, Toshiki Fukui, Yoshihide Fujisawa, Matlubur Rahman, Run-Xia Tian, Shoji Kimura, and Youichi Abe. Systemic and regional hemodynamic responses to tempol in angiotensin ii-infused hypertensive rats. *Hypertension*, 37(1):77–83, 2001.
- [114] Akira Nishiyama and Hiroyuki Kobori. Independent regulation of renin–angiotensin–aldosterone system in the kidney. *Clinical and experimental nephrology*, 22(6):1231–1239, 2018.
- [115] Akira Nishiyama, Dale M Seth, and L Gabriel Navar. Renal interstitial fluid concentrations of angiotensins I and II in anesthetized rats. *Hypertension*, 39(1):129–134, 2002.
- [116] Akira Nishiyama, Dale M Seth, and L Gabriel Navar. Angiotensin II type 1 receptor-mediated augmentation of renal interstitial fluid angiotensin II in angiotensin II-induced hypertension. *Journal of hypertension*, 21(10):1897–1903, 2003.
- [117] Jean Luc Pasquié, Abderraouf Herizi, Bernard Jover, and Albert Mimran. Chronic bradykinin infusion and receptor blockade in angiotensin ii hypertension in rats. *Hypertension*, 33(3):830–834, 1999.
- [118] CORINN M Pawloski and GREGORY D Fink. Circulating angiotensin II and drinking behavior in rats. *American Journal of Physiology-Regulatory, Integrative and Comparative Physiology*, 259(3):R531–R538, 1990.

- [119] Karl D Pendergrass, Nancy T Pirro, Brian M Westwood, Carlos M Ferrario, K Bridget Brosnihan, and Mark C Chappell. Sex differences in circulating and renal angiotensins of hypertensive mRen. lewis but not normotensive Lewis rats. *American Journal of Physiology-Heart and Circulatory Physiology*, 295(1):H10–H20, 2008.
- [120] Marcus Pohl, Henriette Kaminski, Hayo Castrop, Michael Bader, Nina Himmerkus, Markus Bleich, Sebastian Bachmann, and Franziska Theilig. Intrarenal renin angiotensin system revisited: role of megalin-dependent endocytosis along the proximal nephron. *Journal of Biological Chemistry*, 285(53):41935–41946, 2010.
- [121] John Pooler. *Vander’s renal physiology*. McGraw-Hill Companies, Incorporated, 2009.
- [122] Minolfa C Prieto-Carrasquero, Lisa M Harrison-Bernard, Hiroyuki Kobori, Yuri Ozawa, Kathleen S Hering-Smith, L Lee Hamm, and L Gabriel Navar. Enhancement of collecting duct renin in angiotensin II-dependent hypertensive rats. *Hypertension*, 44(2):223–229, 2004.
- [123] Sergej Ramusovic and Stephanie Laeer. An integrated physiology-based model for the interaction of raa system biomarkers with drugs. *Journal of Cardiovascular Pharmacology*, 2022.
- [124] LBA Rangel, C Caruso-Neves, LS Lara, and AG Lopes. Angiotensin ii stimulates renal proximal tubule na⁺-atpase activity through the activation of protein kinase c. *Biochimica et Biophysica Acta (BBA)-Biomembranes*, 1564(2):310–316, 2002.
- [125] Jane F Reckelhoff and J Carlos Romero. Role of oxidative stress in angiotensin-induced hypertension. *American Journal of Physiology-Regulatory, Integrative and Comparative Physiology*, 284(4):R893–R912, 2003.
- [126] Wolfgang F Richter, Suraj G Bhansali, and Marilyn E Morris. Mechanistic determinants of biotherapeutics absorption following sc administration. *The AAPS journal*, 14(3):559–570, 2012.
- [127] Eberhard Ritz and Volker Haxsen. Angiotensin ii and oxidative stress: an unholy alliance, 2003.
- [128] J Carlos Romero and Jane F Reckelhoff. Role of angiotensin and oxidative stress in essential hypertension. *Hypertension*, 34(4):943–949, 1999.

- [129] Gian Paolo Rossi. Losartan metabolite exp3179: An at1-receptor-independent treatment strategy for patients with the metabolic syndrome?, 2009.
- [130] George C Roush and Domenic A Sica. Diuretics for hypertension: a review and update. *American journal of hypertension*, 29(10):1130–1137, 2016.
- [131] Peter Spencer Russell, Jiwon Hong, John Albert Windsor, Maxim Itkin, and Anthony Ronald John Phillips. Renal lymphatics: anatomy, physiology, and clinical implications. *Frontiers in physiology*, 10:251, 2019.
- [132] Javid Sadjadi, Gerald L Kramer, Chun-hua Yu, M Burrell Welborn III, and J Gregory Modrall. Angiotensin II exerts positive feedback on the intrarenal renin-angiotensin system by an angiotensin converting enzyme-dependent mechanism1. *Journal of Surgical Research*, 129(2):272–277, 2005.
- [133] Amanda K Sampson, Karen M Moritz, Emma S Jones, Rebecca L Flower, Robert E Widdop, and Kate M Denton. Enhanced angiotensin ii type 2 receptor mechanisms mediate decreases in arterial pressure attributable to chronic low-dose angiotensin ii in female rats. *Hypertension*, 52(4):666–671, 2008.
- [134] Kiran V Sarikonda, Ralph E Watson, Oluchi C Opara, and Donald J DiPette. Experimental animal models of hypertension. *Journal of the American Society of Hypertension*, 3(3):158–165, 2009.
- [135] MADH Schalekamp and AHJ Danser. Angiotensin II production and distribution in the kidney: I. A kinetic model. *Kidney international*, 69(9):1543–1552, 2006.
- [136] JEFFREY R Schelling and STUART L Linas. Angiotensin II-dependent proximal tubule sodium transport requires receptor-mediated endocytosis. *American Journal of Physiology-Cell Physiology*, 266(3):C669–C675, 1994.
- [137] Detlef Schlöndorff. Roles of the mesangium in glomerular function. *Kidney international*, 49(6):1583–1585, 1996.
- [138] HERIBERT Schunkert, JULIE R Ingelfinger, HOWARD Jacob, BRUCE Jackson, BOUTROS Bouyounes, and VICTOR J Dzau. Reciprocal feedback regulation of kidney angiotensinogen and renin mrna expressions by angiotensin II. *American Journal of Physiology-Endocrinology And Metabolism*, 263(5):E863–E869, 1992.
- [139] VL Schuster, JP Kokko, HR Jacobson, et al. Angiotensin II directly stimulates sodium transport in rabbit proximal convoluted tubules. *The Journal of clinical investigation*, 73(2):507–515, 1984.

- [140] Ioannis Sgouralis, Roger G Evans, and Anita T Layton. Renal medullary and urinary oxygen tension during cardiopulmonary bypass in the rat. *Mathematical medicine and biology: a journal of the IMA*, 34(3):313–333, 2017.
- [141] Weijian Shao, Dale M Seth, and L Gabriel Navar. Augmentation of endogenous intrarenal angiotensin II levels in Val5-ANG II-infused rats. *American Journal of Physiology-Renal Physiology*, 296(5):F1067–F1071, 2009.
- [142] Weijian Shao, Dale M Seth, and L Gabriel Navar. Angiotensin II type 1 receptor-mediated augmentation of urinary excretion of endogenous angiotensin II in val5-angiotensin II-infused rats. *Hypertension*, 56(3):378–383, 2010.
- [143] Delaney Smith and Anita Layton. The intrarenal renin-angiotensin system in hypertension: insights from mathematical modelling. *Journal of Mathematical Biology*, 86(58), 2023.
- [144] Matthew A Sparks, Steven D Crowley, Susan B Gurley, Maria Mirotsoy, and Thomas M Coffman. Classical renin-angiotensin system in kidney physiology. *Comprehensive Physiology*, 4(3):1201, 2014.
- [145] Melissa M Stadt and Anita T Layton. Adaptive changes in single-nephron gfr, tubular morphology, and transport in a pregnant rat nephron: modeling and analysis. *American Journal of Physiology-Renal Physiology*, 322(2):F121–F137, 2022.
- [146] Jerome Sugarman, Meyer Friedman, Evalyn Barrett, and T Addis. The distribution, flow, protein and urea content of renal lymph. *American Journal of Physiology-Legacy Content*, 138(1):108–112, 1942.
- [147] Jennifer C Sullivan. Sex and the renin-angiotensin system: inequality between the sexes in response to ras stimulation and inhibition. *American Journal of Physiology-Regulatory, Integrative and Comparative Physiology*, 294(4):R1220–R1226, 2008.
- [148] Sangita Swapnasrita, Aurélie Carlier, and Anita T Layton. Sex-specific computational models of kidney function in patients with diabetes. *Frontiers in physiology*, page 14, 2022.
- [149] Nobuyuki Takahashi, John R Hagaman, Hyung-Suk Kim, and Oliver Smithies. Minireview: computer simulations of blood pressure regulation by the renin-angiotensin system. *Endocrinology*, 144(6):2184–2190, 2003.

- [150] Tsuneo Takenaka, Hiromichi Suzuki, Tomohiro Furukawa, Yasuhide Ogata, and Takao Saruta. Role of intrarenal renin-angiotensin system on pressure-natriuresis in spontaneously hypertensive rats. *Clinical and Experimental Hypertension. Part A: Theory and Practice*, 12(8):1377–1394, 1990.
- [151] Toshiaki Tamaki, Akira Nishiyama, Shoji Kimura, Yasuharu Aki, Masanori Yoshizumi, Hitoshi Houchi, Kyoji Morita, and Youichi Abe. EXP3174: the major active metabolite of losartan. *Cardiovascular drug reviews*, 15(2):122–136, 1997.
- [152] S Randall Thomas, Pierre Baconnier, Julie Fontecave, Jean-Pierre Françoise, François Guillaud, Patrick Hannaert, Alfredo Hernandez, Virginie Le Rolle, Pierre Maziere, Fariza Tah, et al. Saphir: a physiome core model of body fluid homeostasis and blood pressure regulation. *Philosophical Transactions of the Royal Society A: Mathematical, Physical and Engineering Sciences*, 366(1878):3175–3197, 2008.
- [153] WG Thomas, TJ Thekkumkara, and KM Baker. Molecular mechanisms of angiotensin II (AT1A) receptor endocytosis. *Clinical and experimental pharmacology & physiology. Supplement*, 3:S74–80, 1996.
- [154] Anitha Toke and Timothy W Meyer. Hemodynamic effects of angiotensin II in the kidney. *Contributions to nephrology*, 135:34–46, 2001.
- [155] Rhian M Touyz. The role of angiotensin ii in regulating vascular structural and functional changes in hypertension. *Current hypertension reports*, 5(2):155–164, 2003.
- [156] Michael R Turner and Sathy V Balu-Iyer. Challenges and opportunities for the subcutaneous delivery of therapeutic proteins. *Journal of pharmaceutical sciences*, 107(5):1247–1260, 2018.
- [157] Patricia Valles, Jan Wysocki, and Daniel Battle. Angiotensin II and renal tubular ion transport. *TheScientificWorldJOURNAL*, 5:680–690, 2005.
- [158] Jorge P van Kats, Larissa M de Lannoy, AH Jan Danser, Jan R van Meegen, Pieter D Verdouw, and Maarten ADH Schalekamp. Angiotensin II type 1 (AT1) receptor-mediated accumulation of angiotensin II in tissues and its intracellular half-life in vivo. *Hypertension*, 30(1):42–49, 1997.
- [159] Jorge P Van Kats, Maarten ADH Schalekamp, Pieter D Verdouw, Dirk J Duncker, and AH Jan Danser. Intrarenal angiotensin II: interstitial and cellular levels and site of production. *Kidney international*, 60(6):2311–2317, 2001.

- [160] ANNETTE M Von Thun, RICHARD C Vari, SAMIR S el Dahr, and L GABRIEL Navar. Augmentation of intrarenal angiotensin II levels by chronic angiotensin II infusion. *American Journal of Physiology-Renal Physiology*, 266(1):F120–F128, 1994.
- [161] Miriam A Wallace. Anatomy and physiology of the kidney. *AORN journal*, 68(5):799–820, 1998.
- [162] Chi-Tarng Wang, L Gabriel Navar, and Kenneth D Mitchell. Proximal tubular fluid angiotensin II levels in angiotensin II-induced hypertensive rats. *Journal of hypertension*, 21(2):353–360, 2003.
- [163] Fei Wang, Xiaohan Lu, Mi Liu, Yumei Feng, Shu-Feng Zhou, and Tianxin Yang. Renal medullary (pro) renin receptor contributes to angiotensin II-induced hypertension in rats via activation of the local renin–angiotensin system. *BMC medicine*, 13(1):1–11, 2015.
- [164] Ning Wei, Michelle L Gumz, and Anita T Layton. Predicted effect of circadian clock modulation of nhe3 of a proximal tubule cell on sodium transport. *American Journal of Physiology-Renal Physiology*, 315(3):F665–F676, 2018.
- [165] Christopher S Wilcox and Victor J Dzau. Effect of captopril on the release of the components of the renin-angiotensin system into plasma and lymph. *Journal of the American Society of Nephrology*, 2(7):1241–1250, 1992.
- [166] JM Willemsen, TJ Rabelink, P Boer, and CA Gaillard. Disparate systemic and renal blocking properties of angiotensin ii antagonists during exogenous angiotensin ii administration: implications for treatment. *Journal of human hypertension*, 18(12):857–863, 2004.
- [167] Gunter Wolf, Ulrike Butzmann, and Ulrich O Wenzel. The renin-angiotensin system and progression of renal disease: from hemodynamics to cell biology. *Nephron physiology*, 93(1):p3–p13, 2003.
- [168] Haiyan Wu, Yaoxian Liang, Yimu Zheng, Qiong Bai, Zheng Zhuang, A Lata, Danxia Zheng, and Yue Wang. Up-regulation of intrarenal renin-angiotensin system contributes to renal damage in high-salt induced hypertension rats. *Kidney and Blood Pressure Research*, 39(6):526–535, 2014.
- [169] Peng Wu, Zhong-Xiuzi Gao, Dan-Dan Zhang, Xin-Peng Duan, Andrew S Terker, Dao-Hong Lin, David H Ellison, and Wen-Hui Wang. Effect of angiotensin ii on enac in the distal convoluted tubule and in the cortical collecting duct of mineralocorticoid

- receptor deficient mice. *Journal of the American Heart Association*, 9(7):e014996, 2020.
- [170] Feichao Xu, Caiping Mao, Yujuan Liu, Lei Wu, Zhice Xu, and Lubo Zhang. Losartan chemistry and its effects via at1 mechanisms in the kidney. *Current medicinal chemistry*, 16(28):3701–3715, 2009.
- [171] Kazuo Yamada, Shridhar N Iyer, Mark C Chappell, Detlev Ganten, and Carlos M Ferrario. Converting enzyme determines plasma clearance of angiotensin-(1–7). *Hypertension*, 32(3):496–502, 1998.
- [172] Licy L Yanes, Damian G Romero, Joshua W Iles, Radu Iliescu, Celso Gomez-Sanchez, and Jane F Reckelhoff. Sexual dimorphism in the renin-angiotensin system in aging spontaneously hypertensive rats. *American Journal of Physiology-Regulatory, Integrative and Comparative Physiology*, 291(2):R383–R390, 2006.
- [173] Rui Yang, Ilse Smolders, and Alain G Dupont. Blood pressure and renal hemodynamic effects of angiotensin fragments. *Hypertension Research*, 34(6):674–683, 2011.
- [174] Tianxin Yang and Chuanming Xu. Physiology and pathophysiology of the intrarenal renin-angiotensin system: an update. *Journal of the American Society of Nephrology*, 28(4):1040–1049, 2017.
- [175] Hyung Eun Yim and Kee Hwan Yoo. Renin-angiotensin system-considerations for hypertension and kidney. *Electrolyte & Blood Pressure*, 6(1):42–50, 2008.
- [176] BRAD H Yuan, JOHN B Robinette, and JOHN D Conger. Effect of angiotensin ii and norepinephrine on isolated rat afferent and efferent arterioles. *American Journal of Physiology-Renal Physiology*, 258(3):F741–F750, 1990.
- [177] Oleg Zaika, Mykola Mamenko, Alexander Staruschenko, and Oleh Pochynyuk. Direct activation of enac by angiotensin ii: recent advances and new insights. *Current hypertension reports*, 15(1):17–24, 2013.
- [178] Michael Zeisberg and Raghu Kalluri. Physiology of the renal interstitium. *Clinical Journal of the American Society of Nephrology*, 10(10):1831–1840, 2015.
- [179] Yongjun Zhu, Hongwang Cui, Jie Lv, Haiqin Liang, Yanping Zheng, Shanzhi Wang, Min Wang, Huanan Wang, and Feng Ye. At1 and at2 receptors modulate renal tubular cell necroptosis in angiotensin ii-infused renal injury mice. *Scientific reports*, 9(1):1–13, 2019.

- [180] Jia L Zhuo, John D Imig, Timothy G Hammond, Sheyla Orengo, Edmund Benes, and L Gabriel Navar. Ang II accumulation in rat renal endosomes during ang II-induced hypertension: role of AT1 receptor. *Hypertension*, 39(1):116–121, 2002.
- [181] Jialong Zhuo, Ingrid Moeller, Trisha Jenkins, Siew Yeen Chai, Andrew M Allen, Mitsuru Ohishi, and Frederick AO Mendelsohn. Mapping tissue angiotensin-converting enzyme and angiotensin AT1, AT2 and AT4 receptors. *Journal of hypertension*, 16(12):2027–2037, 1998.
- [182] Jialong Zhuo, Mitsuru Ohishi, and Frederick AO Mendelsohn. Roles of AT1 and AT2 receptors in the hypertensive Ren-2 gene transgenic rat kidney. *Hypertension*, 33(1):347–353, 1999.
- [183] Li-Xian Zou, John D Imig, Anka Hymel, and L Gabriel Navar. Renal uptake of circulating angiotensin II in Val5-angiotensin II infused rats is mediated by AT1 receptor. *American journal of hypertension*, 11(5):570–578, 1998.
- [184] Li-Xian Zou, John D Imig, Annette M Von Thun, Anka Hymel, Hidehiko Ono, and L Gabriel Navar. Receptor-mediated intrarenal angiotensin II augmentation in angiotensin II-infused rats. *Hypertension*, 28(4):669–677, 1996.

APPENDICES

Appendix A

Intrarenal RAS model equations

Below, the model equations for each compartment are summarized.

A.1 Glomerular compartment

$$\frac{d[AngI]_{Gl}^{Ext}}{dt}(t) = \frac{\phi_{Gl}}{V_{Gl}^{Ext}} ([AngI]_{circ}(t) - [AngI]_{Gl}^{Ext}(t)) \quad (A.1)$$

$$\begin{aligned} \frac{d[AngII]_{Gl}^{Ext}}{dt}(t) &= \frac{\phi_{Gl}}{V_{Gl}^{Ext}} ([AngII]_{circ}(t) - [AngII]_{Gl}^{Ext}(t)) \\ &+ k_{diss}[AT1R - bound AngII]_{Gl}^{Memb}(t) \\ &- k_{ass}[AT1R]_{Gl}^{Memb}(t)[AngII]_{Gl}^{Ext}(t) \end{aligned} \quad (A.2)$$

$$\begin{aligned} \frac{d[AT1R - bound AngII]_{Gl}^{Memb}}{dt}(t) &= k_{ass}[AT1R]_{Gl}^{Memb}(t)[AngII]_{Gl}^{Ext}(t) \\ &- k_{diss}[AT1R - bound AngII]_{Gl}^{Memb}(t) \\ &- k_{int}[AT1R - bound AngII]_{Gl}^{Memb}(t) \end{aligned} \quad (A.3)$$

$$\begin{aligned}
\frac{d[AT1R - \text{bound } AngII]_{Gl}^{Cell}}{dt}(t) &= k_{int} \frac{V_{Gl}^{Ext}}{V_{Gl}^{Cell}} [AT1R - \text{bound } AngII]_{Gl}^{Memb}(t) \\
&+ k_{ass} [AT1R]_{Gl}^{Cell}(t) [AngII]_{Gl}^{Cell}(t) \\
&- k_{diss} [AT1R - \text{bound } AngII]_{Gl}^{Cell}(t)
\end{aligned} \tag{A.4}$$

$$\begin{aligned}
\frac{d[AngII]_{Gl}^{Cell}}{dt}(t) &= k_{diss} [AT1R - \text{bound } AngII]_{Gl}^{Cell}(t) \\
&- k_{ass} [AT1R]_{Gl}^{Cell}(t) [AngII]_{Gl}^{Cell}(t) \\
&- k_{lys} [AngII]_{Gl}^{Cell}(t)
\end{aligned} \tag{A.5}$$

$$\begin{aligned}
\frac{d[AT1R]_{Gl}^{Cell}}{dt}(t) &= k_{diss} [AT1R - \text{bound } AngII]_{Gl}^{Cell}(t) \\
&- k_{ass} [AT1R]_{Gl}^{Cell}(t) [AngII]_{Gl}^{Cell}(t) \\
&- k_{rec} [AT1R]_{Gl}^{Cell}(t)
\end{aligned} \tag{A.6}$$

$$\begin{aligned}
V_{Gl}^{Ext} [AT1R]_{Gl}^{Memb}(t) &= AT1R_{Gl}^{tot} - \left(V_{Gl}^{Ext} [AT1R - \text{bound } AngII]_{Gl}^{Memb}(t) \right. \\
&+ V_{Gl}^{Cell} [AT1R - \text{bound } AngII]_{Gl}^{Cell}(t) \\
&\left. + V_{Gl}^{Cell} [AT1R]_{Gl}^{Cell}(t) \right)
\end{aligned} \tag{A.7}$$

A.2 Tubular compartment

$$\begin{aligned}
\frac{d[AngI]_{Tb}^{Ext}}{dt}(t) &= \frac{\phi_{GFR}}{V_{Tb}^{Ext}} [AngI]_{circ}(t) + \frac{\phi_{Gl}}{V_{Tb}^{Ext}} [AngI]_{Gl}^{Ext}(t) \\
&+ k_{AngI}^{Tb}(t) - \left(c_{ACE}^{Tb} + \frac{k_{diff} + \phi_U}{V_{Tb}^{Ext}} \right) [AngI]_{Tb}^{Ext}(t)
\end{aligned} \tag{A.8}$$

$$\begin{aligned}
\frac{d[AngII]_{Tb}^{Ext}}{dt}(t) &= \frac{\phi_{GFR}}{V_{Tb}^{Ext}}[AngII]_{circ}(t) + c_{ACE}^{Tb}[AngI]_{Tb}^{Ext}(t) \\
&+ \frac{\phi_{Gl}}{V_{Tb}^{Ext}}[AngII]_{Gl}^{Ext}(t) - \left(\frac{k_{meg} + \phi_U}{V_{Tb}^{Ext}} \right) [AngII]_{Tb}^{Ext}(t) \\
&+ k_{diss}[AT1R - bound AngII]_{Tb}^{Memb}(t) \\
&- k_{ass}[AngII]_{Tb}^{Ext}(t)[AT1R]_{Tb}^{Memb}(t)
\end{aligned} \tag{A.9}$$

$$\begin{aligned}
\frac{d[AT1R - bound AngII]_{Tb}^{Memb}}{dt}(t) &= k_{ass}[AT1R]_{Tb}^{Memb}(t)[AngII]_{Tb}^{Ext}(t) \\
&- k_{diss}[AT1R - bound AngII]_{Tb}^{Memb}(t) \\
&- k_{int}[AT1R - bound AngII]_{Tb}^{Memb}(t)
\end{aligned} \tag{A.10}$$

$$\begin{aligned}
\frac{d[AT1R - bound AngII]_{Tb}^{Cell}}{dt}(t) &= k_{int} \frac{V_{Tb}^{Ext}}{V_{Pt,Tb}^{Cell}} [AT1R - bound AngII]_{Tb}^{Memb}(t) \\
&+ k_{ass}[AT1R]_{Tb}^{Cell}(t)[AngII]_{Tb}^{Cell}(t) \\
&- k_{diss}[AT1R - bound AngII]_{Tb}^{Cell}(t)
\end{aligned} \tag{A.11}$$

$$\begin{aligned}
\frac{d[AngII]_{Tb}^{Cell}}{dt}(t) &= k_{diss}[AT1R - bound AngII]_{Tb}^{Cell}(t) \\
&- k_{ass}[AT1R]_{Tb}^{Cell}(t)[AngII]_{Tb}^{Cell}(t) \\
&+ k_{meg} \frac{V_{Tb}^{Ext}}{V_{Tb,Pt}^{Cell}} [AngII]_{Tb}^{Ext}(t) \\
&- (k_{lys} + k_{trans})[AngII]_{Tb}^{Cell}(t)
\end{aligned} \tag{A.12}$$

$$\begin{aligned}
\frac{d[AT1R]_{Tb}^{Cell}}{dt}(t) &= k_{diss}[AT1R - bound AngII]_{Tb}^{Cell}(t) \\
&- k_{ass}[AT1R]_{Tb}^{Cell}(t)[AngII]_{Tb}^{Cell}(t) \\
&- k_{rec}[AT1R]_{Tb}^{Cell}(t)
\end{aligned} \tag{A.13}$$

$$\begin{aligned}
\frac{d[AT1R]_{Tb}^{Memb}}{dt}(t) &= k_{rec} \frac{V_{Tb}^{Ext}}{V_{Pt,Tb}^{Cell}} [AT1R]_{Tb}^{Cell}(t) \\
&+ k_{diss} [AT1R - \text{bound } AngII]_{Tb}^{Memb}(t) \\
&- k_{ass} [AT1R]_{Tb}^{Memb}(t) [AngII]_{Tb}^{Ext}(t) \\
&+ fb_{Tb}^{AT1R} ([AT1R - \text{bound } AngII]_{Tb}^{Memb}(t))
\end{aligned} \tag{A.14}$$

A.3 Peritubular compartment

$$\begin{aligned}
\frac{d[AngI]_{Pt}^{Ext}}{dt}(t) &= k_{AngI}^{Pt} + \frac{k_{diff}}{V_{Pt}^{Ext}} [AngI]_{Tb}^{Ext}(t) \\
&- \left(c_{ACE}^{Pt} + \frac{\phi_{Pv} + \phi_L}{V_{Pt}^{Ext}} \right) [AngI]_{Pt}^{Ext}(t)
\end{aligned} \tag{A.15}$$

$$\begin{aligned}
\frac{d[AngII]_{Pt}^{Ext}}{dt}(t) &= k_{trans} \frac{V_{Tb,Pt}^{Cell}}{V_{Pt}^{Ext}} [AngII]_{Tb}^{Cell}(t) + c_{ACE}^{Pt} [AngI]_{Pt}^{Ext}(t) \\
&- \left(\frac{\phi_{Pv} + \phi_L}{V_{Pt}^{Ext}} \right) [AngII]_{Pt}^{Ext}(t) \\
&+ k_{diss} [AT1R - \text{bound } AngII]_{Pt}^{Memb}(t) \\
&- k_{ass} [AT1R]_{Pt}^{Memb}(t) [AngII]_{Pt}^{Ext}(t)
\end{aligned} \tag{A.16}$$

$$\begin{aligned}
\frac{d[AT1R - \text{bound } AngII]_{Pt}^{Memb}}{dt}(t) &= k_{ass} [AT1R]_{Pt}^{Memb}(t) [AngII]_{Pt}^{Ext}(t) \\
&- k_{diss} [AT1R - \text{bound } AngII]_{Pt}^{Memb}(t) \\
&- k_{int} [AT1R - \text{bound } AngII]_{Pt}^{Memb}(t)
\end{aligned} \tag{A.17}$$

$$\begin{aligned}
\frac{d[AT1R - \text{bound } AngII]_{Pt}^{Cell}}{dt}(t) &= k_{int} \frac{V_{Pt}^{Ext}}{V_{Pt,Tb}^{Cell}} [AT1R - \text{bound } AngII]_{Pt}^{Memb}(t) \\
&+ k_{ass}[AT1R]_{Pt}^{Cell}(t)[AngII]_{Pt}^{Cell}(t) \\
&- k_{diss}[AT1R - \text{bound } AngII]_{Pt}^{Cell}(t)
\end{aligned} \tag{A.18}$$

$$\begin{aligned}
\frac{d[AngII]_{Pt}^{Cell}}{dt}(t) &= k_{diss}[AT1R - \text{bound } AngII]_{Pt}^{Cell}(t) \\
&- k_{ass}[AT1R]_{Pt}^{Cell}(t)[AngII]_{Pt}^{Cell}(t) - k_{lys}[AngII]_{Pt}^{Cell}(t)
\end{aligned} \tag{A.19}$$

$$\begin{aligned}
\frac{d[AT1R]_{Pt}^{Cell}}{dt}(t) &= k_{diss}[AT1R - \text{bound } AngII]_{Pt}^{Cell}(t) \\
&- k_{ass}[AT1R]_{Pt}^{Cell}(t)[AngII]_{Pt}^{Cell}(t) \\
&- k_{rec}[AT1R]_{Pt}^{Cell}(t)
\end{aligned} \tag{A.20}$$

$$\begin{aligned}
\frac{d[AT1R]_{Pt}^{Memb}}{dt}(t) &= k_{rec} \frac{V_{Pt}^{Ext}}{V_{Pt,Tb}^{Cell}} [AT1R]_{Pt}^{Cell}(t) \\
&+ k_{diss}[AT1R - \text{bound } AngII]_{Pt}^{Memb}(t) \\
&- k_{ass}[AT1R]_{Pt}^{Memb}(t)[AngII]_{Pt}^{Ext}(t) \\
&+ fb_{Pt}^{AT1R} ([AT1R - \text{bound } AngII]_{Pt}^{Memb}(t))
\end{aligned} \tag{A.21}$$

A.4 Post-glomerular blood vasculature compartment

$$\begin{aligned}
\frac{d[AngI]_{Pv}}{dt}(t) &= \frac{\phi_{RPF} - \phi_{GFR} - \phi_{Gl}}{V_{Pv}} [AngI]_{circ}(t) + \frac{\phi_{Pv}}{V_{Pv}} [AngI]_{Pt}^{Ext}(t) \\
&- \left(\frac{\phi_{RPF} - \phi_L - \phi_U}{V_{Pv}} + \frac{\ln 2}{h_{AngI}} \right) [AngI]_{Pv}(t)
\end{aligned} \tag{A.22}$$

$$\begin{aligned}
\frac{d[AngII]_{Pv}}{dt}(t) &= \frac{\phi_{RPF} - \phi_{GFR} - \phi_{Gl}}{V_{Pv}} [AngII]_{circ}(t) + \frac{\phi_{Pv}}{V_{Pv}} [AngII]_{Pt}^{Ext}(t) \\
&\quad - \left(\frac{\phi_{RPF} - \phi_L - \phi_U}{V_{Pv}} + \frac{\ln 2}{h_{AngII}} \right) [AngII]_{Pv}(t) \\
&\quad + k_{diss}[AT1R - \text{bound } AngII]_{Pv}^{Memb}(t) \\
&\quad - k_{ass}[AngII]_{Pv}(t)[AT1R]_{Pv}^{Memb}(t)
\end{aligned} \tag{A.23}$$

$$\begin{aligned}
\frac{d[AT1R - \text{bound } AngII]_{Pv}^{Memb}}{dt}(t) &= k_{ass}[AngII]_{Pv}(t)[AT1R]_{Pv}^{Memb}(t) \\
&\quad - k_{diss}[AT1R - \text{bound } AngII]_{Pv}^{Memb}(t)
\end{aligned} \tag{A.24}$$

$$[AT1R]_{Pv}^{Memb}(t) = [AT1R]_{Pv}^{tot} - [AT1R - \text{bound } AngII]_{Pv}^{Memb}(t) \tag{A.25}$$

Appendix B

Intrarenal Losartan and EXP3174 model equations

Below, the model equations describing the dynamics of metabolite X ($X = Los$ or $EXP3174$) in each extracellular intrarenal sub-compartment C ($C = Gl, Tb, Pt,$ or Pv) are summarized.

$$\begin{aligned} \frac{d[X]_{Gl}^{Ext}}{dt}(t) &= \frac{\phi_{Gl}}{V_{Gl}^{Ext}} ([X]_{circ}(t) - [X]_{Gl}^{Ext}(t)) \\ &+ k_{diss}^X [AT1R - bound X]_{Gl}^{Emb}(t) - k_{ass}^X [AT1R]_{Gl}^{Emb}(t) [X]_{Gl}^{Ext}(t) \end{aligned} \quad (B.1)$$

$$\begin{aligned} \frac{d[X]_{Tb}^{Ext}}{dt}(t) &= \frac{\phi_{GFR}}{V_{Tb}^{Ext}} [X]_{circ}(t) + \frac{\phi_{Gl}}{V_{Tb}^{Ext}} [X]_{Gl}^{Ext}(t) \\ &- \left(\frac{k_{diff} + \phi_U}{V_{Tb}^{Ext}} \right) [X]_{Tb}^{Ext}(t) \\ &+ k_{diss}^X [AT1R - bound X]_{Tb}^{Emb}(t) - k_{ass}^X [X]_{Tb}^{Ext}(t) [AT1R]_{Tb}^{Emb}(t) \end{aligned} \quad (B.2)$$

$$\begin{aligned}
\frac{d[X]_{Pt}^{Ext}}{dt}(t) &= \frac{k_{diff}}{V_{Pt}^{Ext}} [X]_{Tb}^{Fl}(t) \\
&\quad - \left(\frac{\phi_{Pv} + \phi_L}{V_{Pt}^{Ext}} \right) [X]_{Pt}^{Ext}(t) \\
&\quad + k_{diss}^X [AT1R - \text{bound } X]_{Pt}^{Memb}(t) - k_{ass}^X [AT1R]_{Pt}^{Memb}(t) [X]_{Pt}^{Ext}(t)
\end{aligned} \tag{B.3}$$

$$\begin{aligned}
\frac{d[X]_{Pv}}{dt}(t) &= \frac{\phi_{RPF} - \phi_{GFR} - \phi_L}{V_{Pv}} [X]_{circ}(t) + \frac{\phi_{Pv}}{V_{Pv}} [X]_{Pt}^{Ext}(t) - \left(\frac{\phi_{RPF} - \phi_L - \phi_U}{V_{Pv}} \right) [X]_{Pv}(t) \\
&\quad + k_{diss}^X [AT1R - \text{bound } X]_{Pv}^{Memb}(t) - k_{ass}^X [X]_{Pv}(t) [AT1R]_{Pv}^{Memb}(t)
\end{aligned} \tag{B.4}$$

Appendix C

Blood pressure model equations

Unless otherwise specified in Chapter 5, all equations listed below are taken directly from Ahmed and Layton [1]’s long-term blood pressure regulation model in the male rat. All model parameters and steady state variable values are provided in Table C.1 and Table C.2, respectively.

C.1 Cardiovascular function

The equations describing mean arterial pressure (P_{ma}), cardiac output (ϕ_{co}), venous return (ϕ_{vr}), mean filling pressure (P_{mf}), and the resistance to venous return (R_{vr}) are provided below. Equations describing total peripheral resistance (R_{tp} ; Eq. 5.4) and arterial resistance (R_a ; Eq. 5.3) can be found in Chapter 5.

$$P_{ma}(t) = \phi_{co}(t) \times R_{tp}(t) \quad (\text{C.1})$$

$$\phi_{co}(t) = \phi_{vr}(t) \quad (\text{C.2})$$

$$\phi_{vr}(t) = \frac{P_{mf}(t) - P_{ra}}{R_{vr}(t)} \quad (\text{C.3})$$

$$P_{mf}(t) = \frac{7.4360}{SF_V} \times V_b(t) - 30.18 \quad (\text{C.4})$$

$$R_{vr}(t) = \frac{SF_R \times 8R_{bv} + R_a(t)}{31} \quad (\text{C.5})$$

C.2 Renal hemodynamics

As outlined in Chapter 5, both renal blood flow ϕ_{RBF} and the glomerular filtration rate ϕ_{GFR} are assumed constant. From these now parameters, we compute the renal plasma flow ϕ_{RPF} and the filtered sodium load ϕ_{filsod} , respectively.

$$\phi_{RPF} = \phi_{RBF} \times (1 - Hct) \quad (\text{C.6})$$

$$\phi_{filsod}(t) = W_K \times \phi_{GFR} \times [Na^+]_{circ}(t) \quad (\text{C.7})$$

C.3 Renal fluid handling

All equations related to renal sodium handling (Eqs. 5.5 – 5.19) are provided in Chapter 5. The equations governing renal fluid handling are detailed below.

$$\phi_{pt-wreab}(t) = W_K \times \phi_{GFR} \times \eta_{pt-wreab}(t) \quad (\text{C.8})$$

$$\phi_{md-u}(t) = W_K \times \phi_{GFR} - \phi_{pt-wreab}(t) \quad (\text{C.9})$$

$$\phi_{dt-wreab}(t) = \phi_{md-u}(t) \times \eta_{dt-wreab}(t) \quad (\text{C.10})$$

$$\phi_{dt-u}(t) = \phi_{md-u}(t) - \phi_{dt-wreab}(t) \quad (\text{C.11})$$

$$\phi_{cd-wreab}(t) = \phi_{dt-u}(t) \times \eta_{cd-wreab}(t) \quad (\text{C.12})$$

$$\phi_u(t) = \phi_{dt-u}(t) - \phi_{cd-wreab}(t) \quad (\text{C.13})$$

$$\phi_L(t) = 0.02 \times (\phi_{pt-wreab}(t) + \phi_{dt-wreab}(t) + \phi_{cd-wreab}(t)) \quad (C.14)$$

$$\phi_{Pv}(t) = \phi_{GFR} - \phi_u(t) \quad (C.15)$$

$$\eta_{pt-wreab}(t) = \eta_{pt-wreab}^{eq} \times \mu_{pt-sodreab}(t) \quad (C.16)$$

$$\eta_{dt-wreab}(t) = \eta_{dt-wreab}^{eq} \times \mu_{dt-sodreab}(t) \quad (C.17)$$

$$\eta_{cd-wreab}(t) = \eta_{cd-wreab}^{eq} \times \mu_{cd-sodreab}(t) \quad (C.18)$$

$$\mu_{pt-sodreab}(t) = 0.12 \tanh \left(10 \left(\frac{\eta_{pt-sodreab}(t)}{\eta_{pt-sodreab}^{eq}} - 1 \right) \right) + 1 \quad (C.19)$$

$$\mu_{dt-sodreab}(t) = 0.12 \tanh \left(10 \left(\frac{\eta_{dt-sodreab}(t)}{\eta_{dt-sodreab}^{eq}} - 1 \right) \right) + 1 \quad (C.20)$$

$$\mu_{cd-sodreab}(t) = 0.12 \tanh \left(10 \left(\frac{\eta_{cd-sodreab}(t)}{\eta_{cd-sodreab}^{eq}} - 1 \right) \right) + 1 \quad (C.21)$$

C.4 Renin-angiotensin systems

All equations relating to the intrarenal and systemic RASs are provided in Appendix A. The aldosterone release model is described below. N_{ALD} and $[ALD]_{circ}$ represent the normalized and un-normalized circulating aldosterone concentrations, respectively.

$$\frac{dN_{ALD}}{dt}(t) = \frac{1}{\tau_{ALD}} (\xi_{k/sod}(t) \times \xi_{MAP}(t) \times \xi_{AT1R}(t) - N_{ALD}(t)) \quad (C.22)$$

$$[ALD]_{circ}(t) = [ALD]_{circ}^{eq} \times N_{ALD} \quad (C.23)$$

$$\xi_{k/sod}([Na^+]_{circ}(t)) = \frac{\xi_{k/sod}^a}{1 + \exp\left(\xi_{k/sod}^b \left([K^+]_{circ}/[Na^+]_{circ}(t) - \xi_{k/sod}^c\right)\right)} \quad (C.24)$$

$$\xi_{map}(P_{ma}(t)) = \begin{cases} \xi_{map}^a \exp(-\xi_{map}^b P_{ma}(t)) & \text{if } P_{ma} \leq 100 \\ 1 & \text{if } P_{ma} > 100 \end{cases} \quad (C.25)$$

$$\xi_{AT1R}(R_{circ}(t)) = \xi_{AT1R}^a + \frac{\xi_{AT1R}^b}{1 + \exp(\xi_{AT1R}^c (R_{circ}(t) - \xi_{AT1R}^d))} \quad (C.26)$$

C.5 Miscellaneous

The equations governing extracellular fluid volume (V_{ecf}), blood volume (V_B), plasma volume (V_{circ}), total amount of sodium (M_{Na^+}), and plasma sodium concentration ($[Na^+]_{circ}$) are detailed below. As in [1], we compute the initial (and steady state) blood volume $V_b(0)$ from total body weight W_b .

$$\frac{dV_{ecf}}{dt}(t) = \phi_{win} - \phi_u(t) \quad (C.27)$$

$$V_b(t) = SF_V \times \left(V_b^a + \frac{V_b^b}{1 + \exp(-V_b^c (V_{ecf}(t)/SF_V - V_b^d))} \right), \quad (C.28)$$

$$V_b(0) = 0.06 \times W_b + 0.77$$

$$V_{circ}(t) = V_b(t) \times (1 - Hct) \quad (C.29)$$

$$\frac{dM_{Na^+}}{dt}(t) = \phi_{sodin} - \phi_{u-sod}(t) \quad (C.30)$$

$$[Na^+]_{circ}(t) = \frac{M_{Na^+}(t)}{V_{ecf}(t)} \quad (C.31)$$

Symbol	Description	Value	Unit
Cardiovascular Function			
P_{ra}	Right atrial pressure	0	mmHg
R_{ba}	Arterial resistance	1.03	$\frac{mmHg}{mL/min}$
R_{bv}	Basic venous resistance	0.210	$\frac{mL/min}{mL/min}$
τ_{OXST}	Time constant for the oxidative stress intermediate	9.86	days
Renal Hemodynamics			
ϕ_{RBF}	Renal blood flow	13.4	$\frac{mL/min}{g\ kidney}$
ϕ_{GFR}	Glomerular filtration rate	2.02	$\frac{mL/min}{g\ kidney}$
Renal sodium handling			
<i>pt</i>			
γ_{hyp}^b	Effect of perfusion pressure	3	—
γ_{hyp}^d		0.8	—
γ_{AT1R}^a		0.025	—
γ_{AT1R}^b		1.8	—
<i>dt</i>			
ψ_{ALD}^a	Effect of aldosterone	11.55	—
ψ_{ALD}^b		0.1	—
ψ_{ALD}^c		00081	$\frac{L}{ng\ ALD}$
ψ_{ALD}^d		10.5	—
ψ_{AT1R}^a	Effect of Ang II	0.234	—
ψ_{AT1R}^b		0.1	—
<i>cd</i>			
λ_{dt}^a	Effect of <i>dt</i> sodium outflow	0.8	—
λ_{dt}^b		0.275	—
λ_{dt}^c		2.314	$\frac{\mu eq}{meq}$
λ_{dt}^d		53.5	$\frac{mL}{min}$

Renin-angiotensin-aldosterone systems			
<i>Aldosterone</i>			
τ_{ALD}	Time constant for aldosterone secretion	60	min
<i>Intrarenal Positive Feedback</i>			
K_{circ}^{AGT}	Strength of feedback on hepatic AGT production	562.5	
K_{circ}^{ACE}	Strength of feedback on ACE activity	3.9	$\frac{fmol/mL}{min}$
K_{Pt}^{AT1R}	Strength of feedback on peritubular AT1R production	0.620	
K_{Tb}^{AT1R}	Effect of AT1R-bound Ang II on tubular AT1R production	0.0575	
$AT1R_T^*$	Whole kidney AT1R	1316	$fmol$
<i>Ang II Infusion</i>			
k_a	Rate of Ang II reabsorption from the subcutaneous tissue	1.44e-4	/min
F	Ang II bio-availability	0.056	
Miscellaneous			
W_b	Body weight	284	g
W_K	Kidney weight	1.49	g
$W_{K/b}$	Kidney-to-body weight ratio	5.23	$\frac{mg}{g}$
Hct	Hematocrit	0.42	—
ϕ_{win}	Water intake	0.0372	$\frac{mL}{min}$
ϕ_{sodin}	Na ⁺ intake	3.03	$\frac{\mu eq}{min}$
$[K^+]$	Plasma K ⁺ concentration	5	$\frac{\mu eq}{mL}$
SF_S	Human to Sprague Dawley rat sodium flow scaling factor	24.0	$\frac{\mu eq}{mL}$
SF_U	Human to Sprague Dawley rat urine flow scaling factor	37.2	$\frac{mL}{L}$
SF_V	Human to Sprague Dawley rat volume scaling factor	3.56	$\frac{mL}{L}$
SF_R	Human to Sprague Dawley rat resistance scaling factor	0.0618	$\frac{L}{mL}$

Table C.1: Long-term blood pressure regulation model parameters. Unlisted intrarenal and systemic RAS parameters can be found in Tables 2.2, 2.3, and 3.2.

Symbol	Description	Value	Unit
Cardiovascular Function			
P_{mf}	Mean filing pressure	7.28	
P_{ma}	Mean arterial pressure	103	mmHg
ϕ_{vr}	Venous return	83.3	$\frac{mL}{min}$
ϕ_{co}	Venous return	83.3	
R_a	Arterial resistance	1.03	
R_{vr}	Resistance to venous return	0.0874	
R_{tp}	Total peripheral resistance	1.24	$\frac{mmHg}{mL/min}$
ϵ_{OXST}	Effect of oxidative stress on vascular resistance	1	
Renal sodium and fluid handling			
<i>Sodium</i>			
ϕ_{filsod}	Filtered sodium load	432	
$\phi_{pt-sodreab}$	pt sodium reabsorption rate	346	
ϕ_{md-sod}	Macula densa sodium flow	86.5	
$\phi_{dt-sodreab}$	dt sodium reabsorption rate	43.2	$\frac{\mu eq}{min}$
ϕ_{dt-sod}	dt sodium flow	43.2	
$\phi_{cd-sodreab}$	cd sodium reabsorption rate	40.2	
ϕ_{u-sod}	Urine sodium flow	3.03	
$\eta_{pt-sodreab}$	Fractional pt sodium reabsorption	0.80	
$\eta_{dt-sodreab}$	Fractional dt sodium reabsorption	0.50	—
$\eta_{cd-sodreab}$	Fractional cd sodium reabsorption	0.93	
γ_{hyp}	Effect of perfusion pressure on pt reabsorption	1	
γ_{AT1R}	Effect of Ang II on pt reabsorption	1	
ψ_{ALD}	Effect of aldosterone on dt reabsorption	1	
ψ_{AT1R}	Effect of Ang II on dt reabsorption	1	—
λ_{dt}	Effect of dt sodium outflow on cd reabsorption	1	
<i>Water</i>			
$\phi_{pt-wreab}$	pt water reabsorption rate	2.59	
ϕ_{md-u}	Macula densa flow	0.422	$\frac{mL}{min}$
$\phi_{dt-wreab}$	dt water reabsorption rate	0.253	

ϕ_{dt-u}	dt flow	0.169	
$\phi_{cd-wreab}$	cd water reabsorption rate	0.132	
ϕ_u	Urine flow	0.0372	$\frac{mL}{min}$
ϕ_{Pv}	Flow from peritubular interstitium to renal vasculature	2.0	
ϕ_L	Renal lymphatic flow rate	0.04	
$\eta_{pt-wreab}$	Fractional pt water reabsorption	0.86	
$\eta_{dt-wreab}$	Fractional dt water reabsorption	0.60	—
$\eta_{cd-wreab}$	Fractional cd water reabsorption	0.78	
$\mu_{pt-sodreab}$	Effect of osmotic gradient on pt water reabsorption	1	
$\mu_{dt-sodreab}$	Effect of osmotic gradient on dt water reabsorption	1	
$\mu_{cd-sodreab}$	Effect of osmotic gradient on cd water reabsorption	1	—
Renin-angiotensin-aldosterone systems			
N_{ALD}	Normalized aldosterone concentration	1	
$[ALD]$	Aldosterone concentration	387	$\frac{ng}{L}$
Miscellaneous			
V_{ecf}	Extracellular fluid volume	54.2	
V_b	Blood volume	17.9	mL
V_{circ}	Plasma volume	10.4	
M_{sod}	Total amount of sodium	7761	μeq
$[Na^+]$	Plasma sodium concentration	143	$\frac{\mu eq}{mL}$

Table C.2: Long-term blood pressure regulation model steady state variable values. Unlisted intrarenal and systemic RAS variable values can be found in Table 2.5.

Glossary

Afferent arterioles Blood vessels that supply blood to the glomerulus. [3](#)

Aldosterone Hormone released by the adrenal glands that stimulates sodium reabsorption in the distal tubule and collecting duct of the nephron. It's secretion is increased by Ang II binding to AT1Rs. [7](#)

Ang II infusion Protocol used to induce hypertension in pre-clinical models, relying on the constant administration of Ang II intravenously or subcutaneously. [14](#), [35](#), [148](#)

Ang II-induced hypertension Hypertension induced by [Ang II infusion](#). [8](#), [35](#)

Chymase Enzyme that mediates the production of [Ang II](#) from [Ang I](#) in an ACE-independent manner. [5](#), [24](#), [29](#)

Efferent arterioles Blood vessels that take what remains of the blood after filtration away from the glomerulus. [3](#)

Endocytosis Cellular internalization process by which substances are brought into the cell by way of membrane invagination and the formation of an endosome. [20](#), [29](#)

EXP3174 The bio-active product of [Losartan](#). [xii](#), [12](#), [59](#), [61](#), [75](#)

Feedback parameters Model parameters that impact the system only when it is perturbed from this steady state. [43](#)

Filtrate Fluid within the renal tubule that has been filtered by the nephron. [3](#)

Glomerular compartment Compartment of the intrarenal RAS model that comprises the mesangial matrix and extra-glomerular fluid (extracellular region) as well as mesangial cells (intracellular compartment). Abbreviation: *Gl*. [15](#), [28](#)

- Glomerular filtration rate** Volume of plasma filtered by the glomerular capillaries per unit time [4](#), [7](#), [27](#), [28](#)
- Glomerulus** Tightly interconnected cluster of capillaries within the nephron responsible for filtering the incoming blood. [3](#), [4](#), [20](#)
- Interstitial space** Extracellular matrix and interstitial fluid of the renal interstitial space. Forms the extracellular region of the glomerular and peritubular compartments of the intrarenal RAS model. [3](#), [15](#), [19–21](#), [24](#), [27–29](#), [41](#), [61](#), [90](#), [150](#), [151](#)
- Juxtaglomerular apparatus** Structure adjacent to the glomerulus that secretes renin into the circulation. [4](#), [23](#), [54](#), [66](#)
- Losartan** An [ARB](#) used to treat hypertension. [xii](#), [8](#), [11](#), [12](#), [14](#), [55](#), [59–61](#), [71](#), [72](#), [75](#), [109](#), [148](#)
- Luminal fluid** Fluid filtered into the tubules of the nephron that lies inside the tubular lumen. Forms the extracellular region of the [tubular compartment](#) of the intrarenal RAS model. [3](#), [15](#), [19](#), [27–29](#), [32](#), [36](#), [41](#)
- Macula densa** Area of specialized sodium-sensing cells that line the beginning of the distal tubule adjacent to the glomerulus. [87](#)
- Megalin** Large endocytic receptor on the apical membrane of proximal [tubular epithelial cells](#) that aids in the reabsorption of proteins from the luminal fluid. [15](#), [20](#), [29](#), [32](#)
- Mesangial cells** The cells comprising the space between the glomerular capillaries (the mesangium). [3](#), [15](#), [27](#), [28](#)
- Mesangial matrix** The extracellular matrix of the space between the glomerular capillaries (the mesangium). [3](#), [15](#), [28](#)
- Nephron** Functional unit of the kidney. [iv](#), [3](#)
- Peritubular capillaries** Capillary network that supplies renal cells with the oxygen and nutrients they need to survive while facilitating the reabsorption and secretion of substances between the blood and the renal tubules. [3](#)

Peritubular compartment Compartment of the intrarenal [RAS](#) model that comprises the peritubular [interstitial space](#) (extracellular region) and basolaterally-derived molecular structures of tubular epithelial cells (intracellular region). Abbreviation: *Pt.* [15](#)

Pressure natriuresis Predominant mechanism by which the kidney regulates blood pressure, whereby increases in renal perfusion pressure result in greater sodium, and therefore fluid excretion. [4](#), [81](#), [86](#)

Reabsorption Process of solutes or volume being removed from the filtrate to re-enter the circulation via the peritubular capillaries. [3](#)

Renal blood flow Volume of blood (including cells) delivered to the kidneys per unit time [3](#)

Renal corpuscle Blood-filtering component of the nephron. Contains the glomerulus and Bowman’s capsule. [3](#)

Renal plasma flow Volume of plasma delivered to the kidneys per unit time [19](#), [21](#), [27](#), [28](#), [61](#)

Renal tubule Component of the nephron responsible for fine-tuning the filtrate via reabsorption and secretion of solutes and fluid. [3](#)

Renin First enzyme involved in the [RAS](#) enzymatic cascade, responsible for cleaving [AGT](#) into [Ang I](#). [4](#), [39](#)

Secretion Process of solutes being added to the filtrate from the peritubular capillaries. [3](#)

Transcytosis Type of transcellular transport where the macromolecule (eg. peptide) is transported across the interior of a cell. [20](#)

Tubular compartment Compartment of the intrarenal [RAS](#) model that comprises the luminal fluid (extracellular region) and apically-derived molecular structures of [tubular epithelial cells](#) (intracellular region). Abbreviation: *Tb.* [15](#), [149](#)

Tubular epithelial cells Epithelial cells that line the nephron. Their apical membrane faces the luminal fluid (tubular lumen) and their basolateral membrane faces the interstitium. [3](#), [15](#), [19](#), [27](#), [28](#), [30](#), [36](#), [52](#), [149–151](#)

Tubular epithelium Single layer of [tubular epithelial cells](#) that lines the nephron and separates the luminal fluid from the [interstitial space](#). [20](#), [29](#), [32](#)

Vasculature compartment Compartment of the intrarenal RAS model that comprises the lymphatic vasculature and the post-glomerular blood vasculature. Abbreviation: *Pv*. [15](#), [18](#), [28](#)